ROBERT GORDON
UNIVERSITY ABERDEEN

COMPUTATIONAL FLUID DYNAMICS MODELLING OF PIPELINE ON-BOTTOM STABILITY

IBIYEKARIWARIPIRIBO IYALLA

A thesis submitted in partial fulfilment of the requirements of the Robert Gordon University for the degree of Doctor of Philosophy

October 2017

ACKNOWLEDGEMENTS

DEDICATION

This thesis is dedicated to the memory of my late mother **Mrs Basoene Obuba Iyalla** who did not live long enough to see the fruits of her labour.

ABSTRACT

Subsea pipelines are subjected to wave and steady current loads which cause pipeline stability problems. Current knowledge and understanding on the pipeline on-bottom stability is based on the research programmes from the 1980's such as the Pipeline Stability Design Project (PIPESTAB) and American Gas Association (AGA) in Joint Industry Project. These projects have mainly provided information regarding hydrodynamic loads on pipeline and soil resistance in isolation. In reality, the pipeline stability problem is much more complex involving hydrodynamic loadings, pipeline response, soil resistance, embedment and pipe-soil-fluid interaction.

In this thesis Computational Fluid Dynamics (CFD) modelling is used to investigate and establish the interrelationship between fluid (hydrodynamics), pipe (subsea pipeline), and soil (seabed). The effect of soil types, soil resistance, soil porosity and soil unit weight on embedment was examined. The overall pipeline stability alongside pipeline diameter and weight and hydrodynamic effect on both soil (resulting in scouring) and pipeline was also investigated. The use of CFD provided a better understanding of the complex physical processes of fluid-pipe-soil interaction.

The results show that the magnitude of passive resistance is on the average eight times that of lateral resistance. Thus passive resistance is of greater significance for subsea pipeline stability design hence the reason why Coulomb's friction theory is considered as conservative for stability design analysis, as it ignores passive resistance and underestimates lateral resistance.

Previous works (such as that carried out by Lyons and DNV) concluded that soil resistance should be determined by considering Coulomb's friction based on lateral resistance and passive resistance due to pipeline embedment, but the significance of passive resistance in pipeline stability and its variation in sand and clay soils have not be established as shown in this thesis. The results for soil porosity show that increase in pipeline stability with increasing porosity is due to increased soil liquefaction which increases soil resistance. The pipe-soil interaction model by Wagner et al. established the effect of soil porosity on lateral soil resistance but did not attribute it to soil liquefaction. Results showed that the effect of pipeline diameter and weight vary with soil type; for sand, pipeline diameter showed a greater influence on embedment with a 110% increase in embedment (considering combined effect of diameter and weight) and a 65% decrease in embedment when normalised with diameter. While pipeline weight showed a greater influence on embedment in clay with a 410% increase.

The work of Gao et al. did not completely establish the combined effect of pipeline diameter and weight and soil type on stability. Results also show that pipeline instability is due to a combination of pipeline displacement due to vortex shedding and scouring effect with increasing velocity. As scoring progresses, maximum embedment is reached at the point of highest velocity. The conclusion of this thesis is that designing for optimum subsea pipeline stability without adopting an overly conservative approach requires taking into consideration the following; combined effect of hydrodynamics of fluid flow on soil type and properties, and the pipeline, and the resultant scour effect leading

to pipeline embedment. These results were validated against previous experimental and analytical work of Gao et al, Brennodden et al and Griffiths.

Keywords: Drag, Embedment, Hydrodynamic Force, Lateral Resistance, Lift, Passive Resistance, Pipeline, Pressure Coefficient, Scour, Stability.

TABLE OF CONTENTS

LIST OF FIGURES

LIST OF TABLES

NOMENCLATURE

a	acceleration (m/s^2)
A	area (m^2)
C_a	added mass coefficient
C_{AW}	added mass coefficient with wake flow
C_D	drag Coefficient
C_{DS}	steady current drag coefficient
C_S	steady flow force coefficient
C_L	lift coefficient
C_M	coefficient of inertia
C_1, C_2	wake velocity correction parameters in periodic flow
d	average sediment particle diameter (m)
D	diameter (m)
F_D	drag force (N)
F_F	sliding resistance (N/m)
F_H	total lateral resistance (N/m)
F_R	soil lateral resistance (N/m)
F_I	inertia force (N)
F_L	lift force (N)
F_{Pressure}	Froude-Krylov force (N)
g	acceleration due to gravity (m/s^2)
G	shear modulus (Pa)
G_s	specific gravity soil

H	wave height (m)
k	coefficient of soil permeability
K'	apparent bulk modulus of elasticity of water
KC	Keulegan-Carpenter number
P	pressure (Pa)
Re	Reynolds number
t	time (s)
T	wave period (s)
u_w	wake velocity correction (m/s)
U	velocity (m/s)
U_c	critical velocity (m/s)
U_e	effective velocity (m/s)
U_m	Peak Velocity (m/s)
U_t	total free stream velocity of steady current (m/s)
U_W	wake velocity (m/s)
W_s	submerged weight (N)

Greek

γ'	buoyant unit weight of sand (N/m^3)
β	coefficient of passive soil resistance
μ	coefficient of sliding resistance
θ_c	critical Shields Number
ρ	density (kg/m^3)
ν	kinematic viscosity (m^2/s)

ϕ	phase angle (°)
υ	Poisson's ratio
p	pore-water pressure (Pa)
θ	Shields number
ϕ	soil porosity (%)
γ_w	specific weight of water (N/m³)
ε	volume expansion per unit volume of soil.
ω	wave frequency (Hz)
λ	wavelength (m)

CHAPTER 1: INTRODUCTION

Petroleum reserves located under the seabed have resulted in the development of offshore structures and facilities to support the activities of the oil and gas industry which include exploration, drilling, storage, and transportation of oil and gas. Offshore structures constructed on or above the continental shelve and on adjacent continental slopes take many forms including pipeline system for transporting reservoir fluids from wells to tieback installations or onshore location, and platforms (Wilson 2002). Producing oil and gas from offshore and deepwater wells by means of subsea pipelines has proven to be the most convenient, efficient, reliable and economic means of large scale continuous transportation to existing offshore installation or onshore location on a regular basis (Guo et al 2005).

A pipeline on the seabed has to be stable to avoid possible breakage and eventual spill of hydrocarbons. If the pipeline is too light, it will move (i.e. become unstable) under the action of currents and waves. On the other hand, if it is too heavy, it will be difficult and expensive to construct (Palmer and King 2011). To accurately design systems or design operations at sea, an understanding of the working environment is necessary, that is, an understanding of the principal environmental factors which will influence the design. The process of subsea pipeline stability design incorporates wave and current prediction, determination of hydrodynamic loads due to current, and soil lateral resistance analysis. The loads acting on the pipeline due to wave and current are drag, lift and inertia forces. To ensure stability, the friction due to the effective weight of pipeline on the seabed must balance these forces. Where

the weight of pipeline and contents alone is insufficient in achieving stability, other stabilization techniques such as trenching, mattresses, concrete coating, etc, have to be used (Palmer and King 2011, Bai and Bai 2005).

To evaluate the wave-induced forces acting on a subsea pipeline, the surrounding hydrodynamic loads must be known. Hydrodynamic loads are flow-induced loads caused by the relative motion between pipeline and the surrounding water. To assess the structural integrity and stability of subsea pipelines at the design stage, the environmental loads and structural responses must be calculated and evaluated. Both the static and dynamic response of a subsea pipeline can be reasonably predicted at the design stage. To determine the dynamic behaviour of a subsea pipeline, it is important to acquire realistic data on environmental conditions such as wave, current, soil, etc., and to properly account for them in the calculations (Marbus 2007).

Pipeline stability is affected by the interaction between the sea waves and currents and the pipeline (fluid-pipe), the interaction between the pipeline and the seabed (pipe-soil) and the interaction between the sea waves and currents and the seabed (fluid-soil). Fluid-pipe interaction results in hydrodynamic loading on pipeline, pipe-soil interaction results in soil lateral and passive resistance, while fluid-soil interaction results in seabed mobility or liquefaction. There is a complex relationship between these interactions; fluid-soil interaction in the form of seabed liquefaction affects the degree of pipeline embedment, which in turn affects the hydrodynamic loading on the pipeline (fluid-pipe interaction) and the soil passive resistance (pipe-soil interaction) (Ryan et al. 2011). The approach to pipeline stability design is to limit the lateral

movement of the pipeline under wave loading by establishing a balance between wave loading, the submerged weight of pipeline and soil resistance. This is done by determining the submerged weight required to produce a large enough soil lateral resistance that will hold the pipeline in equilibrium against the combination of weight and hydrodynamic loads. Without sufficient resistance from the soil, the pipeline will loose on-bottom stability which may result in the breaking of pipeline. Conventionally, to avoid the occurrence of such instability, the pipeline has to be given a heavy weight coating or alternatively be anchored or trenched into the soil to avoid the occurrence of pipeline instability. However, both methodologies are considered expensive and complicated in terms of design and construction. Thus a better understanding of on-bottom pipeline stability is of utmost importance in subsea pipeline design (Palmer and King 2011; Gao et al. 2006; Gao and Jeng 2005; Gao et al. 2002).

1.1 Research Aim

Current knowledge and understanding of pipeline on-bottom stability is based on research programmes from the 1980's such as the Pipeline Stability Design Project (PIPESTAB) and American Gas Association (AGA) in Joint Industry Project. These projects have mainly provided information regarding hydrodynamic loads on pipeline and soil resistance in isolation. In reality, the pipeline stability problem is much more complex involving cyclic hydrodynamic loadings, pipeline response, soil resistance, embedment and pipe-soil-fluid interaction. Zeitoun et al. (2008) provided a detailed overview of the currently available knowledge on the pipeline stability and concluded that many aspects of the complex interaction of hydrodynamic loads and structural response is not currently fully understood. As a result of the limitations of the current design

methods, there is a need for an on-bottom stability design method that will consider the interdependency between fluid-pipe, pipe-soil and fluid-soil interactions to give an overall fluid-pipe-soil (F-P-S) interaction model as depicted by the Venn diagram in Figure 1.1 below.
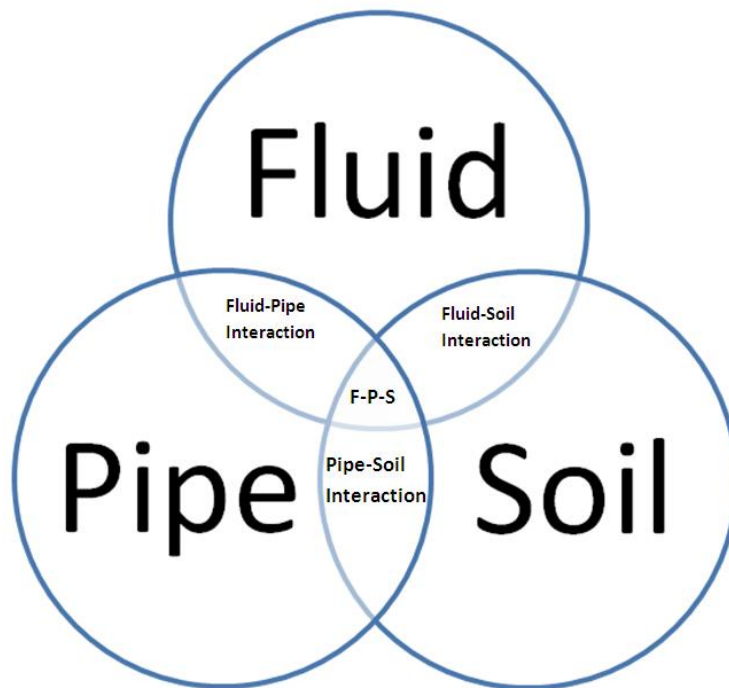
Figure 1.1 Fluid-Pipe-Soil (F-P-S) interaction model

This new approach will reduce the uncertainty in design and thus minimise over-conservatism. This will eliminate the use of costly stabilisation techniques by reducing the uncertainty on the effect of pipe embedment on pipeline stability, and the effect of pipe embedment on the seabed as a result of pipeline self-burial, sediment transport and hydrodynamic loading on pipeline.

This research is thus intended to investigate subsea pipeline on-bottom stability under hydrodynamic loading and soil interaction with a view to further improve the present knowledge of subsea pipeline on-bottom stability and provide a Computational Fluid Dynamics (CFD) model for optimum stability design of subsea pipelines.

1.2 Research Objectives

The main aim of the research is to provide a better understanding of the complex interaction of pipe, seabed and the fluid flow, with specific objectives as follows;

1. To determine the effect of soil resistance on subsea pipeline stability by investigating;

   a) The effect of soil types (sand and clay) on passive resistance

   b) The effect of soil types (sand and clay) on lateral resistance

   c) The effect of hydrodynamic load and embedment on soil resistance

2. To investigate the effect of pipeline embedment and seabed porosity on subsea pipeline stability.

3. To determine degree of pipeline embedment by investigating;

   a) The effect of pipeline diameter and weight on pipeline embedment

   b) The effect of unit weight of soil on pipeline embedment

   c) The effect of hydrodynamic forces on pipeline embedment

4. To investigate the effect of scouring on subsea pipeline embedment by considering velocity, wall shear stress, and pressure coefficient effect.

1.3 Thesis Outline

The thesis is structured as follows;

Chapter 1: Provides an introduction to the concept of subsea pipeline on-bottom stability. The rationale for the research is discussed, and the aim and objectives of the thesis also described.

Chapter 2: Provides a brief description of the factors that influence subsea pipeline on-bottom stability. It also provides review of past and current approaches to on-bottom stability design.

Chapter 3: Computational Fluid Dynamics modelling is a very useful computer based modelling tool for solving a wide range of fluid flow and associated problems. In this chapter the governing equations and supplementary equations used in developing the models described in this thesis is presented.

Chapter 4: Describes the FEA/CFD model created to analyse effect of soil resistance on pipeline stability and presents the results for the effect of soil types on passive and lateral resistance, and effect of hydrodynamic load on embedment and soil resistance.

Chapter 5: Describes the CFD model created to analyse pipeline stability and presents the results for the effect of soil embedment on seabed porosity on pipeline lateral stability

Chapter 6: Describes the CFD model created to analyse pipeline embedment for pipeline stability optimisation and presents the results for the effect of pipe diameter, pipe weight, unit weight of soil, and hydrodynamic forces on pipeline embedment.

Chapter 7: Decribes the CFD model created to analyse seabed scouring effect and presents the results for velocity effect on scouring and scouring effect on wall shear stress and pressure coefficient.

Chapter 8: Final chapter of thesis summarising findings and presenting recommendations for future work.

CHAPTER 2: LITERATURE REVIEW

To accurately design subsea systems or plan subsea operations, an understanding of the working environment is necessary, that is, an understanding of the principal environmental factors which will influence the design and operation. The process of subsea pipeline stability design incorporates wave and current prediction, determination of hydrodynamic loads due to current, and soil lateral resistance analysis. The loads acting on the pipeline due to wave and current are drag, lift and inertia forces. To ensure stability, the friction due to the effective weight of pipeline on the seabed must balance these forces (Figure 1.1) (Palmer and King 2011; Bai and Bai 2005).
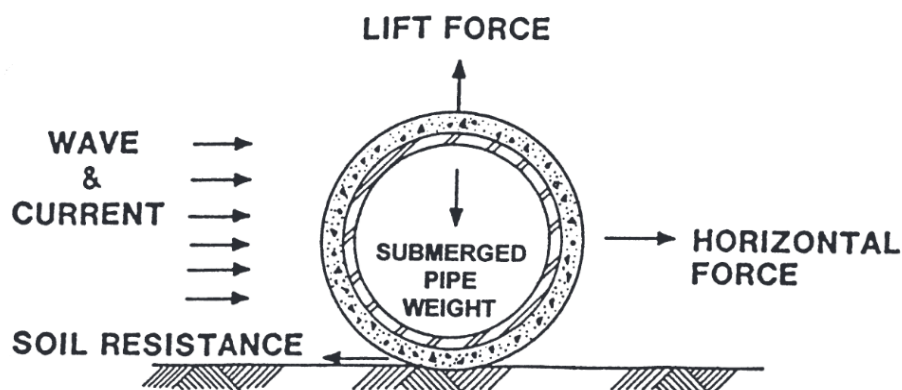
Figure 2.1 On-bottom pipeline stability (Soedigbo, Lambrakos and Edge 1998)

When a pipeline is installed subsea, the presence of the pipe will change the flow pattern in its immediate neighbourhood. The flow condition around the pipeline does not only affect the wave force acting on the pipe, but can also induce sea floor instability. The occurrence of seabed instability is a widespread phenomenon in ocean environments. There is evidence of ocean floor instability in a wide variety of offshore regions, from shallow water, near-shore zones, continental slopes, and beyond to deep ocean floors (Dong 2003).

Analytical study of on-bottom pipeline begins with calculating the wave and current loadings. The widely used load calculation methods are reviewed in the following sections.

2.1 Potential Flow Phenomena on a Cylinder

Pipelines are cylindrical structures, to calculate the forces on these structures, a view of the theory of forces on a cylinder due to wave and current has to be obtained.

The steady flow of a potentially incompressible fluid yields a relationship called the Bernoulli equation. The equation relates the kinetic energy and the work done on a water particle, and is expressed as:

$$\frac{p}{\rho g} + \frac{U^2}{2g} = H \tag{2.1}$$

P - Pressure, U – Velocity, ρ – Density, g – Acceleration due to gravity, and H is a constant.

This formula states that the sum of the piezometric and kinetic pressure is constant along a streamline for the steady flow of an incompressible, non-viscous fluid. If a non-viscous and incompressible fluid is considered, then Bernoulli's equation will apply everywhere in the flow field around a circular cylinder as shown in figure 2.2 below (Marbus 2007; Sumer and Fredsoe 2006).
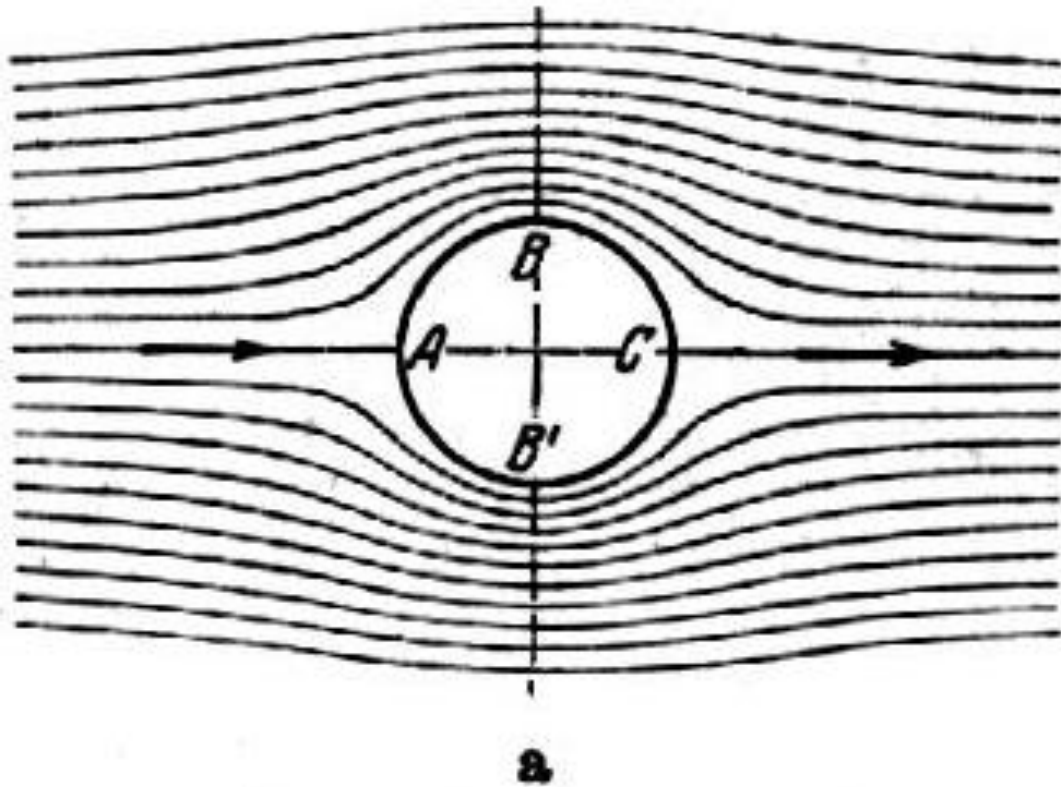
Figure 2.2 Potential flow around a circular cylinder (Marbus 2007)

Point A is considered as $0°$ and point C as $180°$. In a vertical and horizontal sense, the flow is symmetrical through the centre of the cylinder. The cylinder is assumed to be a slender cylinder that is the diameter of the cylinder is relatively small when compared with the wavelength. Point A is referred to as a stagnation point (with normal and tangential component of velocity zero) (Marbus 2007; Sumer and Fredsoe 2006).

2.2 Viscous Fluid

In general, fluids have viscous characteristics. This will have a significant effect on the flow pattern around a cylinder. The viscous nature of the fluid will cause a zero velocity of the fluid at the surface of the cylinder. This viscous effect produces a thin layer called a boundary layer (figure 2.3). The velocity in this

layer changes from zero to the free stream velocity, and the flow in this layer can be either laminar or turbulent. It is relatively stable in front of the cylinder, but once it moves around the cylinder it produces eddies/vortices which are shed from the cylinder. These eddies are shed alternatively from side to side.
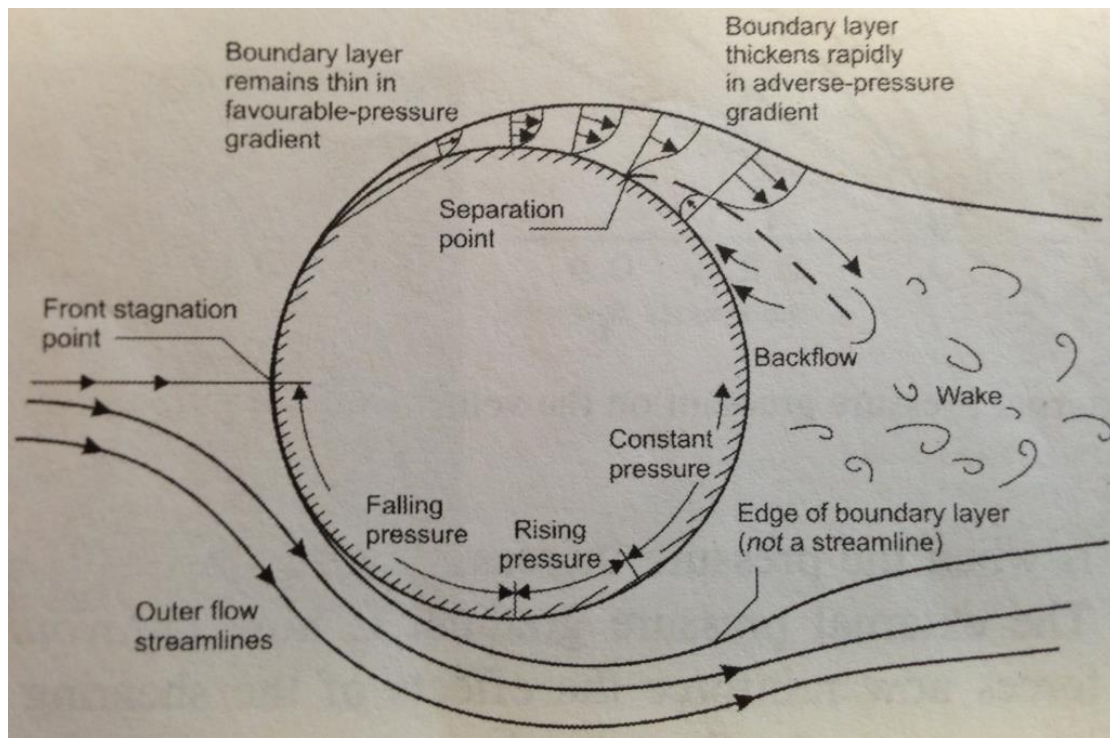
Figure 2.3 Flow around a cylinder with wake (Groh 2016)

The different states of flow around a cylinder described from low velocity to high velocity are shown in figure 2.4 (a-f), and the characteristics of the different states are described in table 2.1.
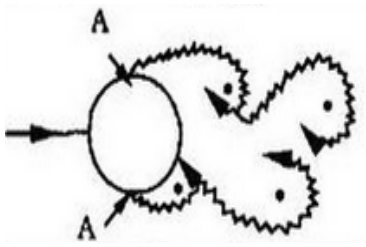
Figure 2.4a Laminar   Figure 2.4b Transition
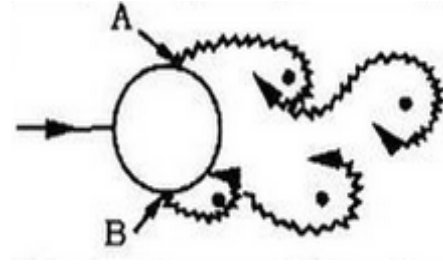
Figure 2.4c Subcritical   Figure 2.4d Critical
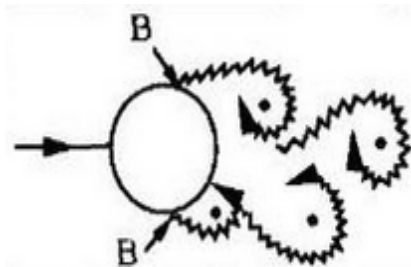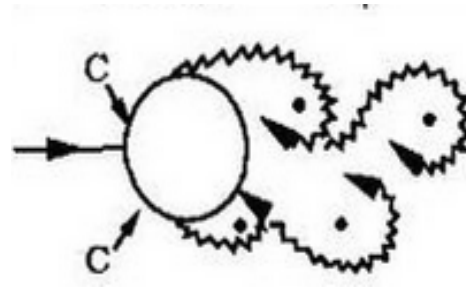
Figure 2.4e Supercritical   Figure 2.4f Transcritical

Figure 2.4 Flow regimes (Sumer and Fredsoe 2006)

Table 2.1 Flow regimes around a circular cylinder (Sumer and Fredsoe 2006)

Flow definition	Characteristics	Reynolds Number
Laminar	Laminar vortex	$Re < 5$
Transition wake	Transition to turbulence wake	$200 < Re < 300$
Subcritical	Wake completely turbulent Laminar boundary layer separation	$300 < Re < 3*10^5$
Critical	Laminar boundary layer separation Start of turbulent boundary layer separation	$3*10^5 < Re < 3.5*10^5$
Supercritical	Turbulent boundary layer separation; partly laminar, partly turbulent	$3.5*10^5 < Re < 1.5*10^6$
Transcritical	Boundary layer completely turbulent	$4*10^6 < Re$

2.3 Drag Forces

With reference to figure 2.3, the pressure increases with distance along the surface downstream of the midsection. The velocity decreases along the surface in the boundary layer, while the pressure increases in the reverse direction. At a point called the separation point, the pressure gradient forces the

fluid to go roundabout the surface. The circular flow behind the cylinder is referred to as the wake.

The wake is thus a low pressure region. This pressure gradient over the cylinder results in a pressure force on the cylinder which is referred to as the drag force (F_D) and is expressed as (Sumer and Fredsoe 2006):

$$F_D = \frac{1}{2}C_D D\rho U|U|$$ (2.2)

C_D - drag coefficient, D - diameter of cylinder (m), ρ - density of water (kg/m³), $U|U|$ - same as velocity squared (U^2) ([m/s]²) but shows that drag force is in the direction of velocity.

2.4 Lift Force

Lift is produced in the same way as a flow over an airfoil. The presence of the seabed introduces an asymmetry between the flow over the top of the pipe and the flow underneath. This causes slower flow (or no flow) underneath the pipeline (high pressure) and higher velocities over the top (low pressure), resulting in lift (Sumer and Fredsoe 2006).

Lift force (F_L) is expressed as follows:

$$F_L = \frac{1}{2}C_L D\rho U^2$$ (2.3)

C_L - coefficient of lift

2.5 Inertia Force

For oscillatory flow, two additional forces contribute to the total in-line force. The flow acceleration is of interest for the inertia forces.

A cylinder inserted within the pressure gradient field of accelerating water particles will experience a force referred to as the pressure gradient force or the Froude-Krylov force ($F_{pressure}$). It is the product of the mass of the water (ρA), which is replaced by the cylinder and the acceleration (a) present in the water (Sumer and Fredsoe 2006).

$$F_{pressure} = \rho Aa \qquad (2.4)$$

ρ - density of water, A - cross-sectional area of cylinder

The cylinder geometry forces the fluid to go around it and thus the velocities and accelerations are modified. The mass of the fluid around the cylinder which is accelerated due to the cylinder causing pressure is referred to as the hydrodynamic mass. This is a result of the force from the cylinder. This force is referred to as the disturbance force ($F_{hydrodynamic}$) and is expressed as follows:

$$F_{hydrodynamic} = C_a \rho Aa \qquad (2.5)$$

C_a - added mass coefficient

These two forces result in the total inertia force expressed as:

$$F_I = \rho \frac{\pi}{4} C_M D^2 a \qquad (2.6)$$

Where:

$$C_M = 1 + C_a$$

C_M is the experimental inertia coefficient, which consists of the coefficient of the two forces. The pressure gradient force is always 1, but the coefficient disturbance force varies for every stream condition and the characteristics of the element (Sumer and Fredsoe 2006).

2.6 Wave Loading

Waves represent the dominant force mechanism acting upon offshore structures such as pipelines. The wave forces are generally periodic, however, non-linearity may result in mean and low frequency steady drift forces. Non-linearity can also induce super harmonic high frequency forces; these are loading frequencies considerably higher than the wave generated frequencies. All forms of wave forces can be significant if they can excite the system resonance. Offshore structures tend to be relatively strained; therefore any stimulation of resonance upon that structure can have an impact on the behaviour of that structure (Faltinsen 1993).

Wave loading for the offshore industry has been applied to developing methods to calculate forces on structural elements such as pipelines and risers. The analysis and interpretation of wave forces have been directed towards the influence of the wave height, diameter of the structural element, and wavelength. Equivalent ratios for wave loading result in a series of non-dimensional coefficients. Wave loading ratios are characterized using the following non-dimensional parameters (Det Norske Veritas 2011):

Keulegan-Carpenter number $KC = \dfrac{U_M T}{D}$ (2.7)

Reynolds number $\mathrm{Re} = \dfrac{U_M D}{v}$ (2.8)

Roughness ratio $= \dfrac{k}{D}$ (2.9)

Froude number $Fr = \dfrac{U_m}{(gD)^{0.5}}$ (2.10)

U_M - maximum flow velocity; T - wave period; v - kinematic viscosity; k - pipe roughness; g - acceleration due to gravity

2.7 Hydrodynamic Forces

A pipeline on the seabed is subjected to a combined effect of waves and currents which results in a pressure difference between the upstream and downstream of the pipeline. This pressure difference creates a hydrodynamic force. Hydrodynamic force is divided into two main components; a horizontal force (drag and inertia) and a vertical force (lift). Figure 2.5 shows a free body diagram of these forces acting on a cross section of a pipeline (Palmer and King 2011; Bai and Bai 2005).
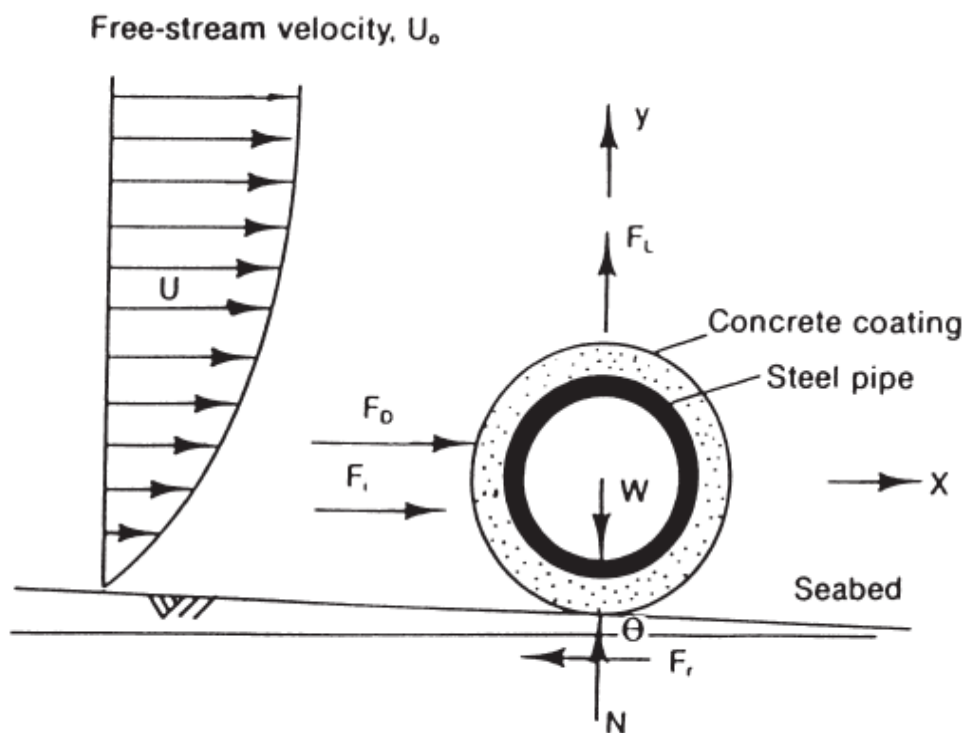
Figure 2.5 Hydrodynamic forces on a pipeline (Mousselli 1981)

Generally, hydrodynamic forces are determined by using the conventional Morison equation with suitable drag, inertia and lift coefficient and pipeline diameter, pipeline roughness and current velocity and acceleration. The steady current and wave induced flow are used for this analysis. The wave and current data used are for extreme conditions such as, wave occurrence probability of one in hundred years used for operational lifetime design and a wave of one

17

year or five years applied for installation design (Sumer and Fredsoe 2002; Mousselli 1981).

2.8 Morison's Equation

Morison's equation was first proposed in the 1950's (Wade and Dwyer 1978) and has been used to calculate hydrodynamic loads on cylindrical bodies such as pipelines. The drag (F_D), inertia (F_I), and lift (F_L) forces traditionally are calculated using an adaptation of Morison's equation (Evans 1970). Morrison equation specifies that the horizontal force (F_H) and lift force (F_L) acting on a subsea pipeline with diameter D can be written as:

$$F_H(t) = \frac{1}{2}.\rho.C_D.D.|U_t|U_t + \frac{\pi.D^2}{4}.\rho.C_M.\dot{U}_t \tag{2.11}$$

$$F_L(t) = \frac{1}{2}.\rho.C_L.D.(U_t)^2 \tag{2.12}$$

U_t - total free stream velocity of steady current and wave component

The flow kinematics U_t and hydrodynamic coefficients to apply to a wide range of flow conditions must be known in order to predict the hydrodynamic loads acting on a subsea pipeline (Zietoun et al 2008). However, it has been found that Morison's equation does not describe with accuracy the forces for combined flow as it applies mainly to small objects where wave kinematics do not change appreciably over a distance equivalent to the width of the structural element (Evans 1970). The measured forces especially for lift forces differ from the calculated forces for regular waves, as lift forces depend on flow history effects (due to wake). In the case of regular waves with current component, Morison's equation gives substantial errors in magnitude, phase relative to velocity, and shape of the lift forces (Det Norske Veritas 2010). This has

18

resulted in the postulation of better design models (Wake II Model) that will best predict the hydrodynamic loads acting on a pipeline on the seabed. One of the difficulties in the calculation of the hydrodynamic forces is the determination of the drag, inertia, and lift coefficients. Extensive measurements have been made in order to define the coefficients as a function of Reynolds number, pipe roughness, and Keulegan-Carpenter number. One of the main sources used for the coefficients is the Norwegian rules Det Norske Veritas (Det Norske Veritas 2010; Marbus 2007).

2.9 Wake Force Model

To assess the adequacy of existing hydrodynamic force models for pipeline design and to provide a reference base for testing improvements to these force models, Exxon operated a field program called Pipeline Field Measurement Program (PFMP) in Washington State. The program lasted six months over the winter of 1980-1981. The objective was to measure design-level forces on a full scale pipe section, and the corresponding flow kinematics (Lambrakos 1982). The PFMP measurements correspond to a wide range of flow conditions. Keulegan-Carpenter numbers, (KC range up to 40), and Reynolds numbers, (Re up to 8×10^5). Water velocity varied from pure steady to pure wave (with velocity ratio ranging from 0.5 to 1.5), and the two pipes relative roughness tested (mean roughness height/pipe diameter) were 10^{-4} (smooth) and 2×10^{-2} (rough) (Lambrakos et al. 1987). The PFMP measurements were in agreement with that predicted by the Wake Force Model, which is an indication of the accuracy of the model with reference to general force characteristics and maximum force values. Pipeline motions determined from predicted forces

19

using the Wake Force Model was also in agreement with motions calculated from PFMP measured forces (Verley, Lambrakos and Reed 1987).

2.9.1 Wake I Model

Lambrakos et al (1987) proposed the Wake I Force Model, based on the data obtained from the Exxon's Pipeline Field Measurement Program (PFMP). This model was intended to incorporate in the Morison's equation the wake velocity behind the cylinder and time dependent hydrodynamic coefficients. The primary difference between the Wake I Model and Morison's equation is that the velocity in the Wake I Model is modified to include the pipe's encounter with the wake flow when the velocity reverses. The effective velocity acting on the pipe is then determined by superimposing the wake generated by the presence of the pipe onto the ambient flow. Time-dependent drag and lift coefficients are also used for this model; this dependence is referred to as a start-up effect (Soedigbo, Lambrakos and Edge 1998).

The basic equations for the drag and lift forces are assumed to be the same as that of Morison's equation. The drag and lift coefficients in the Wake I Model are time dependent (accounting for start-up effect), the effective flow velocity (U_e) is taken to be equal to the sum of the ambient velocity (U), which accounts for the boundary layer of the steady component in the flow, and the wake velocity (U_W). Time dependence for the lift coefficient is particularly important as the relative occurrences of velocity zero-crossings, minimum lift forces, maximum lift forces, and maximum velocities cannot be matched with simple phase shifting of velocities, or the introduction of an internal term.

The Wake I Model expression for the drag (F_D), lift (F_L) and inertial (F_I) forces are:

$$F_D = 0.5\rho D C_D(t)|U_e|U_e \qquad (2.13)$$

$$F_L = 0.5\rho D C_L(t)U_e^{\;2} \qquad (2.14)$$

$$F_I = \frac{\pi D^2}{4}\rho\left[C_M \frac{dU}{dt} - C_{AW} \frac{dU_W}{dt}\right] \qquad (2.15)$$

Where:

$C_D(t)$ - time-dependent coefficient of drag

$C_L(t)$ - time-dependent coefficient of lift

C_{AW} - added mass coefficient with wake flow passing the pipe

The horizontal force is the sum of F_D and F_I.

Figure 2.6 shows the effect of wake velocity (represented as W which is same as U_W) correction in oscillatory pipe motion on the effective velocity encountered by the pipe. The mean wake flow behind the moving pipe is in the same direction as the pipe motion. The wake still flows in the same direction when pipe direction is reversed. The effective velocity is thus equal to the sum of the wake velocity and pipe velocity.
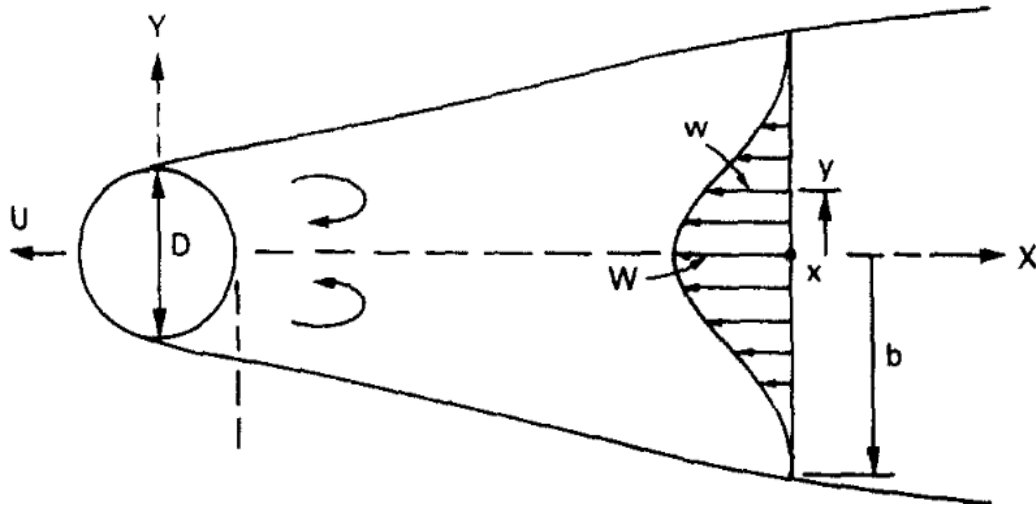
Figure 2.6 Wake velocity effect on effective velocity (Lambrakos et al 1987)

Considering figure 2.6 and using the Prantl's mixing length hypotheses (using eddy viscosity to describe momentum transfer by turbulence Reynolds stresses), far wake velocity (represented as w which is same as U_w) is as follows (Lambrakos et al. 1987);

$$\frac{U_w}{U} = \sqrt{\frac{C_{DS}D}{x}} \left[1 - \left(\frac{y}{b} \right)^{3/2} \right]^2 \tag{2.16}$$

C_{DS} - steady flow drag coefficient; x - distance from pipe along direction of motion; b - wake width; y - distance from x in a direction transverse to the motion.

The average far-wake velocity over the pipe diameter approximates to the wake velocity variation behind the pipe. The wake velocity (U_W) is thus expressed as follows;

$$U_W = U \sqrt{\frac{C_{DS}D}{x}} = kU \text{ for } x > \frac{C_{DS}D}{k^2} \tag{2.17}$$

k is assumed constant with a value less than or equal to 1.

The wake and start-up effect though empirically determined, preserve and reflect theoretical considerations to the extent possible. In developing the Wake I Model, the following assumptions (Lambrakos et al. 1987):

1) The effect of the boundary layer on forces can be represented by the plane of symmetry containing the line of contact between two free pipes whose lines of centre are in a plane normal to the flow (that is, representing the vortex fields and boundary layer effects). To model a pipe on a boundary, the diameter of the pipe (D) in equation (2.17) is taken to be twice the diameter of the pipe ($2D$) to approximate to the two pipes of diameter D.

2) The magnitude of the wake flow for a pipe on a boundary (represented by two free pipes in contact) is similar to the wake flow for a free pipe of twice the diameter.

3) A fixed pipe exposed to wave flow is similar to a pipe in oscillatory motion in still water (Sabag 1999).

The basic findings from the Exxon Pipeline Field Measurement Program (PFMP) and Wake I Model that are not accounted for by Morison's equation are as follows:

1) The lift force shows a large phase difference relative to the velocity.

2) The hydrodynamic forces in a given velocity half cycle is very dependent on the magnitude of the velocity in the preceding half cycle (a velocity half cycle is defined by the consecutive zero crossings).

3) The drag and lift force coefficients from Morison's equation for oscillatory flow are larger than expected; PFMP data range from 0.6 to 1.0 as opposed to 1.0 to 3.0 range for Morison's equation.

4) The mean horizontal forces are very small and practically independent of the presence of current for current to wave velocity ratios less than 0.5 (Sabag 1999).

2.9.2 Wake II Model

The Wake II Model is an improvement of the Wake I Model. The Wake II Model is based upon a closed form correction by solving the linearized Navier-Stokes equation for oscillatory flow. The eddy vorticity in the wake is assumed to be only time-dependent and of a harmonic sinusoidal form (Sabag 1999).

The derivation of the force model expression for the drag, lift, and inertial forces for pipelines is the same as the force model for a cylinder as expressed in equations (2.12), (2.13), and (2.14), except the drag and lift coefficients are based on the start-up effects (Soedigbo, Lambrakos and Edge 1998).

The Wake II Model differs from the Wake 1 Model in that it assumes only a time dependent eddy vorticity in the wake, and the eddy vorticity is of a harmonic sinusoidal form. Thus results in a wake correction with a better analytical basis. The wake correction is described in the following section (2.2.2.1) (Soedigbo, Lambrakos and Edge 1998).

2.9.2.1 The Wake Flow Effect

The Navier-Stokes equations for non-steady state boundary layer are used to solve the wake flow effect for a cylinder in periodic flow. The simplified Navier-Stokes equation for the outer flow of the boundary layer (free stream) is expressed as follows (Soedigbo, Lambrakos and Edge 1998):

$$\frac{\partial U}{\partial t} + U\frac{\partial U}{\partial x} = -\frac{1}{\rho}\frac{\partial p}{\partial x} \qquad (2.18)$$

p - internal pressure; x - distance measured in the flow direction.

The Navier-Stokes equations can also be simplified to what is known as Prandtl's boundary layer equations for wake expressed as:

$$\left(\frac{\partial u}{\partial t}+u\frac{\partial u}{\partial x}+v\frac{\partial u}{\partial y}\right)=-\frac{1}{\rho}\frac{\partial p}{\partial x}+\upsilon\left(\frac{\partial^2 u}{\partial y^2}\right)$$

(2.19)

u - horizontal wake velocity; v - vertical wake velocity; υ - kinematic viscosity

The solution to the wake flow effect is derived by following Lin's method for boundary layer solution as applied by Schlichting (1979) for flows of the form;

$$U(t)=U_0+U_1(t)$$

(2.20)

Where:

$U(t)$ - total ambient velocity

U_0 - steady velocity

$U_1(t)=U_m\sin(\omega t)$ - oscillatory velocity

U_m - peak velocity

The wake velocity correction to the free stream velocity in Morison's equation is thus expressed as follows:

$$u_w=\int U_m C_1\sin^n(\omega t+\phi)e^{\left(-\frac{y^2 C_2^2 \sin^{2n}(\omega t+\phi)}{D}\right)}dy$$

(2.21)

$$U_W=\frac{\sqrt{\pi}\,erf\left(\frac{1}{2}C_2\sin^n(\omega t+\phi)\right)U_m C_1}{C_2}$$

(2.22)

Where

u_w - wake velocity correction with respect to pipe

U_W - wake velocity correction affecting pipe in periodic flow

C_1 and C_2 are constants that determine the rise and decay of the wake velocity correction

ϕ - phase angle

n - exponent which determines the sharpness of the wake velocity correction.

The value of the parameters C_1, C_2, ϕ and n were estimated on the basis of predicted Wake II Force Model for KC numbers 10, 20, 30, 40, 50, 60 and 70. C_1 was found to be 0.50, $C_2 = 0.95$ and $n = 3$ for all values of KC. The value of ϕ varied for different KC numbers; decreasing exponentially from $170°$ (at $KC = 10$) to $150°$ (at $KC = 40$) and then increasing exponentially to $190°$ (at $KC = 70$) (Soedigbo, Lambrakos and Edge 1998). This shows that ϕ is the only parameter affected by KC number (C_1, C_2 and n are all independent of KC number).

Overall the Wake II Model showed an improvement of a 40%-50% increase in the magnitude of lift force predicted over the conventional Morison's equation. The prediction of the model was in line with measured forces. The Wake II Model for pipeline stability design is best suited for regular wave conditions (without current). Adjustments will have to be for all parameters in the model for other sea conditions, and also the boundary condition of the pipeline will have to be taken into account (Soedigbo, Lambrakos and Edge 1998).

2.10 Soil Resistance: Coulomb's Friction Theory

Soil resistance is an important part of subsea pipeline stability design. Friction which depends on the seabed soils and submerged weight of pipeline provide the equilibrium required for stability. Before the 1970's, Coulomb's friction

26

theory was applied in the estimation of the frictional force between submarine pipeline and the seabed under the influence of ocean waves (Gao, Gu and Jeng 2002). Coulomb's friction theory is the simplest method used to estimate lateral resistance of subsea pipelines on the seabed. This theory assumes a constant friction between the subsea pipeline and the seabed, and does not consider any loading history or passive resistance due to pipeline embedment. Coulomb's friction theory is applicable in both static and dynamic analysis, and usually offers a conservative estimate of the lateral resistance. This theory offers an easy solution to model lateral resistance, and is perfectly adequate for subsea pipelines lying on hard rocky seabed, stiff clay or cemented sand. Coulomb's friction theory however underestimates the soil lateral resistance if passive resistance is ignored, and does not model accurately the pipe-soil-interaction in most geotechnical conditions (Zietoun et al. 2008; Bai and Bai 2005).

Lyons (1973) examined the soil resistance to lateral sliding of marine pipelines experimentally and concluded that the Coulomb friction theory is unsuitable for explaining the wave-induced interaction between pipeline and soil particularly when the soil is adhesive clay because the lateral friction between pipeline and soil is a function of pipe, wave and soil properties.

In practice the expression for soil resistance is much more complex than the simple Coulomb's friction theory. This complexity is caused by embedment of pipeline, loading history effect on lateral resistance, and pipe-soil-interaction. Soil resistance should thus be determined by determining the pure Coulomb friction and passive resistance due to soil penetration of pipeline (Det Norske Veritas 2010). The governing equations are as follows;

$$F_f = \mu (W_S - F_L) \tag{2.23}$$

Where F_f, is the frictional force between the pipeline and the soil, μ is the coefficient of friction, W_s is the submerged weight of pipeline and F_L is the hydrodynamic lift force.

The submerged weight of the pipeline is given by:

$$W_S = \rho_s \frac{\pi}{4}\left(D_o{}^2 - D_i{}^2\right)Lg - \rho_w \frac{\pi}{4}D_o{}^2 Lg \qquad (2.24)$$

Where ρ_s and ρ_w are densities of steel pipe and seawater respectively, D_o is outer diameter of pipe, D_i is internal diameter of pipe, L is length of pipeline and g is acceleration due to gravity.

Traditionally, the frictional resistance must be greater than the total horizontal force (F_T) for the pipeline to be stable (Soedigdo, Lambrakos and Edge 1998). That is;

$$\frac{\mu\left(W_S - F_L\right)}{F_T} > 1 \qquad (2.25)$$

$$F_H = F_F + F_R \qquad (2.26)$$

Where F_H is total lateral soil resistance, F_F is sliding resistance and F_R is lateral soil passive resistance

2.11 Seabed Soil Properties

When a structure is installed in a marine environment, the presence of the structure will change the flow pattern in its immediate neighbourhood. The flow condition around the structure does not only affect the wave force acting on the structure, but also can induce sea floor instability. The former has been the main concern in the design of marine structures, which has been intensively studied by marine and structural engineers. However, the latter involves the

foundations of the structure, which has attracted attention from marine geotechnical engineers in recent years. In the past few decades, considerable effort has been devoted to the wave-soil-structure interaction phenomenon. The major reason for the growing interest is that many marine structures such as vertical walls, caissons, pipelines, etc. have been damaged by the wave-induced seabed response, rather than from construction deficiencies. It is common to observe that concrete armour blocks at the toes of many marine structures have been found to subside into the seabed.

Seabed instability is a widespread phenomenon in subsea environments; there is evidence of ocean floor instability in a wide variety of offshore regions, from shallow water, near-shore zones, continental slopes, and beyond to deep ocean floors. Seabed instability has been responsible for the damage and destruction of offshore structures. Recently, significant progress has been made towards the development of both analytical and numerical approaches for some simple modes of instability in the vicinity of marine structures (Dong 2003). An understanding of the seabed soil properties is thus essential for optimising subsea pipeline design.

2.11.1 Soil Classification

Soil classification is used to predict soil behaviour and define design parameters for subsea pipeline. Soil classification is based on particle size and plasticity. Generally, fine grained soil is described as a clay or silt and course grained soil is defined as sand or gravel. BS5930, ISO 14688 and ASTM D-2487 are some of the standards that define soil classification. These standards specify different boundary definition for percentage particle size. ASTM defines a fine soil as having 50% or more of the particles less than 0.075mm in size, while BS 5930

specifies 35% to be less than 0.063mm. The variation in classification boundary (based on different standards) can lead to difficulties as the same soil can be classified differently if the particle size distribution is close to the boundaries (Thusyanthan 2012).

2.11.2 Soil Behaviour

Soil behaviour can be categorised as drained or undrained depending on the rate of loading on the soil and its permeability. If the rate of loading exceeds the rate at which the pore water is able to move out of the soil, it is defined as behaving in an undrained manner. If the rate of loading is lower it behaves in a drained manner. The strength of a soil acting in an undrained manner is given as 'undrained shear strength', measured in kilopascals, and the strength of a drained soil is given in terms of friction angle. Generally, clay behaves in an undrained manner and sand behaves in a drained manner due to the permeability of each. However, it is important to note that if the rate of loading is very low a clay soil can act in a drained manner and rapid loading on a sandy soil can cause it to act in an undrained manner (Thusyanthan 2012).

2.11.3 Sediment Mobility

Increase in local fluid velocity due to the presence of pipeline on the seabed results in sediment mobility and scouring. Scouring is the process by which sediment (soil) is removed from beneath the pipeline as result of pressure difference between the upstream and downstream sides of the pipeline. This leads to the removal of soil in areas on the downstream side of the pipeline, and continues through to the upstream side forming a tunnel. The water velocity through this tunnel is accelerated causing the gap under the pipeline to grow,

eventually allowing the pipeline to sag into the gap. (Bransby et al. 2014). Sediment mobility and scouring result in pipeline embedment, and thus affect the overall pipeline stability. Figure 2.7a, b, c and d shows a representation of the different geometries that a subsea pipeline may assume from the initial time of laying (a) to (b) which is a result of motions during laying process to (c) result of scouring and (d) result of sediment build up.
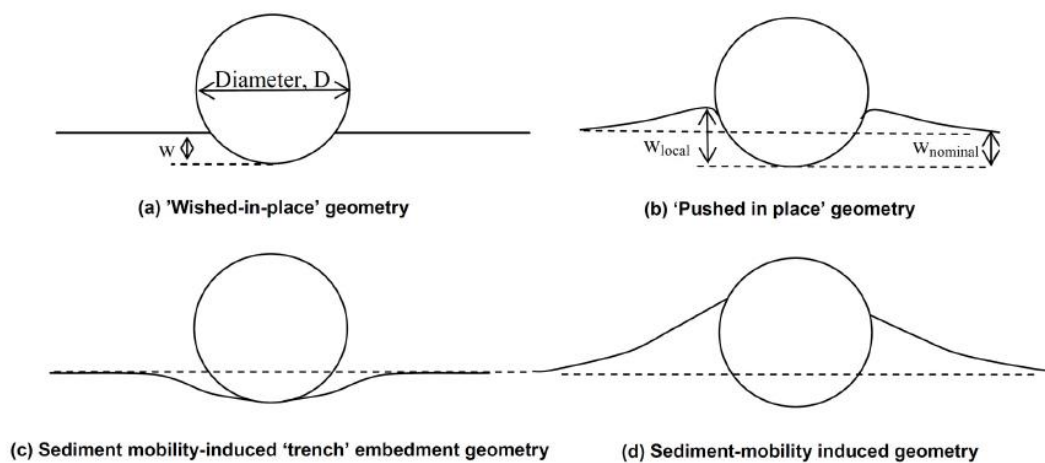
Figure 2.7 Pipeline embedment conditions (Bransby et al. 2014)

Shields' Criteria is used to determine the onset of sediment motion using equation (2.27); Sediment particles will become mobile when Shields Number (θ) is greater than the Critical Shields Number (θ_c).

$$\theta = \frac{U_c^{\,2}}{g(G_s - 1)d} \tag{2.27}$$

Where U_c is critical velocity (when sediment particles begin to move), G_s is the specific gravity of the soil and d is average sediment particle diameter.

When a subsea pipeline is laid on the seabed, there is an initial embedment into

31

the soil due to subsea environmental loads which result in scouring. Scouring underneath pipelines occurs when there is an induced seepage flow in the soil under the pipeline. This is as a result of the pressure difference between the upstream and downstream of the pipeline (Luo and Gao 2008). The pipeline profile also changes the flow pattern around the pipeline which increases the seabed shear stress and flow turbulence. Scouring underneath a pipeline affects the hydrodynamic forces acting on the pipeline and thus its stability (Sumer and Fredsoe 1999). The mechanism for the onset of scour is also known as tunnel erosion (Figure 2.8); where a considerable amount of water is directed towards the gap between the pipeline and the seabed resulting to a very high velocity in the gap and high shear stress on the seabed below the pipeline. Tunnel erosion is calmed as the gap-flow velocity decreases with increasing gap between pipeline and seabed due to scour (Sumer and Fredsoe 2002).
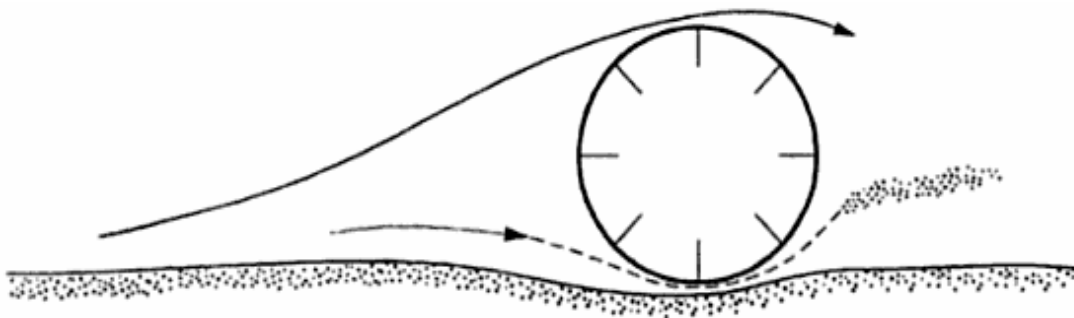
Figure 2.8 Tunnel erosion (Scour) (Sumer and Fredsoe 2002)

There is a rapid increase in scouring with increasing seabed shear stress, resulting in vortex shedding due to increase in gap between pipeline and seabed as shown in Figure 2.9.

Figure 2.9 Seabed sediment motion due to vortex (Sumer and Fredsoe 2002)

Vortex shedding results in lee-wake erosion (Figure 2.10). Lee-wake erosion occurs when sediment transport at the lee side (shielded side) of the pipeline increases great due to vortices shed from the seabed side of the pipe sweeping the seabed as they are transported downstream. The Shields number (θ) in the period of lee-wake erosion is found to be raised up to 4θ (Sumer and Fredsoe 2002).
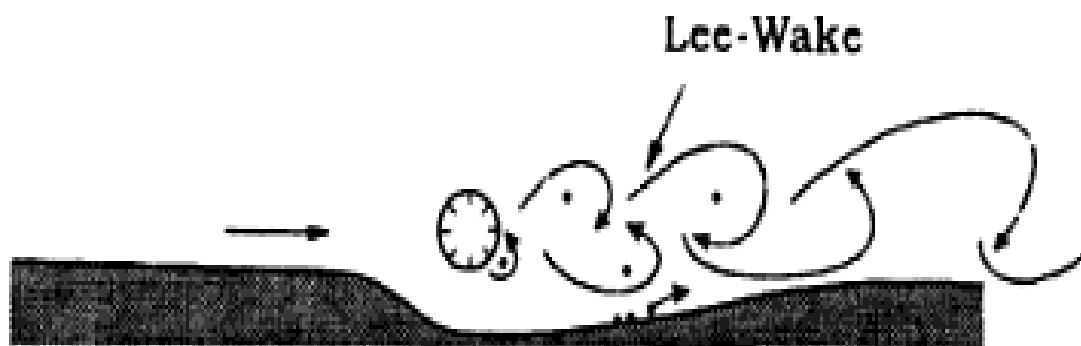
Figure 2.10 Lee-wake effect (Sumer and Fredsoe 2002)

2.11.4 Soil Liquefaction

Liquefaction is a state of the soil where there is a loss of confinement and shear strength between the individual grains of the soil, resulting in the water-soil mixture acting as a fluid. Subsea soils affected by liquefaction under wave action are fine soils (fine sand and silt) and composite soils (silty sand and clayey sand). Wave induced liquefaction can be categorised based on wave mechanism into residual liquefaction (build-up of pore-water pressure) and momentary liquefaction (upward-directed vertical pressure in the soil during passage of wave trough) (Sumer 2014).

2.11.4.1 Residual Liquefaction

A loose soil is susceptible to liquefaction under wave action due to pore-water pressure build-up, this is referred to as residual liquefaction. In this form of liquefaction, the hydrodynamic pressure on the seabed undergo periodic variation due to increased bed pressure under the wave crest and opposite effect under the wave trough as illustrated in Figure 2.11. This results in cyclic shear stresses and deformation of the soil as it compresses under wave crest and expands under wave trough. As pore-water pressure builds up, it may exceed the value of overburden pressure with soil particles becoming unbounded and free resulting in soil liquefaction, that is soil beginning to act like a liquid (Sumer 2014).
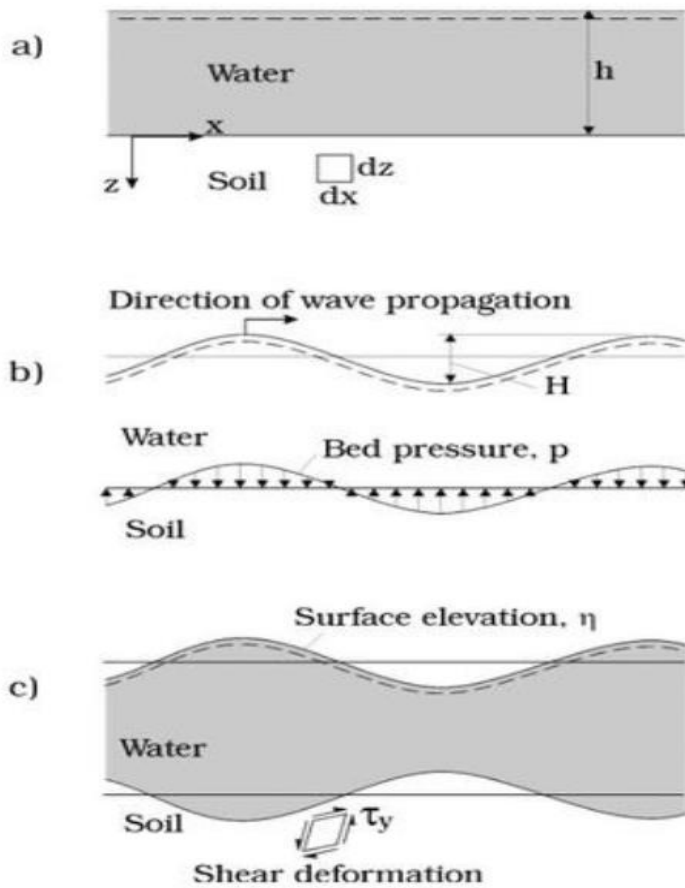
Figure 2.11 Seabed soil deformation (Sumer 2014)

The stages of residual liquefaction is as illustrated in Figure 2.12; pore pressure build-up begins at point A with the introduction of waves, resulting in an increase in pressure gradient. Point B is the onset of liquefaction as increase in pressure gradient drives the water in the liquefied soil upward with soil particles settling through the water until they begin to come in contact with each other.
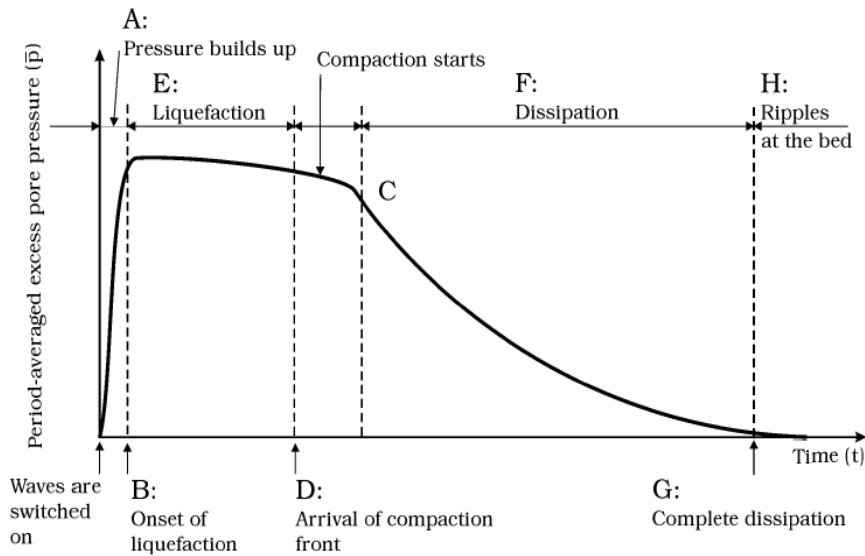
Figure 2.12 Excess pore pressure time series (Sumer 2014)

The onset of liquefaction begins at the surface of the seabed and progresses downwards. This is followed by the compaction process where pore water at the deepest layer moves out of the soil and travels upward (until all of the excess pore-water pressure is dissipated), allowing soil particles to compact and settle in a non-liquefied state (point C to G). Compaction causes the mean seabed level to shift downwards.

Kirca, Sumer, and Fredsoe (2012) carried out a series of controlled liquefaction experiments using video recordings of soil behaviour and pore pressure ($\bar{p}$) to study the onset of liquefaction. The results showed that liquefaction occurred when the pore pressure ($\bar{p}$) reached a value referred to as the critical pore pressure ($\bar{p}_{cr}$) which is equal to the initial mean normal effective shear stress (σ'_0); this formed the basis of the onset of liquefaction criterion given as;

Liquefaction occurs when $\bar{p} > \sigma'_0$ or $\dfrac{\bar{p}}{\sigma'_0} > 1$

This finding was contrary to the perception that liquefaction occurs at the time when maximum pore pressure (p_{max}) is reached. Rather liquefaction occurs when $\bar{p}$ reaches $\bar{p}_{cr} = \sigma_0'$ which is much less than p_{max} as shown in Figure 2.13 (Sumer 2014).
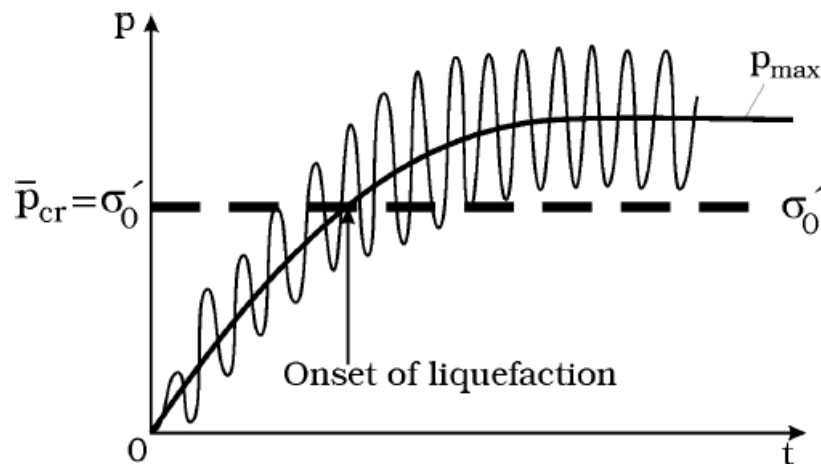
Figure 2.13 Build-up pore pressure and liquefaction (Sumer 2014)

2.11.4.2 Momentary Liquefaction

Momentary liquefaction is related to phase resolved components of the waves and occurs during the passage of wave trough. As shown in figure 2.8b, the pore pressure in the soil beneath the trough (having a negative sign) is less than the hydrostatic pressure due to the calm water height. In unsaturated soils this leads to a high pore pressure gradient at the top layer of the soil which is dissipated at a very fast rate due to soil containing some gas in the pore spaces. The high pressure gradient can generate a lift force which may exceed the submerged weight of the soil. If this happens the soil will fail and momentary period of liquefaction will occur during the passage of the wave trough (Sumer 2014; Sumer and Fredsoe 2006).

2.11.4.3 Biot Equations for Soil Shear Stresses

Wave induced shear stresses in the soil, pore pressure, and ground-water flow which are essential components of soil liquefaction are governed by Biot's equations. Figure 2.14 shows equilibrium condition for a stress field, with shear stresses denoted as τ normal forces as σ.
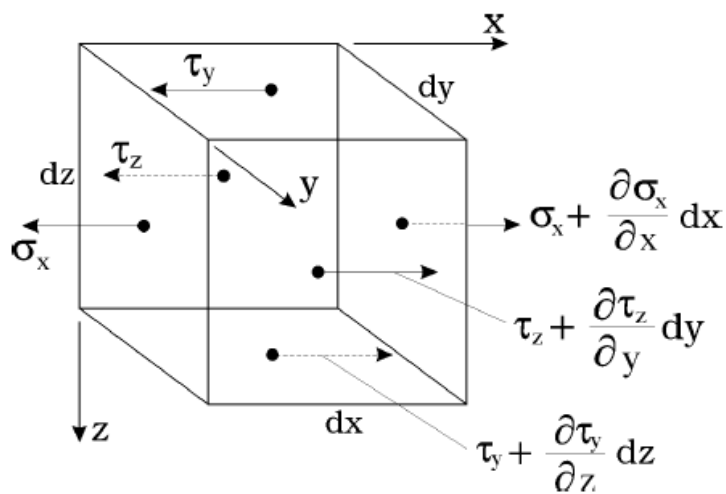
Figure 2.14 Surface stresses on a small soil element (Sumer 2014)

Sumer (2014) gives a detailed derivation of the equations, where the soil is treated as a poro-elastic material. The equilibrium conditions for a stress field, stress-strain relationships, equilibrium equations for a poro-elastic soil and Darcy's law are used along with the conservation of mass equation of pore water to obtain equation 2.28.

$$\frac{k}{\gamma_w}\nabla^2 p = \frac{\phi}{K'}\frac{\partial p}{\partial t} + \frac{\partial \varepsilon}{\partial t} \qquad (2.28)$$

Where k is the coefficient of permeability of the soil, γ_w is the specific weight of water, p is the pore-water pressure, ϕ is the porosity of the soil, K' is the apparent bulk modulus of elasticity of water, ε is the volume expansion per unit

volume of soil. ε and ∇^2 are represented by equation 2.29 and 2.30 respectively.

$$\varepsilon = \frac{\partial u}{\partial x} + \frac{\partial v}{\partial y} + \frac{\partial w}{\partial z} \qquad (2.29)$$

$$\nabla^2 = \frac{\partial^2}{\partial x^2} + \frac{\partial^2}{\partial y^2} + \frac{\partial^2}{\partial z^2} \qquad (2.30)$$

Where u, v and w are components of soil displacement in the x, y and z directions respectively.

Equation 2.16 is referred to as the storage equation and can be used along with Biot Consolidation Equations (2.31 to 2.33) to find the individual components of soil displacement and the pore pressure. This information can also be used to find the stresses in the soil.

$$G\nabla^2 u + \frac{G}{1-2\upsilon}\frac{\partial \varepsilon}{\partial x} = \frac{\partial p}{\partial x} \qquad (2.32)$$

$$G\nabla^2 v + \frac{G}{1-2\upsilon}\frac{\partial \varepsilon}{\partial y} = \frac{\partial p}{\partial y} \qquad (2.32)$$

$$G\nabla^2 w + \frac{G}{1-2\upsilon}\frac{\partial \varepsilon}{\partial z} = \frac{\partial p}{\partial z} \qquad (2.33)$$

Where G is the shear modulus and υ is Poisson's ratio.

2.12 Past and Current Stability Analysis Methods

There has been much interest and research over the past few decades to understand the dynamics of the complex interaction of fluid-pipe-soil in pipeline on-bottom stability. Current application of pipeline stability design is based on pipe-soil interaction models proposed following Joint Industry Projects such as the Pipeline Stability Design Project (PIPESTAB), American Gas Association AGA) and Danish Hydraulic Institute (DHI) project (Zeitoun et al. 2008; Gao et

al. 2006). The following sections give an overview of the various approaches to subsea pipeline stability design.

2.12.1 Pipe-Soil Interaction Stability Design Methods

The conventional approach for pipeline stability design was the static stability (static analysis) approach based on a force balance calculation (equation 2.34) in which the submerged weight required to give a large enough lateral resistance to prevent pipeline movement against the combination of submerged weight pipeline and hydrodynamic force (horizontal and lift forces) is determined (Palmer and King 2011; Knut et al. 2009; Zeitoun et al. 2008).

$$\gamma_s F_H = \mu \left(W_s - F_L \right) \tag{2.34}$$

$$F_H = F_I + F_D \tag{2.35}$$

Where γ_s is safety factor (typically taken as 1.1 (Det Norske Veritas 2000)), F_H is horizontal force, F_I is inertia force, F_D is drag force, μ is Coulomb friction factor, W_s is submerged weight of pipeline, and F_L is lift force.

This approach does not allow for horizontal pipeline movement when exposed to extreme environmental conditions. Pipeline movement is assumed as a failure criteria, which is not the case for most design conditions, and thus leads to costly stabilisation requirements (Zeitoun et al. 2008).

To improve on the conventional design method, extensive research work was carried out to further investigate the physical phenomena of pipeline on-bottom stability. The research work involved two joint industry projects (JIPs); Pipeline Stability Design (PIPESTAB) and the Pipeline Research Committee of the American Gas Association (AGA) which were run concurrently between 1983 and 1987(Knut et al. 2009; Allen et al. 1989).

2.12.1.1 PIPESTAB Project (Wolfram, Getz and Verley 1987)

The PIPESTAB project was aimed at investigating the physical phenomenon involved in predicting subsea pipeline lateral stability with a view to provide a better application for on-bottom pipeline stability analysis. The project included an experimental investigation from which analytical models were developed for predicting hydrodynamic forces and soil resistance forces acting on a pipeline on the seabed (Wolfram, Getz and Verley 1987). The project involved developing a computer program (PONDUS) to model pipeline response (predict pipeline movement and strain) under applied hydrodynamic loads. The program was validated with a structural response model and a finite element model. The results showed a high degree of accuracy and a reduction in computing time. The project was also aimed at verifying the Wake Force Model proposed by Lambrakos et al. (1987) by carrying out a large-scale test. Measured forces from the test were in agreement with predicted forces using Wake Force Model, confirming a much improved maximum force prediction of the Wake Force Model when compared to the conventional approach using Morison's equation. Another part of the project was to develop a pipe-soil interaction model to account for load history effect and its impact on soil resistance. A soil test flume was used to measure soil resistance for coarse sand, silty fine sand, soft clay and stiff clay. The results showed a higher total soil resistance when compared to the simple Coulomb friction theory. The empirical model developed included a frictional term and a passive resistance term which is dependent on soil load history but independent of pipeline weight (Wolfram, Getz, and Verley 1987).

2.12.1.2 The AGA project (Allen et al. 1989)

The AGA project had similar objectives as the PIPESTAB project, to obtain accurate assessment and verification of forces associated with pipeline stability, produced an analytical procedure and software program (Pipeline Research Council International (PRCI)) that can predict hydrodynamic forces and their effect on pipeline stability. As with the PIPESTAB project, the AGA project was carried out in various parts; a large-scale test of about 1000 tests (with varying conditions of current only, regular or irregular wave only, combination of current and either regular or irregular waves, and varying non-dimensional parameters such as KC, Re, pipe and seabed roughness, and current to wave ratio) was carried out and an analytical model (New Force Model) developed to accurately predict hydrodynamic forces. A pipe-soil interaction test was also carried out in a soil test flume and the measured data used to develop an empirical pipe-soil interaction model implemented into the PRCI software program. The AGA project showed that pipelines designed using the conventional method were more than sufficiently weighted to withstand movement. However in very hard soils with no pipe seabed penetration the new design procedure from this project showed that conventionally designed pipes may move.   The general conclusion from the AGA project is as follows;

A pipeline designed to be stable using the conventional approach,

   I.   will be stable in clay (with undrained shear strength < 80psf) and sand (with relative density < 50%) with little pipeline movement;

  II.   gives a conservative result in soft clay and loose sand;

III.   shows pipeline movement in harder clay and denser sand (Allen et al. 1989).

2.12.1.3 Summary of PIPESTAB and AGA Projects

Both PIPESTAB and AGA projects resulted in the development of special purpose dynamic finite element model programs; PRCI for AGA and PONDUS for PIPESTAB, which made allowance for pipeline movement within defined limits of lateral displacements and is thus referred to as dynamic stability approach. This dynamic stability approach provided a better understanding of pipeline response and displacement patterns, and thus resulted in much less requirement for pipeline stabilization compared to the static stability approach. The finite element programs were initially developed as three dimensional models, but due to the time requirement for simulations, a simple two dimensional model was developed in order to improve computational efficiency (Knut et al. 2009; Zeitoun et al. 2008; Allen et al. 1989).

The complexity and time requirement of the dynamic stability approach led to the development of calibrated (or empirical) methods (Simplified Method and Generalized Method) which involves calibrating the static stability method with results from the finite element simulations of the dynamic stability method. This approach is applied using simple finite element models or spreadsheets, and provides less conservative results compared to the static stability approach (Knut et al. 2009; Zeitoun et al. 2008).

The simplified method is an empirical approach, as used in AGA Level II, which applies hydrodynamic loading, spectral representation of sea state, and a more complex form of pipe-soil interaction. This approach is still considered to be conservative. The generalized method was developed by Lambrakos (Knut et al. 2009; Zeitoun et al. 2008) based on the dynamic finite element analysis using the PIPESTAB PONDUS software. It involves using a set of design response curves to determine the submerged pipeline weight requirement for

stabilization (for a specified displacement). This generalized approach forms the basis of the Generalized Stability design methodology as presented in the Det Norske Veritas (DNV) guideline RP-F109 (Zeitoun et al. 2008).

The AGA and PIPESTAB projects showed that there is a significant increase in lateral soil resistance (which is not considered in the conventional stability analysis approach) as pipeline is embedded in seabed as a result of pipeline displacement due to oscillation (Allen et al. 1989).

An important difference between the PIPESTAB and AGA pipe-soil models is based on how the soil resistance is determined; while PIPESTAB model uses volume soil displaced to determine soil resistance, the AGA model uses the work done on the soil by the pipeline to determine embedment and soil resistance. Thus the PIPESTAB model gives less embedment and soil resistance. Both models however underestimates actual soil resistance when compared to experimental tests on which they are based (Hale, Lammert and Allen 1991).

All the design methods discussed above assume a stationary and immovable seabed in the analysis of pipeline response, and so does not take into account seabed mobility and liquefaction (Palmer 1996). Seabed movement occurs in response to hydrodynamic forces (fluid soil interaction), thus pipeline movement and sediment transport occur together. In reality seabed instability and mobility occur before the design conditions for pipeline on-bottom stability are reached (Palmer and King 2011). Damgaard and Palmer (2001) proposed an approach which takes into account seabed liquefaction when assessing requirements for pipeline stabilization. This approach is based on research and observation that pipeline embedment or floatation depends on the specific gravity of the pipeline; the seabed liquefaction potential is assessed and a

design pipeline embedment is specified, which is then used to determine the required pipeline specific gravity. The challenge with this method is specifying the extent of seabed mobility and liquefaction with some degree of certainty, and also applying it to larger diameter (36"– 42") pipelines which normally have low specific gravity which reduces the likelihood of embedment (Zeitoun et al. 2008).

2.12.1.4 Energy-Based Pipe-Soil Interaction Method

Brennodden et al. (1989) describes and presents the results for the full scale pipe-soil interaction tests carried out for loose medium sand, dense sand medium sand and soft clay following a research project carried out by SINTEF (sponsored by AGA). The aim of this project was to investigate the interaction between an unburied subsea pipeline and the seabed with the pipeline exposed to hydrodynamic loading. The test parameters included pipeline diameter, pipeline weight and soil properties. The results showed that soil resistance is to a greater extent determined by pipeline embedment; in both sand and clay soil resistance increased with increasing degree of pipeline embedment. It was observed that any load condition (e.g. pipeline weight) that causes an increase in pipeline embedment, increases soil resistance. Generally, soil resistance in loose soils (that is, soils with relatively low load bearing capacity), was greater than in dense soils as a result of greater pipeline embedment in loose soil; soil resistance increased from 0.18kN/m to 0.80kN/m for a test case of pipe diameter 0.5m and submerged weight of 0.25kN/m with corresponding embedment increasing from 0.7cm to 5.5cm.

As with previous research work, a much higher lateral soil resistance than predicted by Coulomb's friction model was also observed in this project.

2.12.1.5 Det Norske Veritas (DNV) Recommended Practice

The current on-bottom stability design method is based on modelling fluid-pipe and pipe-soil interactions interdependently without fluid-soil interaction. There are three design methods currently recommended by DNV for lateral on-bottom stability design. These methods are; Dynamic Lateral Stability Analysis, Generalised Lateral Stability Analysis, and Absolute Lateral Static Stability Design (Ryan et al. 2011).

The dynamic lateral stability method determines the lateral displacement of a pipeline due to hydrodynamic loads from a given combination of waves and current during a design sea state by analysing the pipeline response to applied hydrodynamic loads and time domain simulation of soil resistance for the given design sea condition. DNV RP F109 (2010) specifies a soil resistance consisting of a Coulomb's friction component and a passive resistance (FR) due to soil embedment with pipeline lateral displacement. The soil passive resistance versus lateral displacement relationship (Figure 2.15) shows an elastic region with very little pipeline lateral displacement, a region with significant lateral displacement which increases pipeline embedment, a breakout region where there is a decrease in soil resistance and pipeline embedment, and a very high lateral region after breakout where soil passive resistance and embedment remain fairly constant. This is in agreement with the wave-pipe-soil interaction model proposed by Gao, Gu and Jeng (2003) with the characteristic times corresponding to the regions specified in DNV RP F109 (2010).
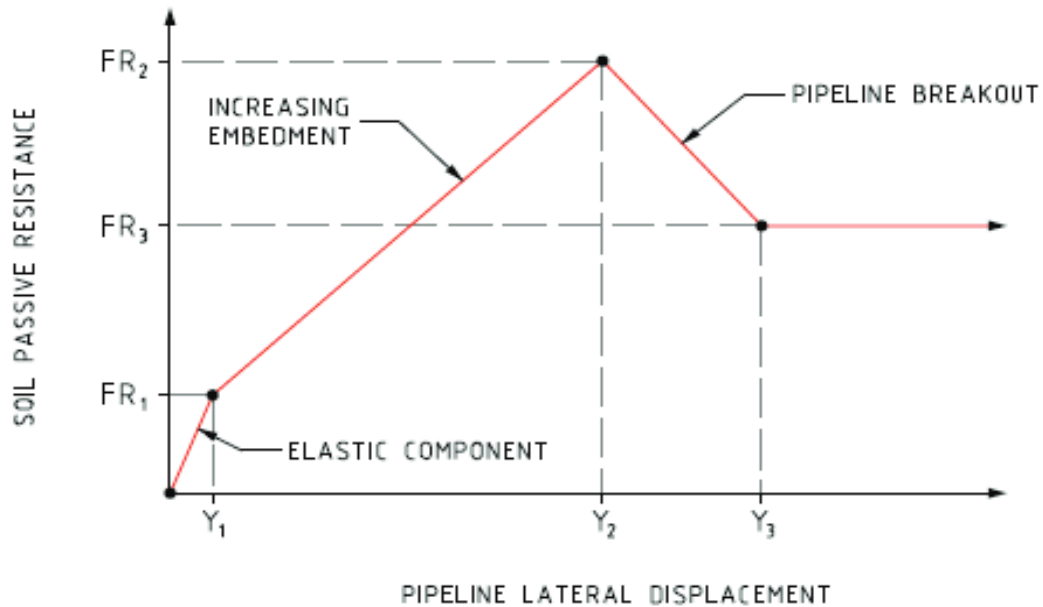
Figure 2.15 Soil passive resistance (Ryan et al 2011)

The generalised lateral stability method makes allowance for displacement of the pipeline in a design spectrum of oscillatory wave induced velocities perpendicular to the pipeline.

The absolute lateral static stability method is a simplistic approach that is based on static equilibrium of hydrodynamic forces on pipeline and soil resistance. No pipeline movement is permitted on the seabed under extreme environmental conditions.

These design methods all provide an indication of the effect of hydrodynamic loads on pipeline response. The pipeline response needs to be assessed against defined acceptance criteria and limit states (serviceability, ultimate, fatigue, and accidental) as specified in DNV offshore standard F101 (Det Norske Veritas 2013). The problem with this approach is that pipeline on-bottom stability analysis is a non-linear process especially when soil resistance and pipeline embedment is considered. Considering the non-linear process of pipeline stability together with the various limit states adds to the complexity of pipeline

response assessment. It is thus necessary to seek an alternative design approach that will allow for the assessment of the different factors (soil resistance, pipeline displacement, pipeline embedment, etc.) that influence pipeline on-bottom stability (Zeitoun et al. 2008).

2.12.2 Fluid-Pipe-Soil Interaction Stability Design Methods

Pipe-soil interaction tests carried out by both the Pipeline Stability Design Project (PIPESTAB) and American Gas Association (AGA) show that the process of pipeline instability was either displacement controlled or force controlled. Both experiments show that in the process of lateral instability, the pipe pushes the nearby soil back and forth, and sand scouring was not involved. The PIPESTAB and AGA experiments have generally showed that any loading history causing additional pipeline penetration would result in an increase of lateral resistance (Wolfram, Getz and Verley 1987). It is also noteworthy that in the pipe-soil methods discussed, wave loads were modelled with mechanical actuators rather than hydrodynamic methods. Thus, wave induced scour around the pipeline was not considered.

Some of the attempts made to improve upon the pipe-soil interaction is discussed as follows.

2.12.2.1 Wave-Pipe-Soil Interaction Model

Gao, Gu and Jeng (2003) investigated the mechanism of wave induced pipeline on-bottom stability using a U-shaped oscillatory flow tunnel in which the critical conditions for pipeline instability was investigated by varying submerged weight and diameter of pipeline, soil parameters and loading histories. The experiment showed that an increase in the oscillatory flow amplitude results in three

48

characteristic times, $t = t_s$, $t = t_r$ and $t = t_b$ during pipe losing on-bottom stability.

Onset of scour ($t = t_s$) (see figure 2.16): Sand ripples gradually form in the vicinity of the pipe as a result of increasing water particle velocity thus triggering local scouring. In the process of local scouring, the sands in front of the pipe move towards the pipe, and the sands behind the pipe are scoured away from the pipe. The sand scour zone enlarges as the flow velocity increases.
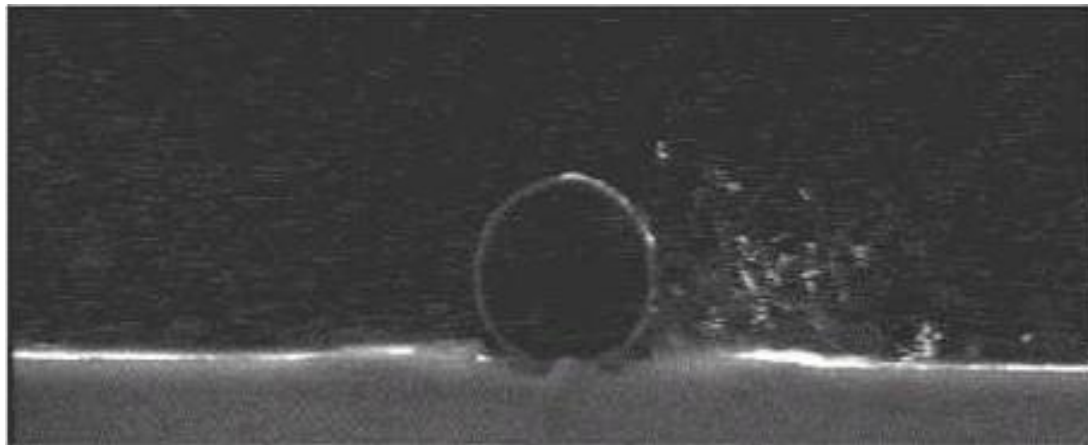
Figure 2.16 Onset of sand scour (Gao, Jeng and Wu 2006)

Pipe rocking ($t = t_r$) (see figure 2.17): At a certain flow velocity the pipe rocks slightly periodically at its original location with approximately same frequency of oscillatory flow. The pipe pushes the soil with a noticeable horizontal displacement, accompanied by pipe rolling. Local scouring is also involved in this phase and later phases.

49
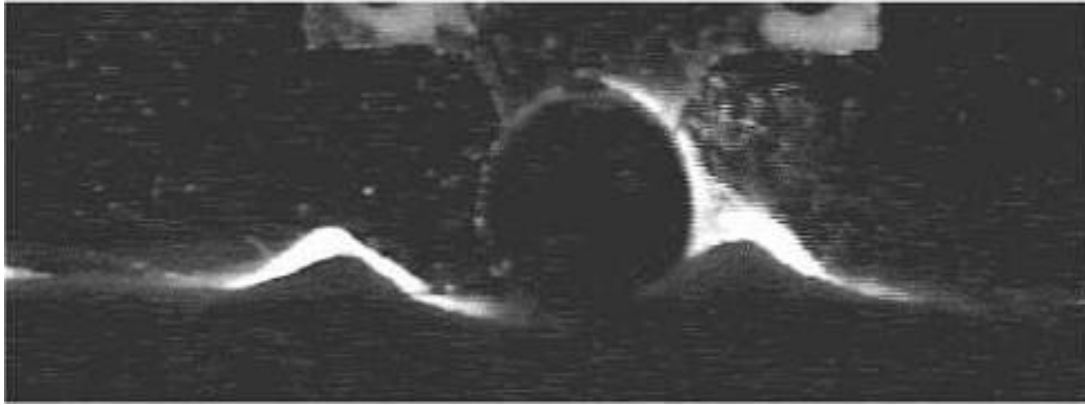
Figure 2.17 Pipeline rocks (Gao, Jeng and Wu 2006)

Pipe breakout ($t = t_b$) (see figure 2.18): As the flow velocity further increases after a period of slight pipe rocking, the pipe is displaced from its original location losing on-bottom stability. That is, the pipe breaks out suddenly from its original location with a large lateral displacement (Gao, Jeng and Wu 2006).
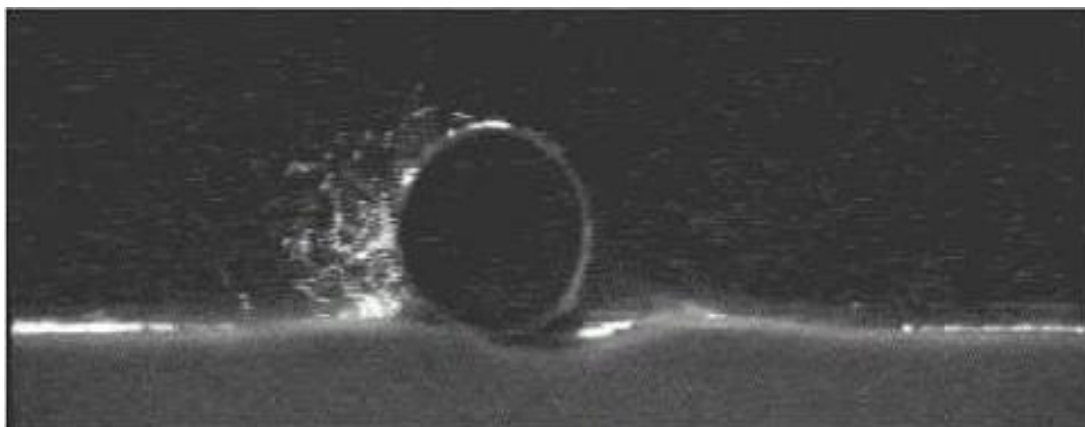
Figure 2.18 Pipeline breakout (Gao, Jeng and Wu 2006)

The experiment showed a correlation between the dimensionless pipeline weight ($G = \dfrac{W_s}{\gamma'D^2}$ where W_s is submerged weight of pipeline, γ' is buoyant weight of soil, and D is pipeline diameter) and KC number for the constraint conditions of freely laid pipeline and anti-rolling pipeline. For both constraint

conditions there is a linear relationship between G and KC as pipeline loses stability for same diameter, but different for different diameters. This shows the significance of pipeline diameter in stability analysis. Similarly, a correlation between Fr and G was also established; for the same soil type with different pipeline diameters there is a linear relationship between Fr and G, but results differ with different soil types which is an indication of the influence of soil type on pipeline stability. These relationships have been used as stability criteria for subsea pipelines (Gao, Jeng and Wu 2006; Gao, Gu and Jeng 2003).

Comparing the physical phenomena of pipe instability in the pipe-soil interaction experiment and that of wave-pipe-soil interaction shows an additional penetration of pipeline into soil bed under cyclical preloadings which increases the ultimate lateral resistance (Gao, Jeng and Wu 2006; Gao et al. 2006). The wave-pipe-soil interaction experiment showed that sand scouring occurred around pipe and sediment transport had significant influence on pipe on-bottom stability. The wave-pipe-soil interaction model thus provides a better understanding of the pipeline on-bottom stability (Gao et al. 2005).

2.12.2.2 Conceptual Fluid-Pipe-Soil Stability Design Approach

Ryan et al (2011) proposed a fluid-pipe-soil interaction approach which includes physical model testing and numerical stability analysis that will allow for the combination of fluid-soil, pipe-soil and fluid-pipe effects to be investigated. The physical model testing is intended to provide a better understanding of changes in pipeline embedment, soil strength and soil resistance with time, and the changes in hydrodynamic loading on pipeline with changes in pipeline embedment. The pipe-soil model can then be updated taking into account the

combined effect of scouring, pipe-soil interaction, and soil liquefaction on the overall pipeline response. This is intended to reduce design uncertainty by minimising over-conservatism and also reduce potential under-conservatism in the current design method.

2.12.2.3 2D Pipe-Soil-Fluid Interaction Model

Griffiths (2012) developed a pipe-soil-fluid (PSF) interaction model aimed at accurate modelling of soil scouring and liquefaction at a minimal computational cost (compared to the continuum soil Finite Element Analysis (FEA) approach). A number of seabed shear stress profiles were generated as a function of seabed and pipe geometry under various wave and current flow conditions using 2D CFD models. The PSF model based on Shield's criteria replicates the CFD results and incorporates sediment suspension and transport into a pipe-soil interaction model without requiring the solution of the Navier Stokes equations in a CFD model. The key elements of the PSF model is as follows;

1. Determine soil deformation by first calculating the swept area of soil in front of the pipe (as shown in figure 2.19) considering a $0.2D$ initial pipe embedment with a $0.5D$ and $0.05D$ horizontal (to the right) and downward displacement respectively.
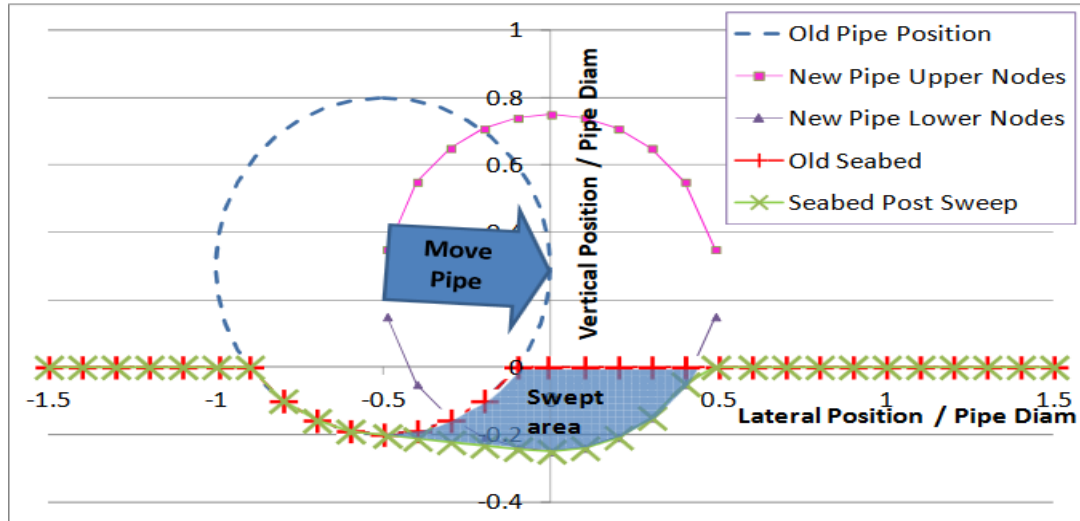
Figure 2.19 Sweep area (Griffiths 2012)

2. The second step is then to calculate the suck area (void created behind the pipe following pipe displacement) as shown in Figure 2.20. The suck area is able to draw in water and sediment to fill the void as pipe is embeded.
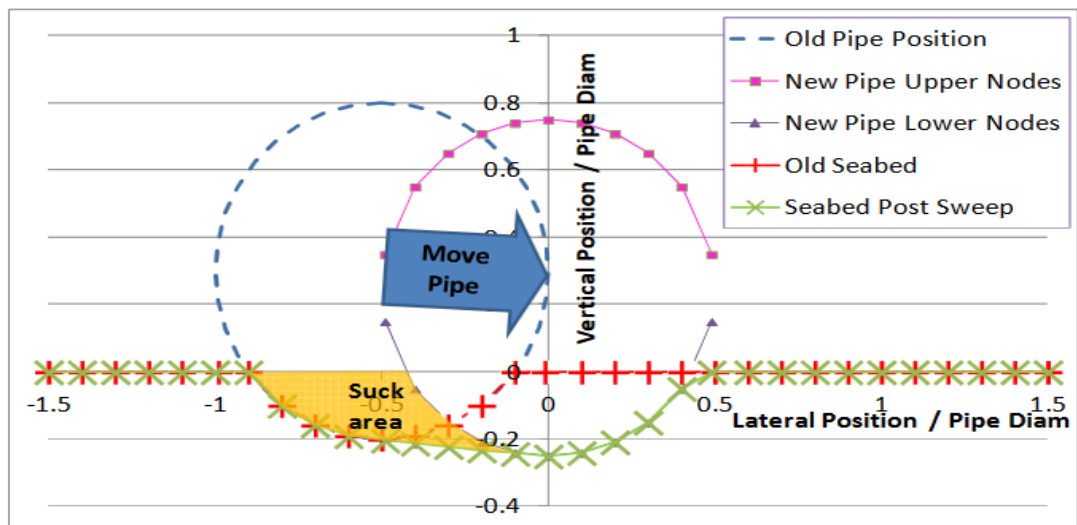
Figure 2.20 Suck area (Griffiths 2012)

3. Determine soil reaction forces using modified equations from DNV RP F109 (2010) to calculate vertical soil reaction force and Verley's theoretical model (Verley , Sortberg and Brennodden 1990) to calculate soil horizontal reaction force.

4. Determine hydrodynamic forces by generating wave velocity time and force time history taking into account force reduction factors such as embedment and pipe movement using DNV RP F109 (2010).

5. Soil-fluid interaction is then modelled by considering sediment transport and deposition and applying Shield's criteria to predict onset of sediment motion.

The PSF model results when compared to results obtained from Brennodden et al (1989)'s Energy-Based Pipe-Soil Interaction model show a similar general behaviour. The limitation with this model is in describing the fluid domain accurately considering turbulence and fluid-soil interaction and its resultant pipeline embedment since CFD is not used. Another limitation is that the PSF fluid-soil interaction algorithm does not account for soil liquefaction. The PSF model is undergoing further refinement, verification and validation with a view to improve current pipeline stability design methodology which makes for costly stabilisation techniques.

This project thus seeks to improve the current methodology for subsea pipeline on-bottom stability design by providing a better understanding of fluid-pipe-soil interaction using CFD modelling to incorporate the effect of seabed scouring and liquefaction which are not presently correctly accounted for. The use of CFD capability to accurately model fluid flow and sediment transport around subsea pipelines have been proven; for example, Zhao et al. (2007) applied a Computational Fluid Dynamics (CFD) model to investigate the flow dynamics around a piggyback pipeline and found that the relative position of the smaller pipe has significant effects on the vortex shedding characteristic and the subsequent hydrodynamic loads on the pipeline. Kamarudin (2005) has shown

using a CFD modelling technique that the current practice of using an equivalent

diameter approach for piggyback pipelines underestimates the drag coefficient.

CHAPTER 3: METHODOLOGY

Computational Fluid Dynamics (CFD) is an advanced computer based modelling tool for solving fluid dynamics (fluid flow, heat transfer and associated phenomena) problems (Contantinides, Oakley and Holmes 2005). Experimental works are expensive to perform and time consuming, sometimes there are risks and environmental issues involved in designing test facilities, and thus computer modelling technique is a very efficient and useful tool to carry out stability analysis of submarine pipelines. With the progress in the development of computational technology, CFD is becoming the most available and useful tool for simulating a wide range of flow, mass, momentum and energy problems. The use of CFD presents the opportunity to simulate different flow conditions and environment faster and without the difficulty and expenses required for experiments (Versteeg and Malalsekera 2007). This will benefit the industry in the understanding of the behaviour of subsea pipelines under various conditions.

CFD codes are based on numerical algorithms that can solve fluid flow related problems. The codes comprises of a pre-processor, solver, and post-processor (figure 3.1).
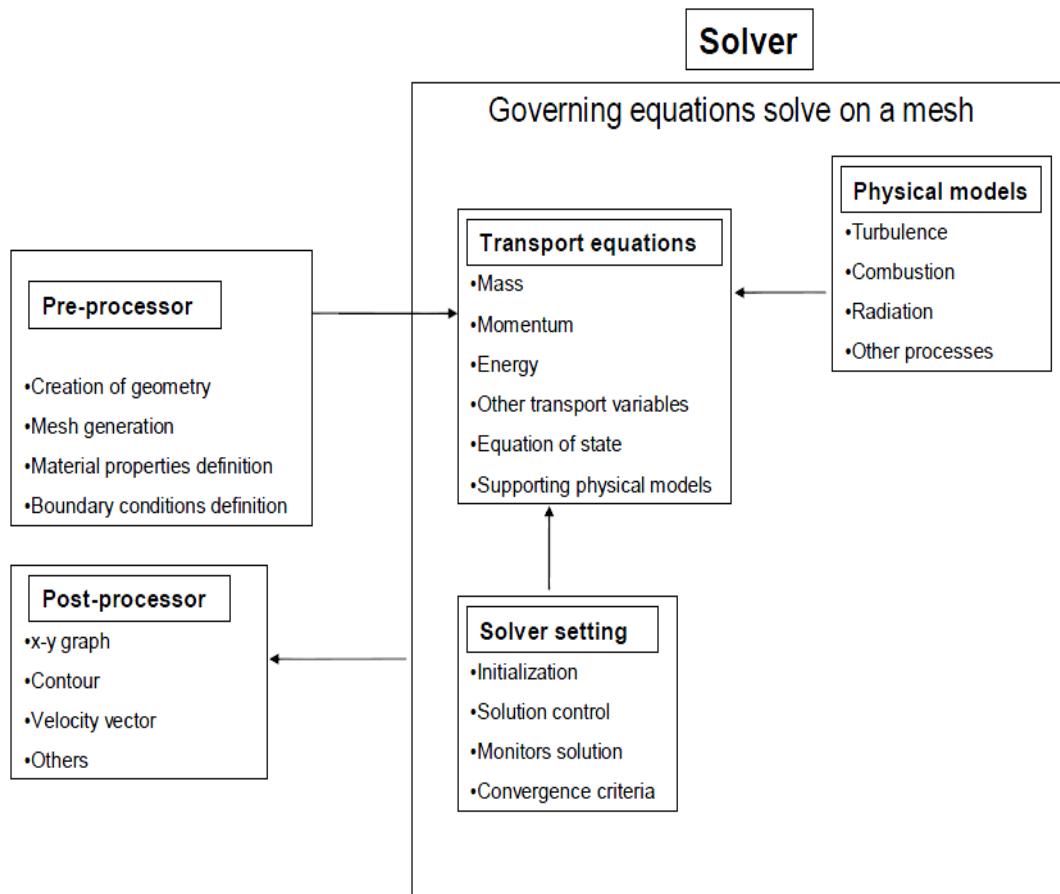
Figure 3.1 Interconnectivity of the main elements of CFD codes (Tu, Yeoh and Liu 2013)

Versteeg and Malalsekera (2007) describe these three elements as follows;

Pre-processor - This is the input element of the code where key parameters are defined. Parameters defined include geometry and computational domain, fluid properties, boundary conditions, and mesh (grid) generation.

Solver - This integrates governing equations of fluid flow (such as continuity Navier Stokes equations) over the computational domain, converting the resulting integral equations into algebraic equations and generating a solution by an iterative method (figure 3.2).
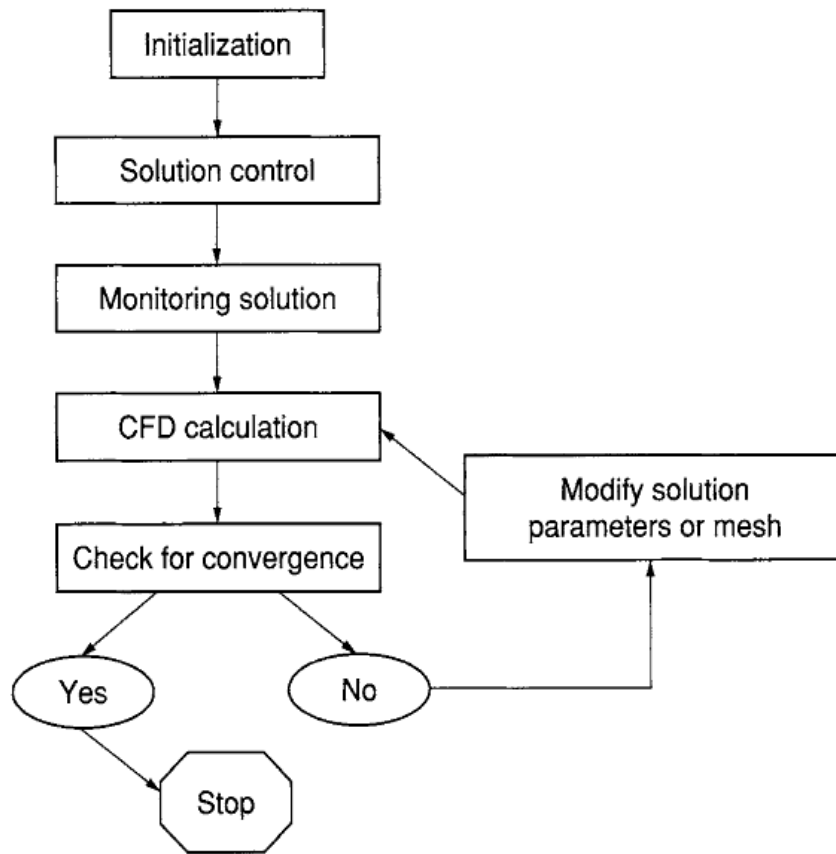
Figure 3.2 Solver process (Tu, Yeoh and Liu 2013)

Post-processor – This is the graphics output element of the code providing data visualisation in the form of geometry and grid display, vector and surface (two-dimensional and three-dimensional) plots, contour plots etc.

This research work is focussed on developing a fluid-pipe-soil model by combining the effect of fluid-pipe, fluid-soil and pipe-soil interaction and using computational fluid dynamics code to solve the model.

This chapter provides an explanation of the governing equations and supplementary equations used in developing the model.

3.1 Governing Equations

CFD modelling for fluid flow is governed by equations of the laws of conservation of physics; continuity equation (equation 3.1) which accounts for mass conservation, momentum equation (equation 3.2 and equation 3.3) which accounts for the force balance between rate of change of momentum and the sum of forces on a fluid particle.

$$\frac{\partial \rho}{\partial t} + \nabla \cdot (\rho v) = 0 \tag{3.1}$$

$$\frac{\partial u}{\partial t} + u\frac{\partial u}{\partial x} + v\frac{\partial u}{\partial y} = -\frac{1}{\rho}\frac{\partial p}{\partial x} + v\frac{\partial^2 u}{\partial x^2} + v\frac{\partial^2 u}{\partial y^2} \tag{3.2}$$

$$\frac{\partial v}{\partial t} + u\frac{\partial v}{\partial x} + v\frac{\partial v}{\partial y} = -\frac{1}{\rho}\frac{\partial p}{\partial y} + v\frac{\partial^2 v}{\partial x^2} + v\frac{\partial^2 v}{\partial y^2} \tag{3.3}$$

$$\frac{\partial T}{\partial t} + u\frac{\partial T}{\partial x} + v\frac{\partial T}{\partial y} = \frac{k}{\rho C_P}\frac{\partial^2 T}{\partial x^2} + \frac{k}{\rho C_P}\frac{\partial^2 T}{\partial y^2} \tag{3.4}$$

Where ρ is the fluid density, u and v are velocity vectors, p is the pressure, ∇ is the vector gradient, T is the temperature, C_P is specific heat capacity and k is thermal conductivity (Tu, Yeoh and Liu 2013).

Many attempts have been made to solve separated flow around marine structures numerically, Navier-Stokes equations (equation 3.5) govern the motion of a fluid around a body (Sumer and Fredsoe 2006).

$$\rho\left(\frac{\partial u}{\partial t} + u.\nabla u\right) = -\nabla p + \mu \nabla^2 u \tag{3.5}$$

Navier-Stokes equations (equation 3.5) representing the conservation of momentum are solved together with the continuity equation (equation 3.6) which represents conservation of mass.

$$\nabla.u = 0 \tag{3.6}$$

Where p is the pressure, ∇^2 is the Laplacian operator and μ is the fluid viscosity.

The Navier-Stokes equations (equation 3.5) and the continuity equation (equation 3.6) for a two dimensional flow in a Cartesian coordinate system are presented as follows;

$$\frac{\partial u}{\partial t} + u\frac{\partial u}{\partial x} + v\frac{\partial u}{\partial y} + \frac{\partial(p/\rho)}{\partial x} = v\left(\frac{\partial^2 u}{\partial x^2} + \frac{\partial^2 u}{\partial y^2}\right) \tag{3.7}$$

$$\frac{\partial v}{\partial t} + u\frac{\partial v}{\partial x} + v\frac{\partial v}{\partial y} + \frac{\partial(p/\rho)}{\partial y} = v\left(\frac{\partial^2 v}{\partial x^2} + \frac{\partial^2 v}{\partial y^2}\right) \tag{3.8}$$

$$\frac{\partial u}{\partial x} + \frac{\partial v}{\partial y} = 0 \tag{3.9}$$

Where u and v are the components of the velocity along the x and y directions respectively.

It is more convenient to write the Navier-Stokes equations in terms of the stream function, ψ and the vorticity function, ω defined by:

$$u = \frac{\partial \psi}{\partial y} \tag{3.10}$$

$$v = -\frac{\partial \psi}{\partial x} \tag{3.11}$$

$$\omega = \frac{\partial v}{\partial x} - \frac{\partial u}{\partial y} \tag{3.12}$$

The continuity equation (equation 3.9) is satisfied by equation 3.10 and equation 3.11. Eliminating the pressure from equation 3.7 and equation 3.8, and making use of equation 3.10, equation 3.11 and equation 3.12, the following equation is obtained:

$$\frac{\partial \omega}{\partial t} + u\frac{\partial \omega}{\partial x} + v\frac{\partial \omega}{\partial y} = v\left(\frac{\partial^2 \omega}{\partial x^2} + \frac{\partial^2 \omega}{\partial y^2}\right) \tag{3.13}$$

This equation is known as the vorticity-transport equation (Sumer and Fredsoe 2006).

3.1.1 Reynolds-averaged Navier-Stokes (RANS) equations

RANS equations solve the unsteady Navier-Stokes equations by introducing averaged and fluctuating components. For incompressible flow with no change in viscosity, the RANS equation are supplemented with turbulence model. The RANS models offer a cost effective approach for computing turbulent flows. In this thesis, the two-equation standard $k-\varepsilon$ turbulence model has been used

with the following key equations (equation 3.14 and equation 3.15). The choice of standard $k-\varepsilon$ model was based on its accuracy for turbulent flow and good convergence, and is widely used for turbulence modelling in industrial applications.

Turbulence kinetic energy k :

$$\frac{\partial}{\partial t}(\rho k)+\frac{\partial}{\partial x_i}(\rho k u_i)=\frac{\partial}{\partial x_j}\left[\left(\mu+\frac{\mu_t}{\sigma_k}\right)\frac{\partial k}{\partial x_j}\right]+G_k-\rho\varepsilon \tag{3.14}$$

Energy dissipation rate, ε:

$$\frac{\partial}{\partial t}(\rho\varepsilon)+\frac{\partial}{\partial x_i}(\rho\varepsilon u_i)=\frac{\partial}{\partial x_j}\left[\left(\mu+\frac{\mu_t}{\sigma_\varepsilon}\right)\frac{\partial\varepsilon}{\partial x_j}\right]+C_{1\varepsilon}\frac{\varepsilon}{k}G_k-C_{2\varepsilon}\rho\frac{\varepsilon^2}{k} \tag{3.15}$$

G_k represents the generation of turbulence kinetic energy due to the mean velocity gradients, $C_{1\varepsilon}$ (1.44) and $C_{2\varepsilon}$ (1.92) are constants, σ_k (1) and σ_ε (1.3) are the turbulent Prandtl numbers for k and ε respectively (Ansys Fluent 2015).

3.2 Calculation of soil resistance

Passive resistance (F_R) on sand and clay is determined as shown in equation 3.16, equation 3.17, and equation 3.18 as follows (Det Norske Veritas 2010);

$$\frac{F_R}{w_s-F_L}=\left(5k_s-0.15k_s^{\,2}\right)\left(\frac{z_p}{D}\right)^{1.25}\text{ for }k_s\leq26.7 \tag{3.16}$$

$$\frac{F_R}{w_s-F_L}=k_s\left(\frac{z_p}{D}\right)^{1.25}\text{ for }k_s>26.7 \tag{3.17}$$

$$\frac{F_R}{w_s-F_L}=\frac{4.1k_c}{G_C^{\,0.39}}\left(\frac{z_p}{D}\right)^{1.31} \tag{3.18}$$

Where

$$z_p = z_{pi} + z_{pm} \qquad k_s = \frac{\gamma_s' D^2}{w_s - F_L} \qquad k_c = \frac{s_u D}{w_s - F_L} \qquad G_c = \frac{s_u}{D\gamma_s}$$

D - pipeline diameter,

z_{pi} - initial embedment

z_{pm} - embedment due to movement

γ_s' - buoyant weight of soil

γ_s - dry weight of soil

w_s - submerged weight of pipeline

F_L - lift force

s_u - undrained shear strength

When pipeline is laid on the seabed, the initial embedment (z_{pi}) which is due to its own weight is determined by equation 3.19 for sand and equation 3.20 for clay (Det Norske Veritas 2010).

$$\frac{z_{pi}}{D} = 0.037 k_s^{-0.67} \tag{3.19}$$

$$\frac{z_{pi}}{D} = 0.0071 \left(\frac{G_c^{0.3}}{k_c} \right)^{3.2} + 0.0062 \left(\frac{G_c^{0.3}}{k_c} \right)^{0.7} \tag{3.20}$$

For initial embedment F_L is assumed to be zero.

Initial embedment is determined by using the submerged unit weight of soil (γ') which is determined from the bulk unit weight of soil (γ_{bulk}) as follows;

$$\gamma_{bulk} = \gamma_w \left(\frac{G_s + eS}{1 + e} \right) \tag{3.21}$$

Where γ_w unit weight of water is, G_s is specific gravity of soil, S is the degree

of saturation and $e = \dfrac{\phi}{1-\phi}$ is the voids ratio (where ϕ is soil porosity).

When the degree of saturation $S = 1$ indicating that the voids are filled with

water (as in dense sands), the bulk unit weight of soil (γ_{bulk}) = saturated unit

weight of soil (γ_{sat}) which is written as;

$$\gamma_{sat} = \gamma_w \left(\frac{G_s + e}{1+e} \right) \tag{3.22}$$

When the degree of saturation $S = 0$ indicating that the voids are filled with air,

the bulk unit weight of soil (γ_{bulk}) = dry unit weight of soil (γ_{dry}) which is written

as;

$$\gamma_{dry} = \gamma_w \left(\frac{G_s}{1+e} \right) \tag{3.23}$$

The submerged unit weight of soil (γ') is then determined as;

$$\gamma' = \gamma_{sat} - \gamma_w$$

Seabed was modelled as porous media to ensure flow through the soil. This was

done by inputting porosity and inertial resistance values in the seabed region.

Porosity values used are as shown in the following chapters. Inertial resistance

is the inverse of the coefficient of permeability (k) of the soil. Assuming an

average soil particle diameter (d) of 0.6mm, equation 3.24 (Yang 2010) was

used to determine the coefficient of permeability (k).

$$k = \frac{c(d^{-2})\phi^2}{(1-\phi)^2} \tag{3.24}$$

ϕ is the porosity and c is 0.003.

In this research work Computational Fluid Dynamics (CFD) software in combination of analytical formulations has been used to model hydrodynamic loadings, pipeline response, soil resistance, pipeline embedment and pipe-soil-wave interaction. ABAQUS was initially used to model pipe-soil interaction (chapter 4) as it able to simulate motion, deformation and fluid flow using continuous function. ANSYS Fluent was used to model fluid-pipe-soil interaction (chapters 5, 6, and 7) as its architecture enables efficient simulation and control, flexible mesh capabilities to solve fluid flow using unstructured meshes generated about complex generates.

Models created were used to analyse; the effect of soil types on passive and lateral resistance and the effect of hydrodynamic loads on total soil resistance; the effect of soil embedment and soil porosity on pipeline lateral stability; the degree of embedment taking into consideration combined effect of pipeline diameter and weight, unit weight of soil, and hydrodynamic forces; the scour phenomenon and its effect on pipeline embedment. Models were created in 2D to represent a finite section of pipeline to gain a better understanding of the fluid-pipe-soil interaction which can be replicated across the pipeline length. Considering the analysis to be carried out are mostly nonlinear, 2D simulation will provide faster and more accurate results allowing for design iterations and optimisation.

All models were created using dimensions from previous work carried out by Gao et al (2007) in the wave-pipe-soil interaction model (discussed in section 1.12.2.1), Brennodden et al (1989) in the energy-based pipe-soil interaction method (discussed in section 2.12.1.4), and Griffiths (2012) in the 2D

pipe-soil-fluid interaction model (discussed in section 2.12.2.3). The results

from the work were also validated by results from these models.

CHAPTER 4: MODELLING THE EFFECT OF SOIL RESISTANCE ON SUBSEA PIPELINE STABILITY

ABAQUS CFD was used to simulate pipe-soil interaction with a view to investigating the effect of soil types (sand and clay) on passive and lateral resistance and the effect of hydrodynamic loading and pipe embedment on soil resistance. A 2D pipeline model with length to diameter ratio (20) of a typical cross-section of full scale pipeline was created (Wang et al 2010). A 0.5m diameter pipe (typical pipeline diameter vary from 2in (0.05m) to 72in (1.8m)) was created with the seabed soil represented as a relatively finite space. To analyse the relationship between passive resistance and displacement and lateral resistance and displacement, the pipeline is assumed to move between a lateral displacement boundary of x=0 to x=0.5m (Figure 4.1).

The soil was modelled as elastic since pipe self-embedment and soil resistance due to soil deformation was not considered. Also as the pipe's Young's Modulus is much greater than that of the soil, the pipe was modelled as non-deformable analytical rigid. As nonlinear deformation of soil is not considered, a tetrahedral 4-node bilinear plane mesh with cell size $50mm \times 50mm$ was generated is as shown in Figure 4.2.
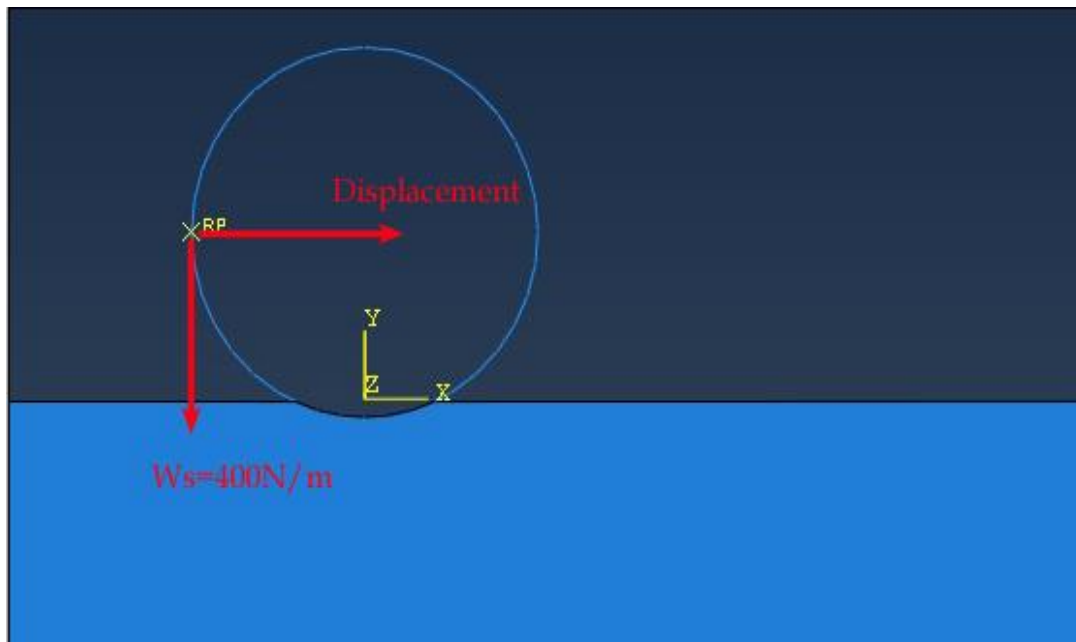
Figure 4.1 Pipeline displacement ($10m \times 5m$)
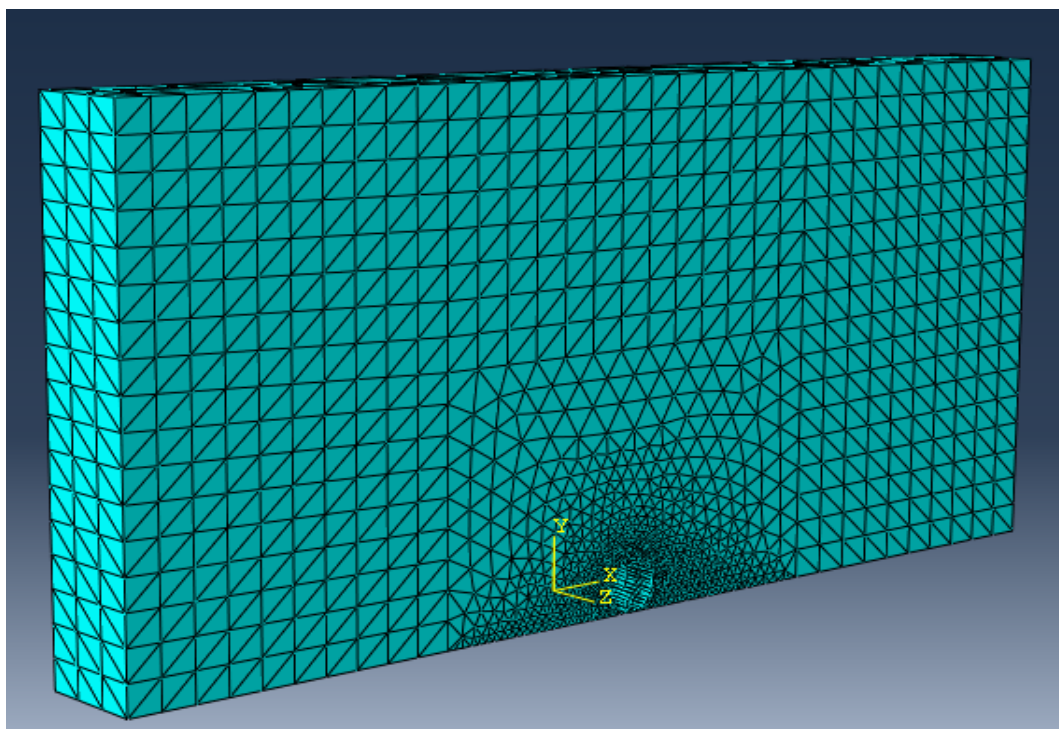
Figure 4.2 $50mm \times 50mm$ Mesh

The boundary conditions (Figure 4.3) defines a series of physical behaviour for the fluid flow process, such as pressure, temperature, and velocity. The boundary names and types, and selected parameters were set as shown in Table 4.1 and Table 4.2 respectively.

Table 4.1 Boundary conditions

Boundary Name	Boundary Type
Inlet	Velocity Inlet
Outlet	Pressure Outlet
Side wall 1	Symmetry Plane
Side wall 2	Symmetry Plane
Top wall	Symmetry Plane
Bottom wall	No-Slip Wall
Pipe wall	No-Slip Wall

Table 4.2 Selected parameters

Parameter	Value	
Density H_2O	1025 kg/m^3	
Viscosity of H_2O	0.001002 Pa-s	
Reference Gravity	0, 0, -9.81 m^2/s	
Young's Modulus	Sand	1.034 × 10^7 Pa
	Clay	6.894 × 10^5 Pa
Poisson's Ratio	Sand	0.3
	Clay	0.3
Friction Coefficient	Sand	0.6
	Clay	0.2
Inlet Velocity	0.2 - 1.6 m/s	
Pipeline weight	400 N	
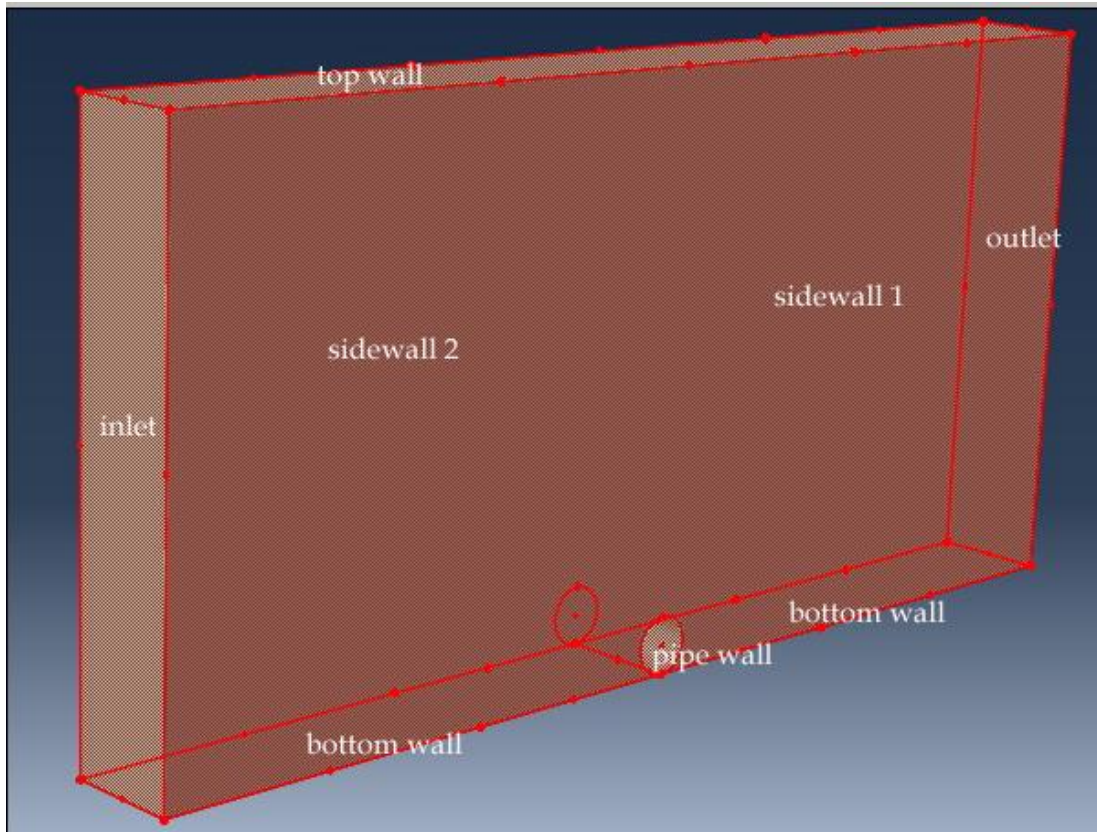
Figure 4.3 Geometry and boundaries

Simulation was carried out for various penetration depth (e) to outer diameter

(D) ratio i.e. embedment as illustrated in Figure 4.4; $\frac{e}{D}$ = 5%, 10%, 15% and

20%.
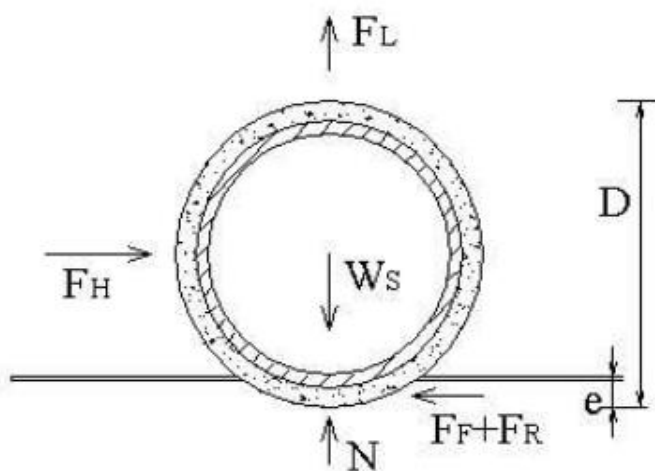
Figure 4.4 Pipe-soil interaction (Ren and Liu 2013)

4.1 Results of the Effect of Soil Types on Passive Resistance

Pipeline embedment causes deformation of the soil, resulting in the build-up of a soil ridge (berm) in front of the pipeline as it slides. The contact pressure exerted by the pipeline together with the hydrodynamic forces acting on the soil will result in a corresponding resistance from the soil. Figure 4.5 and Figure 4.6 show the graph of passive soil resistance on sand and clay respectively. Passive soil resistance increases with displacement until it reaches a maximum and then decreases slightly before becoming fairly constant with further increase in displacement. The increase in initial passive resistance is a result of increased contact pressure and linear elastic deformation of the soil, with the soil swept upwards in front of the pipe forming a berm. As pipe continues to be displaced it gradually mounts up the berm resulting in a decrease in passive resistance. When pipe completely mounts over the berm i.e. breaks out of embedment, passive resistance becomes constant.

The graphs show maximum passive resistance is reached at a displacement of 0.15m for sand and 0.1m for clay for 10%, 15% and 20% embedment, and a slightly less displacement value for 5% embedment. Graphs also show passive resistance increases with increase in embedment which explains the reason for achieving better stability in well-embedded (or trenched) pipelines. Table 4.3 shows the maximum passive resistance for various degrees of embedment in sand and clay soil. The results show that maximum passive resistance for a 20% embedment is approximately ten times that of a 5% embedment for both sand and clay, and the maximum passive resistance for sand approximately twice that of clay (see Figure 4.7).
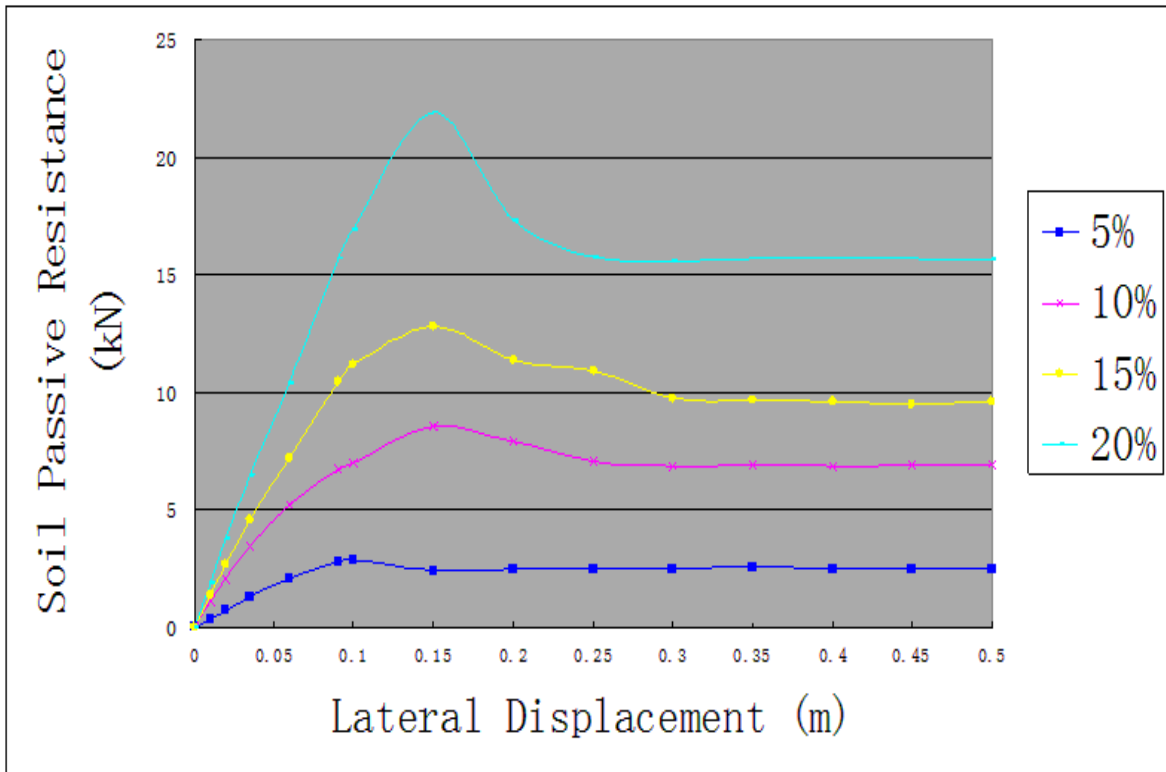
Figure 4.5 Passive resistance on sand with 5%, 10%, 15% and 20% embedment
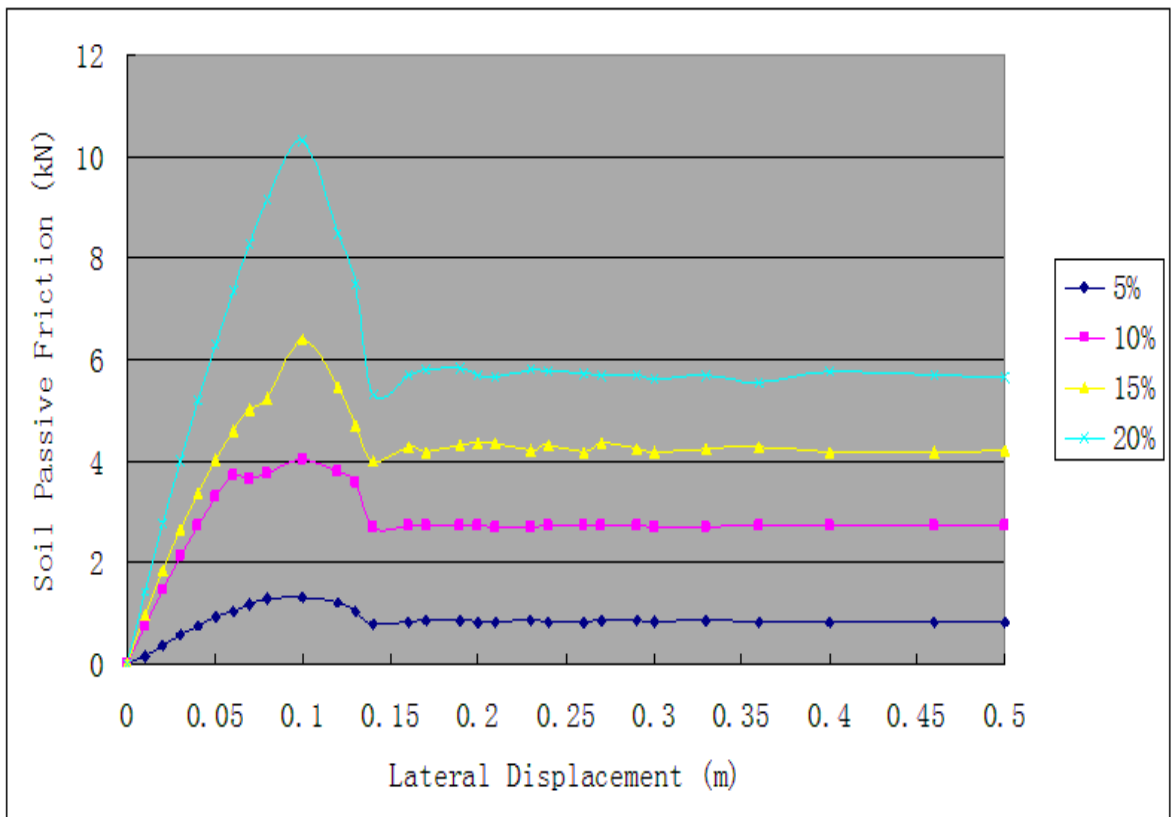
Figure 4.6 Passive resistance on clay at 5%, 10%, 15% and 20% embedment

71

Table 4.3 Maximum passive resistance on sand and clay

Embedment	Maximum Passive Soil Resistance (kN/m)	
	Sand	Clay
5%	2.87	1.32
10%	8.55	4.04
15%	12.77	6.39
20%	21.89	10.31
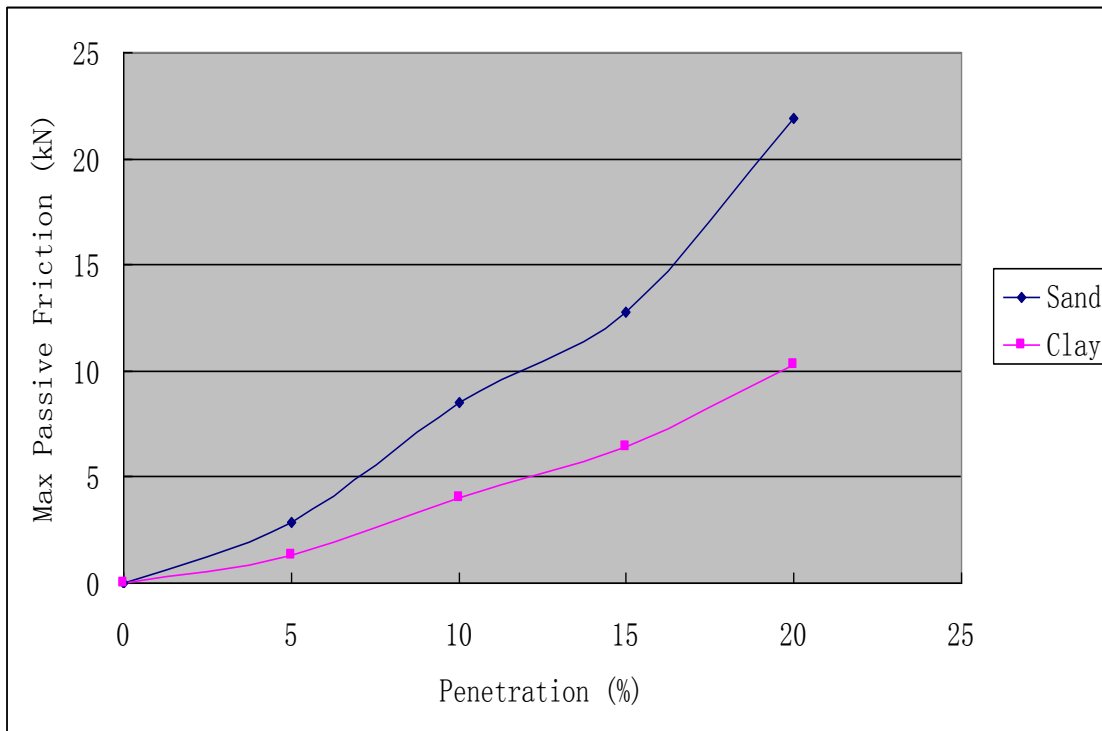
Figure 4.7 Maximum passive resistance on sand and clay

These results are in agreement with the DNV recommended practice (Det
Norske Veritas 2010) model (figure 4.8) which specifies four regions for passive
resistance; a) an elastic region with very little lateral displacement, b) a region
with significant increase in displacement and increased passive resistance as a

result of increased pipe embedment which is due to pipe soil interaction, c) a region of with decreased passive resistance and embedment signifying pipe breakout, and d) a region with very high displacement where passive resistance and embedment are fairly constant. The predicted results conform well with the experimental work (an energy-based pipe-soil interaction model) carried out by Brennoddden et al (1989) as part of research project conducted by SINTEF on behalf of AGA (see Figure 4.8 shown below).
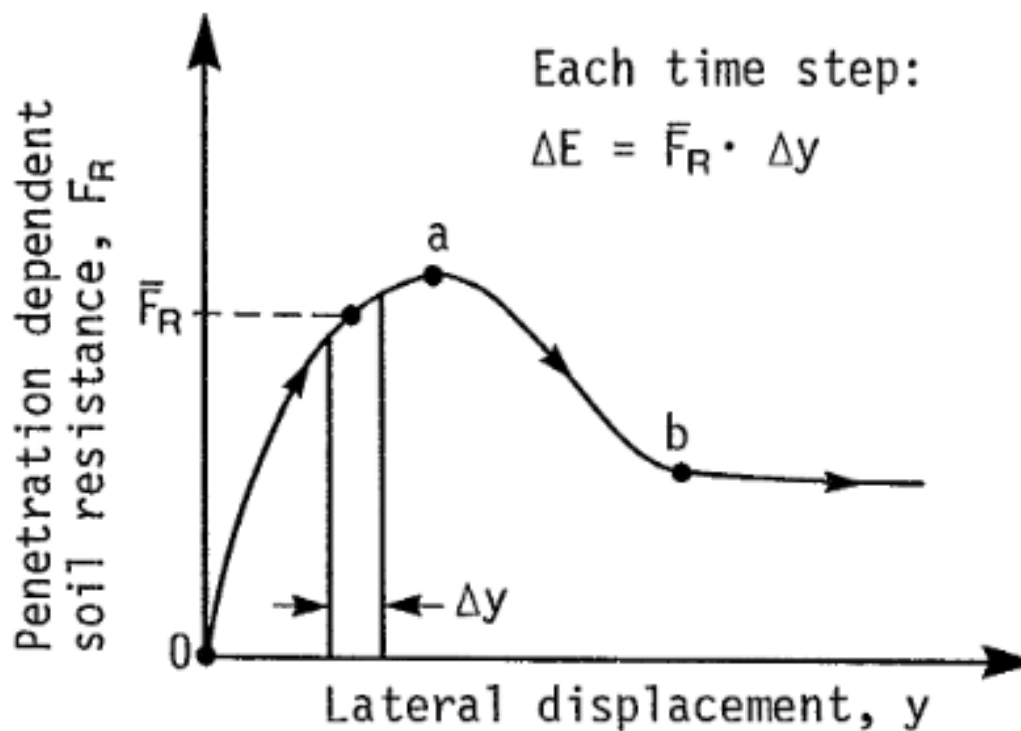
Figure 4.8 Soil resistance versus lateral displacement plot (Brennoddden et al 1989)

4.2 Results of the Effect of Soil Types on Lateral Resistance

Unlike passive soil resistance which is dependent on submerged weight of pipeline, diameter of pipeline, height of berm in front of pipeline and

hydrodynamic loading, lateral soil resistance relates to soil resistance against sliding friction only (that is the ability of soil to resist lateral forces exerted by pipeline). Figure 4.9 and Figure 4.10 show the graph of soil friction variation with displacement at various embedment for sand and clay respectively. As pipe is displaced, soil friction increases for the partially embedded pipe and maintains as a result of elastic deformation of the soil and build-up of mound. This results in an increase of lateral soil resistance. After the breakout of pipe (i.e. pipe going over berm), soil friction remains constant. The total soil friction then becomes equal to the Coulomb's friction. The graphs show that for a pipeline with $W_s = 400N$ at 0% embedment, the sliding friction on sand and clay is 240N and 80N respectively which is same as calculated using the Coulomb's friction equation $F_F = \mu W_s$.

On Sand: $F_F = \mu W_s = 0.6 \times 400N = 240N$

On Clay: $F_F = \mu W_s = 0.2 \times 400N = 80N$
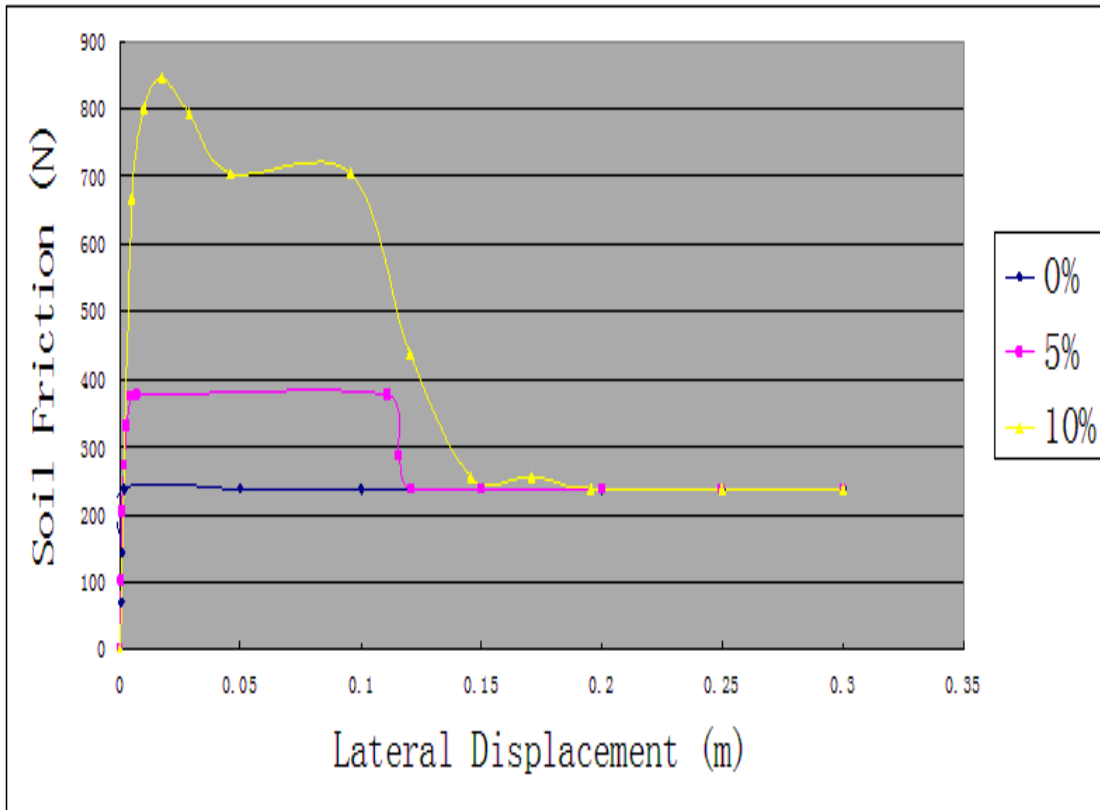
Figure 4.9 Soil friction on sand at 0%, 5% and 10% embedment
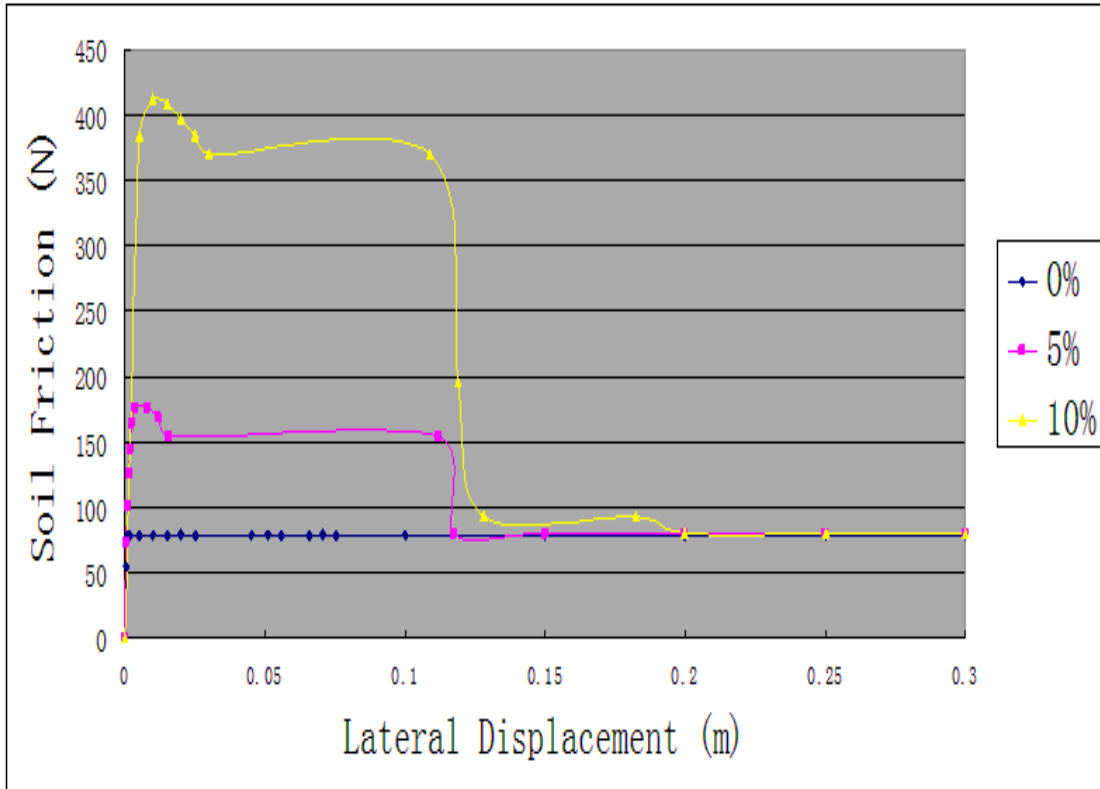
Figure 4.10 Soil friction on clay at 0%, 5% and 10% embedment

The maximum lateral resistance for sand and clay is calculated as shown in Table 4.4 and plotted as shown in Figure 4.11.

Table 4.4 Maximum lateral resistance on sand and clay

Embedment	Maximum lateral resistance (N/m)	
	Sand	Clay
0%	238	80
5%	377	175
10%	845	412
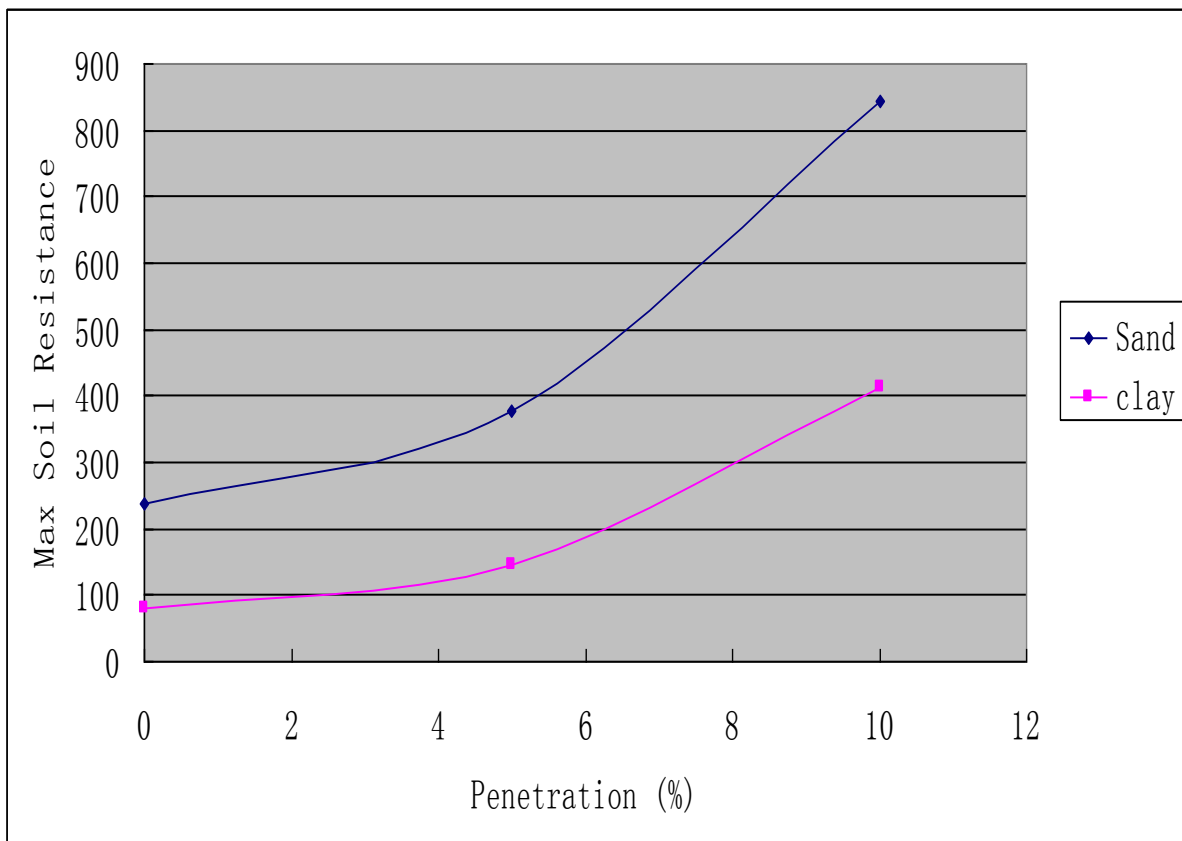
Figure 4.11 Maximum lateral resistance on sand and clay

Table 4.4 and Figure 4.11 show that maximum lateral resistance on sand is greater (approximately twice) than on clay. Clay is more easily yielded and deformed making it easier for pipeline to breakout of embedment. Thus for clay soil a greater degree of embedment is required to maintain pipeline on-bottom stability.

Overall passive resistance is by far greater than lateral resistance, thus passive resistance is of greater significance for pipeline on-bottom stability analysis.

4.3 Results of the Effect of Hydrodynamic Load and Embedment on Soil Resistance

To investigate the effect of hydrodynamic force and pipeline embedment on soil resistance, the maximum lateral resistance was determined for various pipeline submerged weight as shown in Table 4.5 and Table 4.6. Table 4.5 and Table 4.6 show that as submerged weight decreases the maximum lateral resistance also decreases but increases with increasing embedment.

Table 4.5 Effect of submerged weight on maximum lateral resistance on sand

Submerged weight (N/m)	Maximum lateral resistance on Sand (N/m)		
	0%	5%	10%
400	240	377	845
300	180	283	637
200	120	189	441
100	60	95	226
50	30	47	115

Table 4.6 Effect of submerged weight on maximum lateral resistance on clay

Submerged weight (N/m)	Maximum lateral resistance on Clay (N/m)		
	0%	5%	10%
400	80	175	412
300	60	132	312
200	40	88	209
100	20	38	106
50	10	22	54

As the submerged weight of pipeline decreases, lift force increases resulting in a corresponding decrease in lateral soil resistance due to reduced contact pressure. When the lift force becomes equal or exceeds the submerged weight of pipeline, there will be no contact pressure between soil and pipeline, thus soil resistance becomes zero. This is illustrated as shown in the plots of Figure 4.12 and Figure 4.13 for sand and clay respectively.
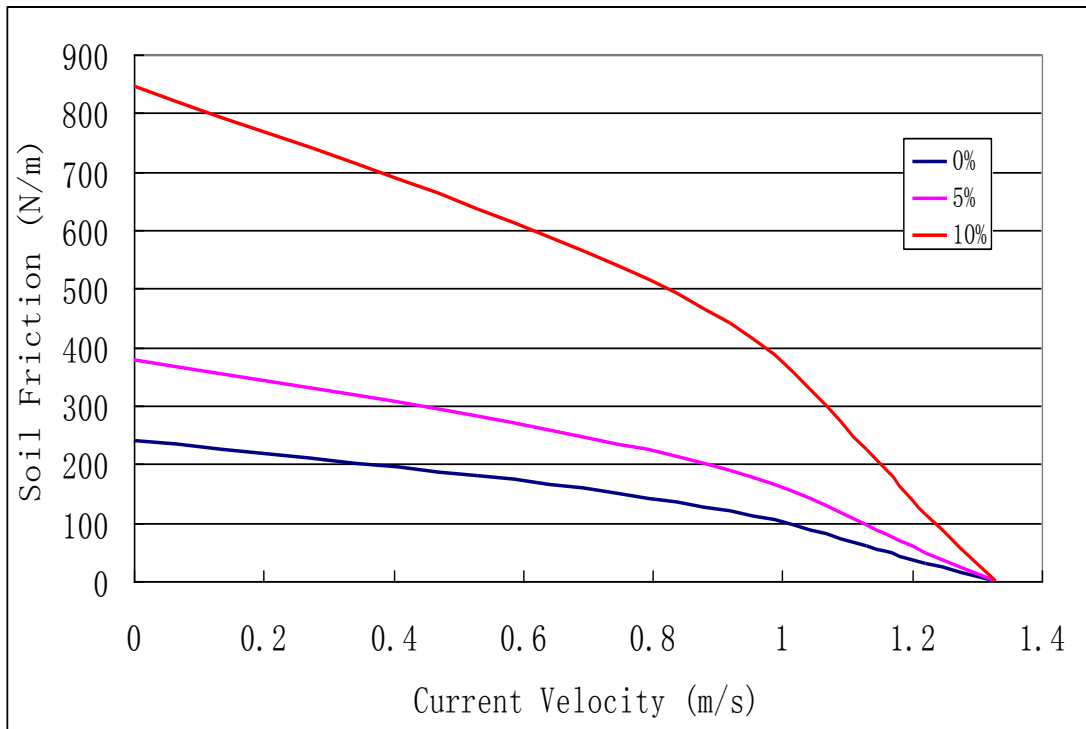
Figure 4.12 Relationship between hydrodynamic loading and soil friction on sand
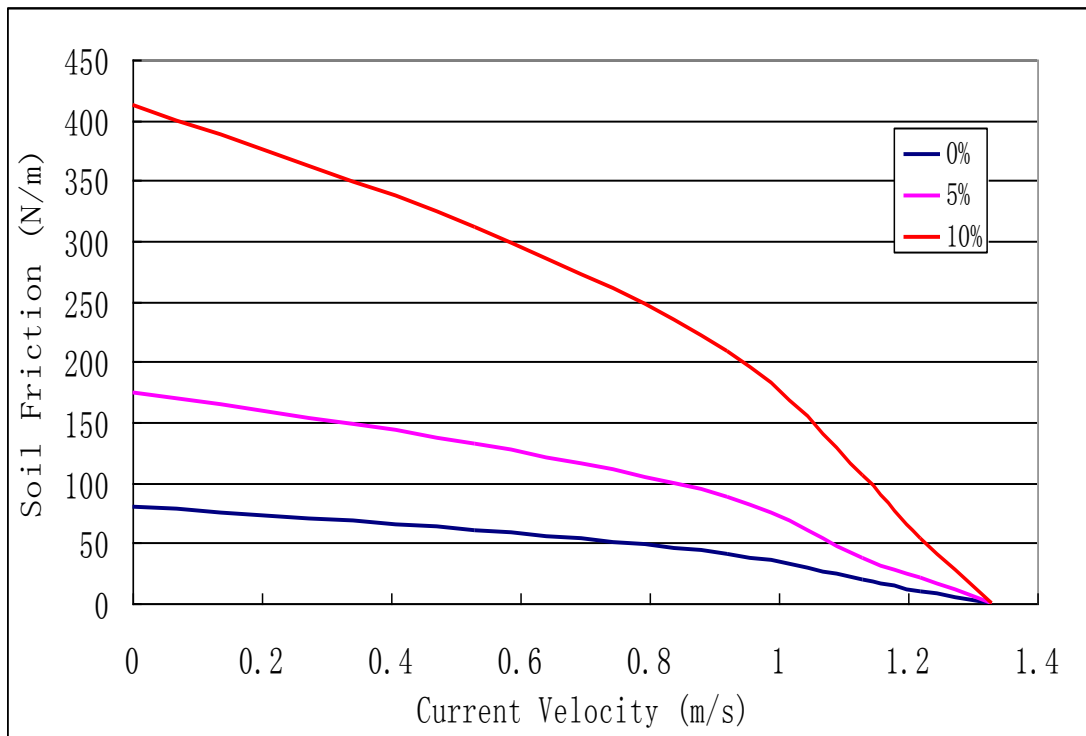
Figure 4.13 Relationship between hydrodynamic loading and soil friction on clay

4.4 Model Validation

The model developed was used to determine the horizontal force acting on the pipeline and the results compared with that calculated from Morison's equation and Wake II Model (applied in DNV code) based on Lambrakos et al (1987) and Chao, Lambrakos and Verley (1989) comparison of Wake Model predictions with measured forces from Exxon's PFMP. The results (Figure 4.14) show that the CFD model predicts a 25% increase when compared to the Wake Model, and the Morison equation values are much higher. Though the CFD and Wake II models both account for wake effect as flow goes past pipeline and velocity reverses resulting in an upstream region of low pressure (hence the closeness of predicted result), the CFD model more accurately accounts for the pipeline boundary conditions and varying sea conditions.
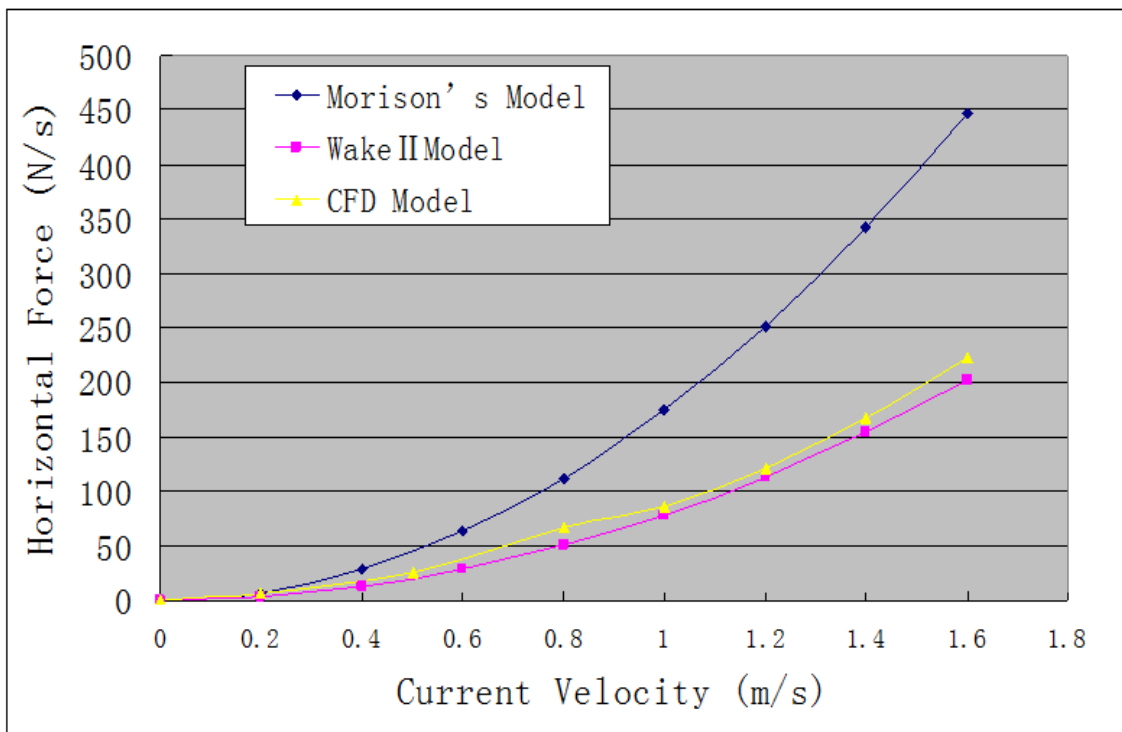
Figure 4.14 Horizontal force comparison with CFD model

4.5 Results Summary

The results from modelling the effect of soil resistance on pipeline stability show that overall soil resistance is a combination of passive and lateral soil resistance. While passive resistance is a function of pipeline weight and height, and hydrodynamic forces, lateral resistance on the other hand is a function of the pipeline's contact with the soil (that is, sliding friction). The results also show that passive resistance is on the average 10 times the value of lateral resistance for both sand and clay soils, which implies that passive resistance is more critical for pipeline on-bottom stability analysis. This confirms the limitation of the Coulomb's friction theory (discussed in section 2:10) which estimates soil resistance based on lateral resistance.

CHAPTER 5: PIPELINE STABILITY ANALYSIS

CFD model was developed to represent a typical pipeline installed on a seabed, with the inlet in the direction of the positive x-axis and the direction of flow perpendicular to the axis of the pipeline using a scale of $10m \times 1.5m \times 2.0m$. Figure 5.1 shows the generated mesh near the pipe-seabed. The geometry of the imported mesh is considered to be a control volume of a pipeline installed on the seabed (Figure 5.2). A polyhedral mesh (with a relative size of 1.5% of model size) was chosen as it uses less memory, gives faster solution and greater accuracy. The boundary names and types, and selected parameters were set as shown in Table 5.1 and Table 5.2 respectively.
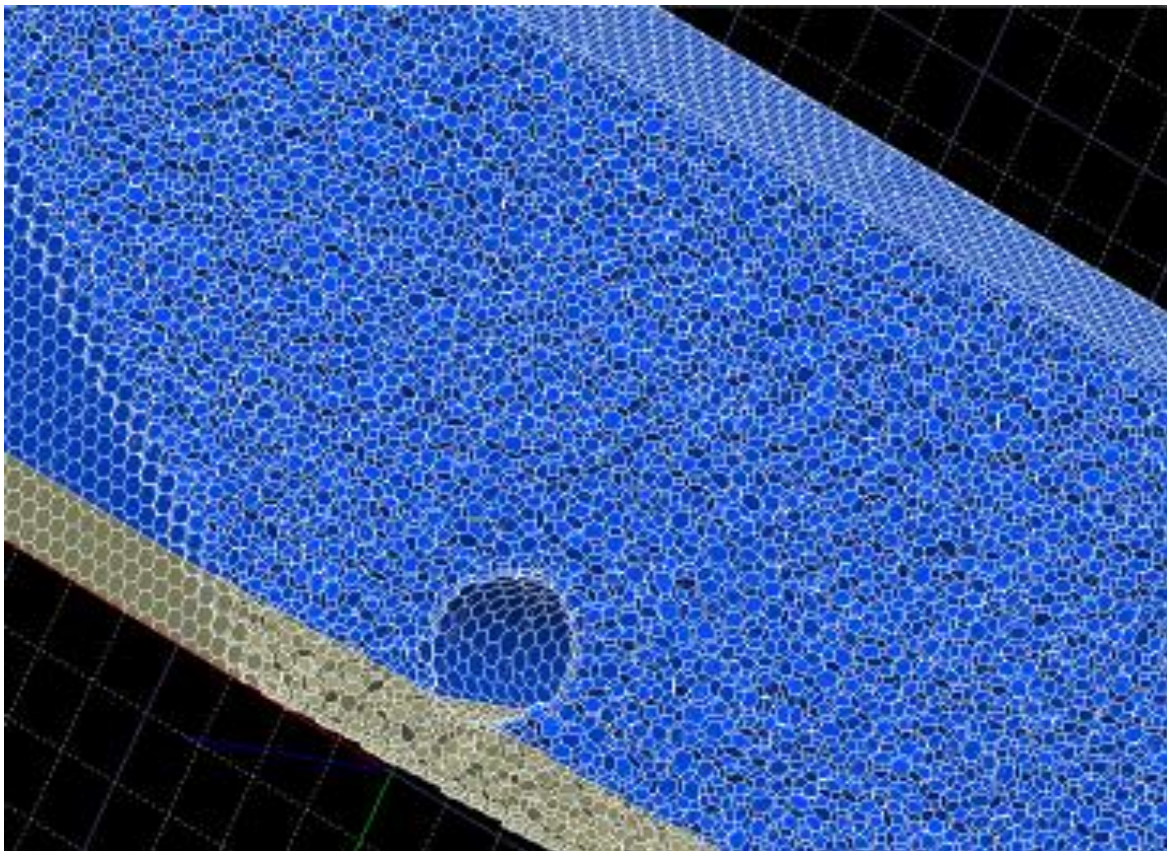
Figure 5.1 Interior volume of mesh ($10m \times 1.5m \times 2.0m$)
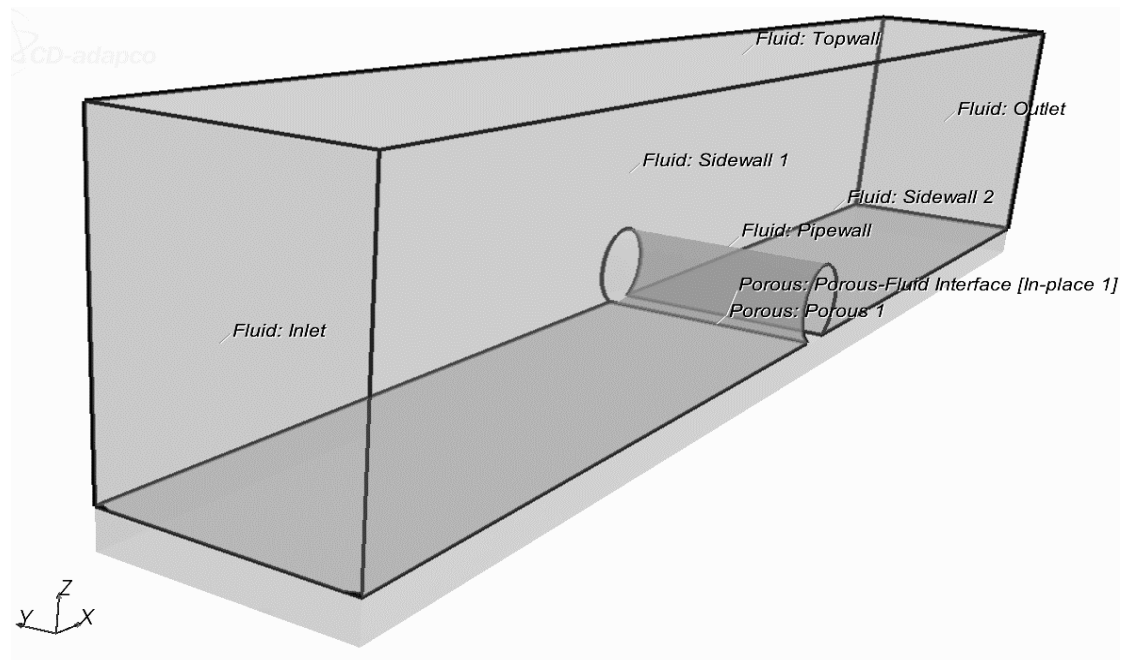
Figure 5.2 Geometry and boundaries

Table 5.1 Boundary conditions

REGION			
Fluid		**Porous**	
Boundary Name	*Boundary Type*	*Boundary Name*	*Boundary Type*
Fluid-Porous Interface	No-Slip Wall	Porous 1	No-Slip Wall
Inlet	Velocity Inlet	Porous 2	No-Slip Wall
Outlet	Pressure Outlet	Porous 3	No-Slip Wall
	No-Slip Wall	Porous-Fluid Interface	No-Slip Wall
Side wall 1	Symmetry Plane		
Side wall 2	Symmetry Plane		
Top wall	Symmetry Plane		

Table 5.2 Selected parameters

Parameter	Value
Density of H_2O	1025 kg/m^3
Viscosity of H2O	0.001002 Pa-s
Reference Gravity	0, 0, -9.81m^2/s
Reference Temperature	273K
Reference Pressure	101325 Pa
Static Temperature	280K
Turbulence Dissipation Rate	0.1 J/kg-s
Turbulence Kinetic Energy	0.001 J/kg
Inlet Velocity	0.2 to 1.5 m/s
Porous Inertial Resistance	50 kg/m^4
Porous Viscous Resistance	3000 kg/m^3-s
Time Step	0.05 seconds
Maximum Inner Iteration	5
Maximum Physical Time	90 seconds

An unsteady, incompressible and turbulent segregated flow model was chosen to solve the flow equations. Segregated flow model solves equations separately and sequentially as opposed to coupled flow model which solves equations together at the same time thus requires more memory space. Considering that the flow is turbulent, the flow was modelled based on RANS equation derived from the Reynolds decomposition of the Navier Stokes equation using the standard k-ε model as described in section 3.1.1.

Hydrodynamic force was simulated by considering a constant flow amplitude of 0.3m/s at varying KC number (40, 50, 60, and 70) based on Soedigbo, Lambrakos and Edge (1998) Wake II Model. Series of simulations were performed by varying inlet flow velocity from 0.2 m/s to 1.5 m/s, to determine the hydrodynamic forces acting on the pipeline. The embedment of the pipeline and the porous resistance of the seabed were also varied in order to determine their effect on pipeline stability. As seabed was modelled as static, the pressure loads and distribution on the pipe wall was used to analyse the pipeline stability.

5.1 Model Validation

The CFD model was validated by comparing its start-up effect with that observed by Soedigbo, Lambrakos and Edge (1998) in the analysis of field work carried out by Exxon Production Research Company (EPRC) to improve the prediction of hydrodynamic forces on subsea pipelines. The start-up effect (discussed in section 2.9.1) for the CFD model and work based on EPRC show that as the relative velocity between pipeline and sea (water) changes, the lift force varied more rapidly compared to the drag force which is the effect of varying time dependent force coefficients as shown in Figure 5.3 (lift coefficient) and Figure 5.4 (drag coefficient). This also in agreement with the results from the full-scale laboratory and field investigation of hydrodynamic force characteristics by Verley, Lambrakos and Reed (1987) which also established that lift coefficient has a stronger start-up effect than the drag coefficient.
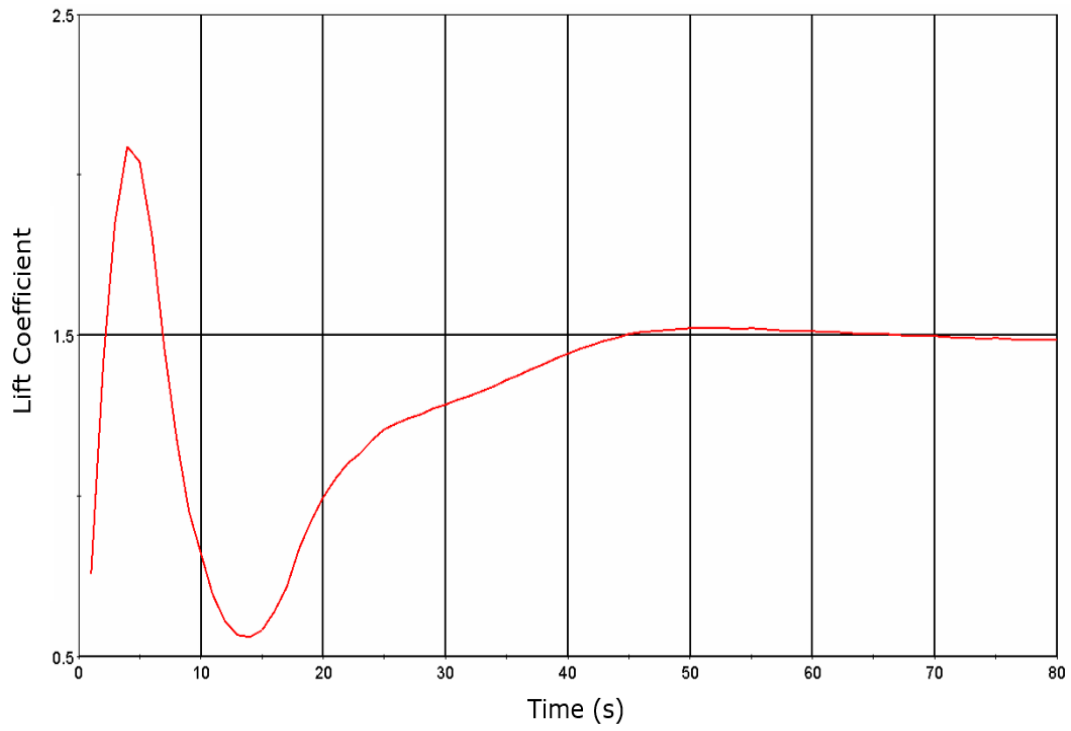
Figure 5.3 Lift coefficient with start-up effect
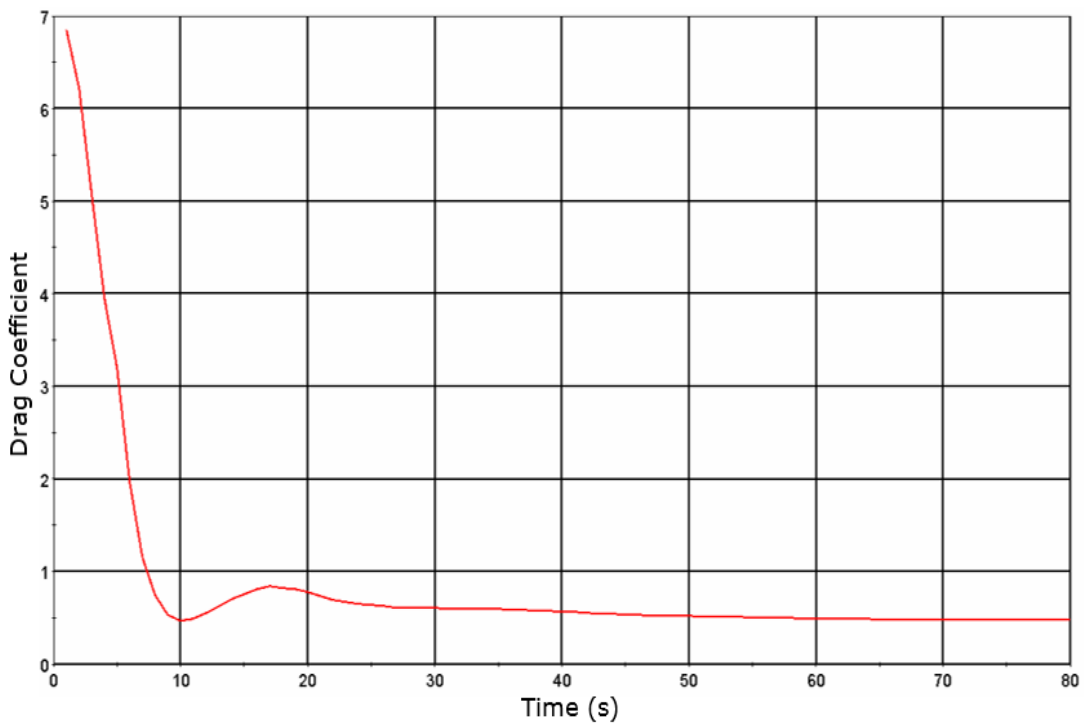
Figure 5.4 Drag coefficient with start-up effect

5.2 Results of Pipeline Stability Analysis

The lateral stability of the pipeline in currents can be achieved by maintaining a balance between the horizontal forces acting on the pipeline and the total lateral soil resistance. Figure 5.5 shows the graph for stability criteria for 0.5m diameter pipeline with 5% embedment. The pipeline will be unstable if the horizontal force becomes greater than the total lateral soil resistance. At the point of intersection between the horizontal force and total lateral soil resistance, the critical velocity of the current U_C above which the pipeline becomes unstable is determined (in figure 5.5 U_C is 0.94m/s). This implies at any current velocity below U_C the pipe will be stable and any current velocity above U_C will result in lateral instability of the pipeline.
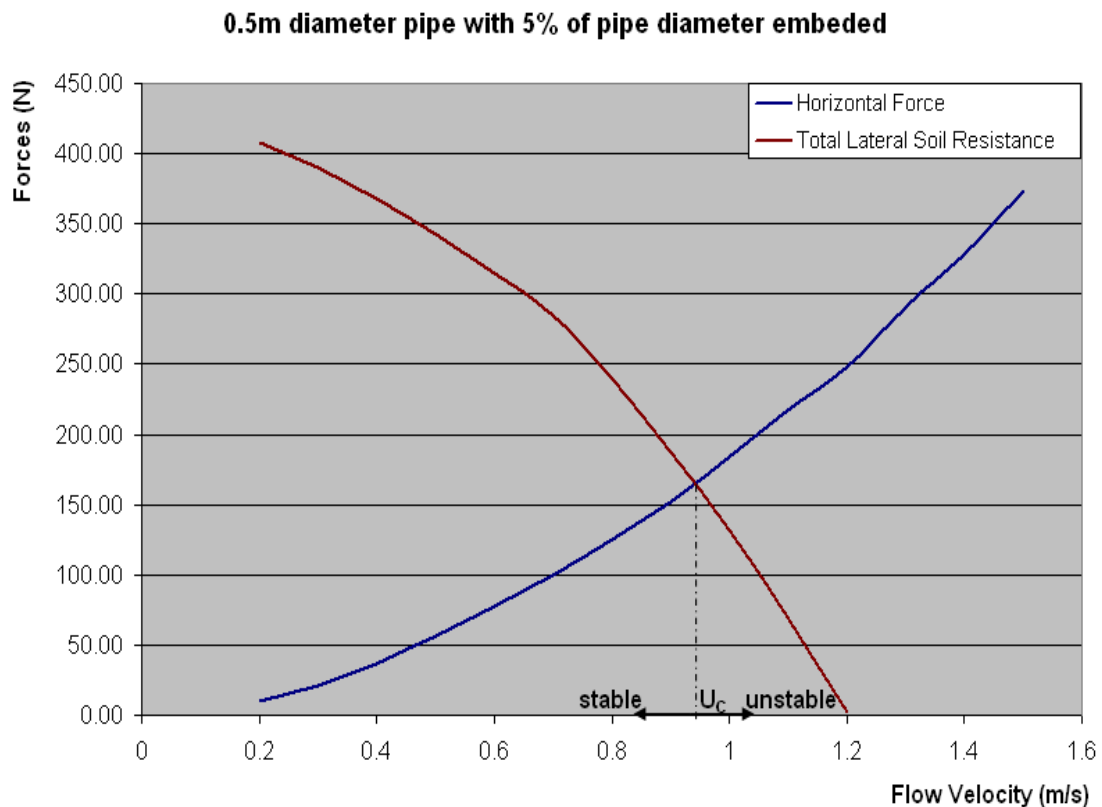
Figure 5.5 Pipeline stability criteria for 0.5m diameter pipeline with 5% embedment

Reducing the diameter to thickness ratio of the pipeline will increase the thickness as well as the submerged weight of the pipeline thus increasing the total lateral soil resistance which will cause the pipeline to be more stable. Any small proportional increase in submerged weight results in a proportional increase in the total lateral soil resistance and the critical velocity that will cause pipeline instability. In Figure 5.6 any submerged weight above weight 1 will keep the pipeline stable in a sea state with critical velocity U_{C1} or less.
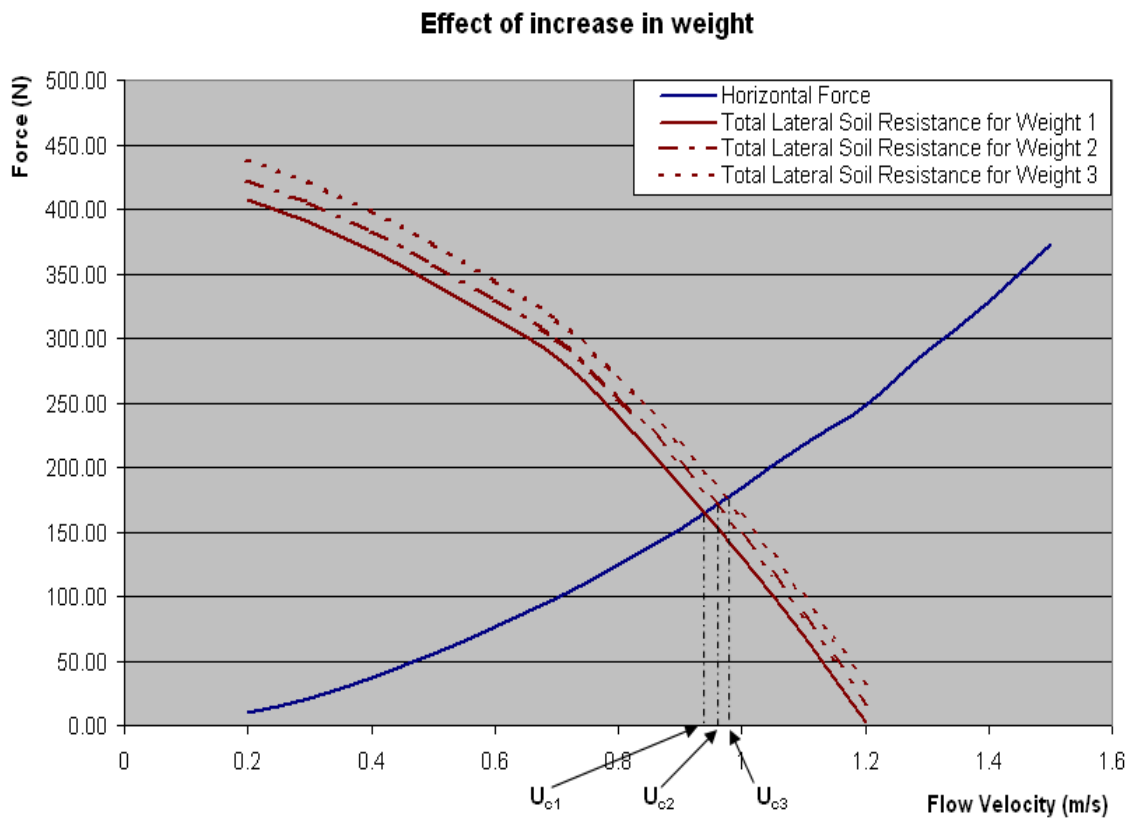
Figure 5.6 Effect of weight increase on 0.5 m diameter pipeline (submerged weight 1 $= 415N$, submerged weight 2 $= 440N$ and submerged weight 3 $= 465N$)

5.2.1 Results of the Effect of Soil Embedment on Pipeline Lateral Stability

The submerged weight of an installed pipeline induces some degree of embedment of the pipeline. The degree of embedment also depends on the properties of the seabed soil. Figure 5.7 shows that a slight reduction (2% i.e. decrease from 5% to 3%) in pipeline embedment reduces the total lateral soil resistance by approximately 23%. This is due to the reduced pipe-soil contact. The effect of reduced embedment on horizontal force was insignificant (as there was no notable difference as can been see in figure 5.7) when compared with the effect on the total lateral soil resistance. This implies that the higher the degree of embedment the more stable the pipeline and vice versa.
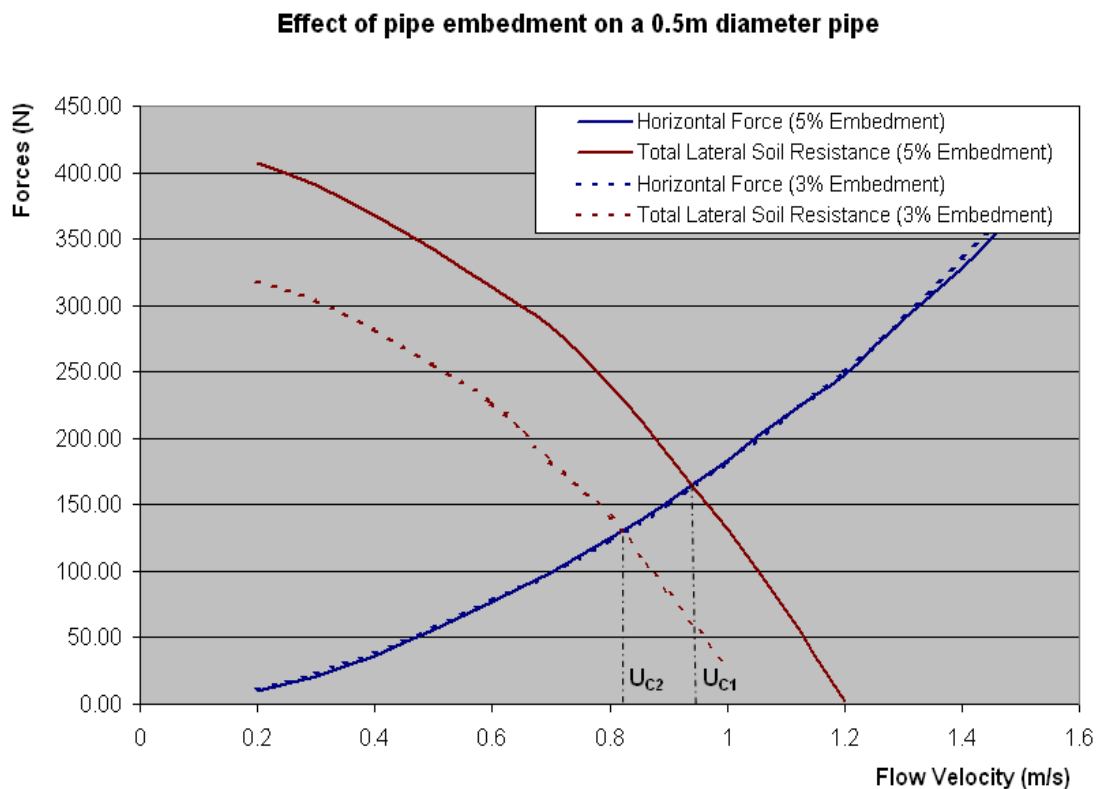
Figure 5.7 Effect of soil embedment on pipeline lateral stability

5.2.2 Results of the Effect of Seabed Porosity on Pipeline Lateral Stability

Increasing the porous inertial resistance and porous viscous resistance by 100% and 67% respectively results in a corresponding reduction in the porosity of the seabed. Figure 5.8 shows that this reduction in porosity results in a slight reduction (5%) in the lateral stability of the pipeline. There is a higher rate of decrease in total lateral soil resistance of the less porous seabed with flow velocity when compared with the higher porous seabed.
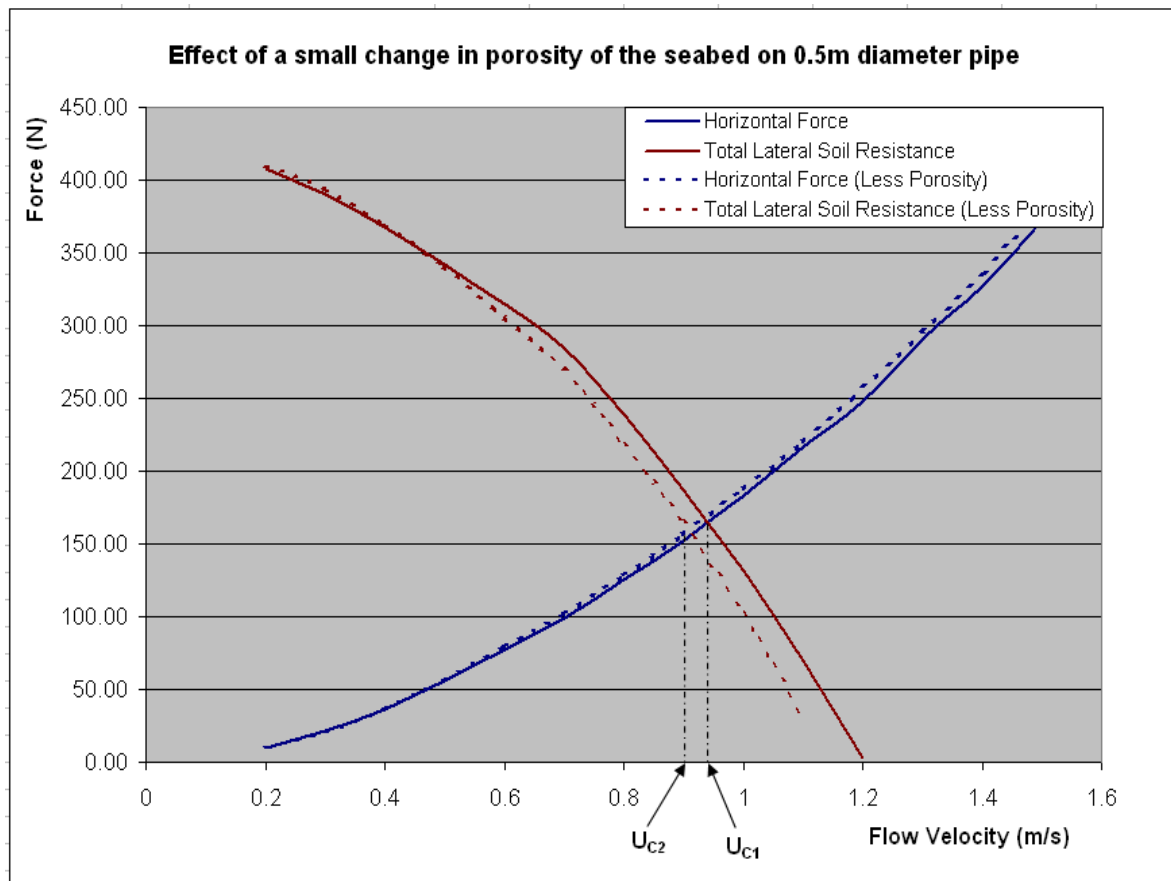
Figure 5.8 Effect of porosity on pipeline lateral stability

A very slight rate of increase in the horizontal force was observed with the less

porous seabed as flow velocity increased. This is due to the reduced fluid-soil interaction; the less porous seabed reduces the ease with which the fluid flows through the soil, thus increasing the pressure acting on the pipeline. As discussed in section 2.11 (sediment mobility), wave induced shear stresses on subsea soils causes pore-water pressure build-up which results in soil liquefaction. Thus, the higher the pore-water pressure build-up, the higher the soil porosity and hence greater soil liquefaction.

5.3 Results Summary

The results from this chapter show the effect of seabed porosity on lateral soil resistance; increasing seabed porosity increases lateral soil resistance. This explains the reason for the decrease in pipeline stability in less porous seabed as higher porosity results in greater soil liquefaction which increases soil resistance and hence pipeline stability. The results obtained are in agreement with the conclusion of Wagner et al. (1987) pipe-soil interaction model, which established that pipeline embedment as a result of soil porosity have a significant effect on lateral soil resistance and thus overall lateral stability of subsea pipelines.

CHAPTER 6: MODELLING PIPELINE EMBEDMENT FOR ON BOTTOM STABILITY OPTIMISATION

The experimental work by Gao et al. (2007) on ocean currents-induced pipeline lateral stability on sandy seabed showed a linear correlation between the Froude number and dimensionless submerged weight of pipeline for various pipeline diameters. The result gave an indication of the influence of pipeline diameter on stability. However the combined effect of change in diameter and submerged weight of pipeline on stability was not fully established. This section seeks to establish the relationship of this combined effect on pipeline stability in sand and clay soils.

CFD model was developed to represent a pipeline on a seabed, with the seabed created as a porous media using dimensions from experimental work on pipeline stability carried out by Gao et al. discussed in section 2.12.2.1 (Gao et al. 2007; Gao, Gu and Jeng 2003; Gao et al. 2002).

To ensure good resolving of boundary layer as the flow is wall bounded, a 410000 cell mesh (Figure 6.1) was generated with inflation applied to accurately calculate effects of non-slip condition on pipe wall. Inflation layer results in correct prediction of hydrodynamic coefficients (drag and lift), wake, turbulence and other surface losses. Considering turbulent conditions, the standard k-ε turbulence model was selected as discussed in section 3.1.1.
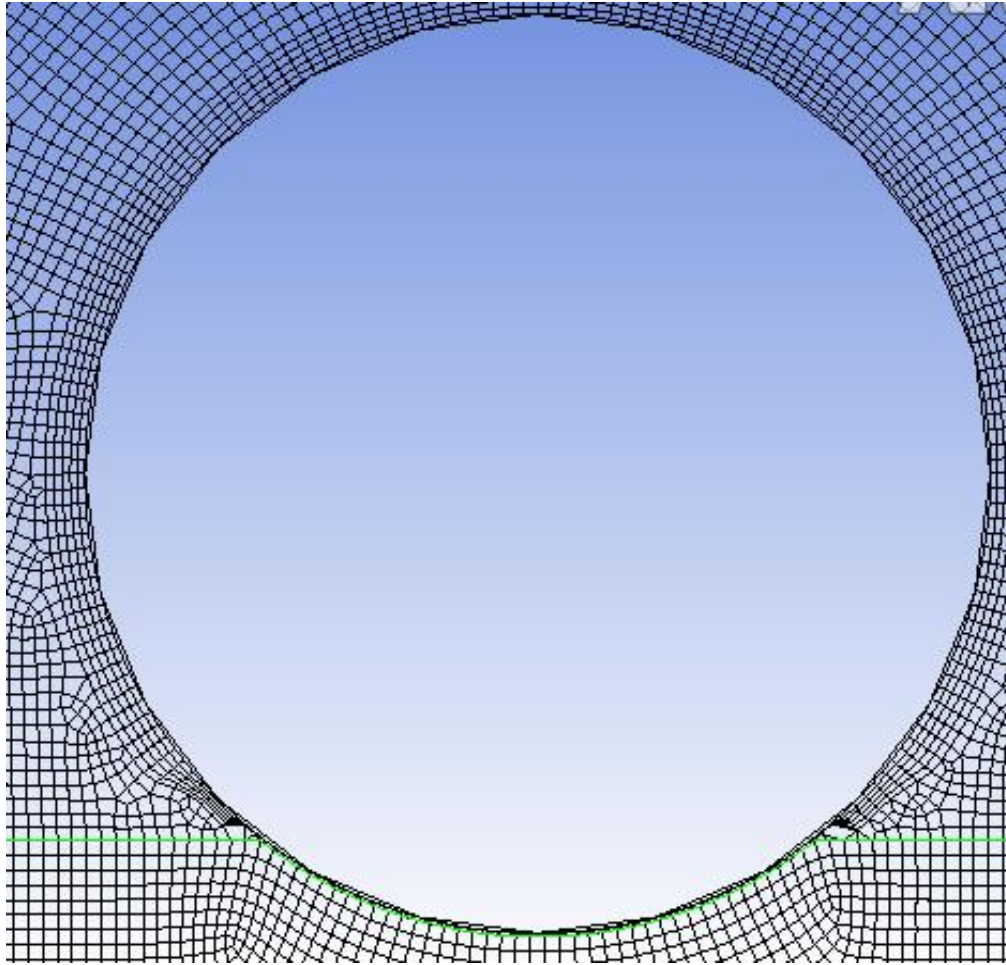
Figure 6.1 Mesh with applied inflation on pipeline wall

Boundary conditions were specified as shown in Figure 6.2. The boundary name and type were set as shown in Table 6.1. Table 6.2 shows the selected parameters. In specifying outlet boundary conditions, the pressure outlet was used rather than outflow to improve rate of convergence. Outflow boundary results in poor convergence if backflow occurs during iteration. Considering a fully developed inlet flow, the intensity and hydraulic diameter specification method was used to specify turbulence length scale. As turbulence derives its characteristic length from the pipeline forming an obstacle in the flow path, the turbulence length scale is based on hydraulic diameter equivalent to the pipeline diameter. Fluid and soil domain were defined as interfaces to enable coupling as a mesh interface over which fluid can flow.

93
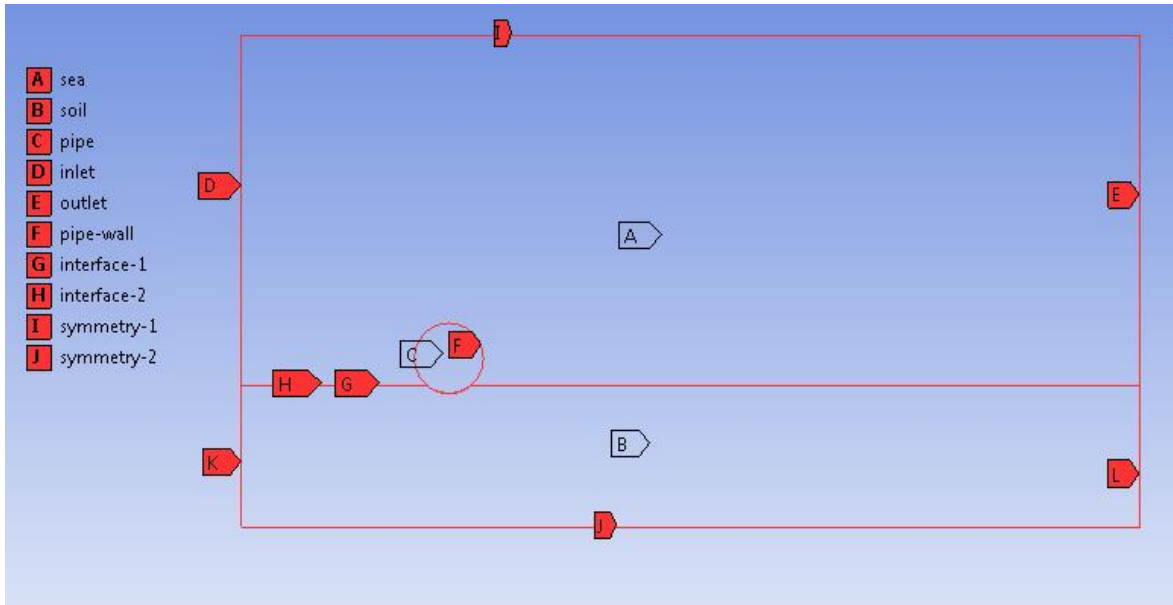
Figure 6.2 Fluid-pipe-soil boundary conditions

Table 6.1 Boundary conditions

Boundary Name	Boundary Type
Inlet	Velocity Inlet
Outlet	Pressure Outlet
Symmetry 1	Symmetry Plane
Symmetry 2	Symmetry Plane
Pipe wall	No-Slip Wall
Interface 1	Mesh Interface
Interface 2	Mesh Interface

Table 6.2 Selected parameters

Parameter	Value		
Inlet Velocity	0.25 to 1.5 m/s		
Pipeline Diameter	0.5m, 1m		
Unit Weight of Soil		Loose Sand	18400 N/m^3
		Dense Sand	19400 N/m^3
		Soft Clay	17300 N/m^3
Unit Weight of Dry Soil		Loose Sand	13900 N/m^3
		Dense Sand	15100 N/m^3
		Soft Clay	11500 N/m^3
Saturation		Loose Sand	94.8%
		Dense Sand	100%
		Soft Clay	100%
Porosity		Loose Sand	48.3
		Dense Sand	43.9
Undrained Shear Strength		Soft Clay	1400 Pa
Static Friction Coefficient		Sand	0.6
		Clay	0.2

Simulation was carried out for various penetration depth (e) to outer diameter

(D) ratio i.e. embedment $\dfrac{e}{D}$ = 5%, 10%, 15%, 20% and 25%.

Three sets (0.5m and 1m diameter pipeline on loose sand and 0.5m diameter

pipeline on dense sand) of thirty-six simulations were carried out for six current

velocities at six embedment conditions with varying pipeline submerged weight

per unit length. Matlab code (see appendix A (I and II), B (I and II), C (I and II), D (I and II), E) was used to determine embedment.

6.1 Results of the Effect of Pipe Diameter and Pipe Weight on Pipeline Embedment

Figures 6.3 (for sand) and 6.4 (for clay) show the relationship between increasing pipe diameter and pipeline embedment (at a fixed weight submerged weight of $1000N/m^3$). The graph shows a decrease in pipeline embedment with increasing diameter, which is due to the increased pipe-soil contact area resulting in increased resistance to embedment, and increase in lift force with increasing diameter. The plots (Figures 6.3 and 6.4) show that the percentage decrease in embedment with increasing diameter (0.2m to 1.2m) is similar for both sand (86%) and clay (83%) with clay having a higher degree of embedment.
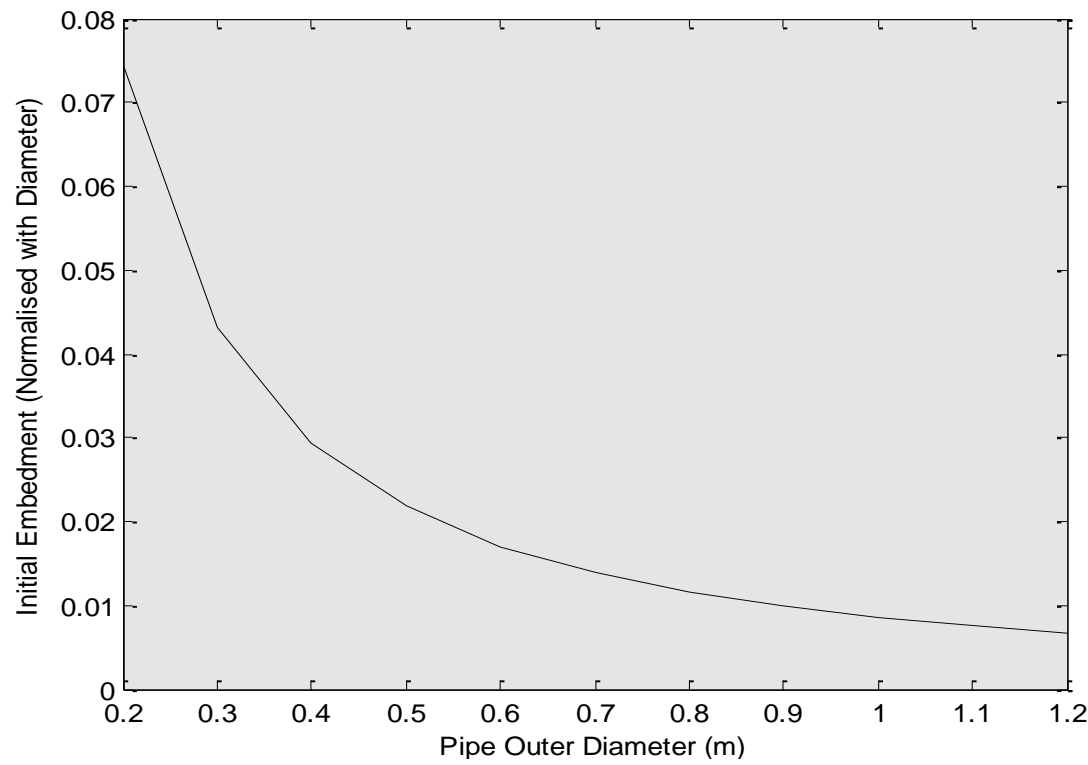
Figure 6.3 Effect of increasing diameter on initial embedment (sand)
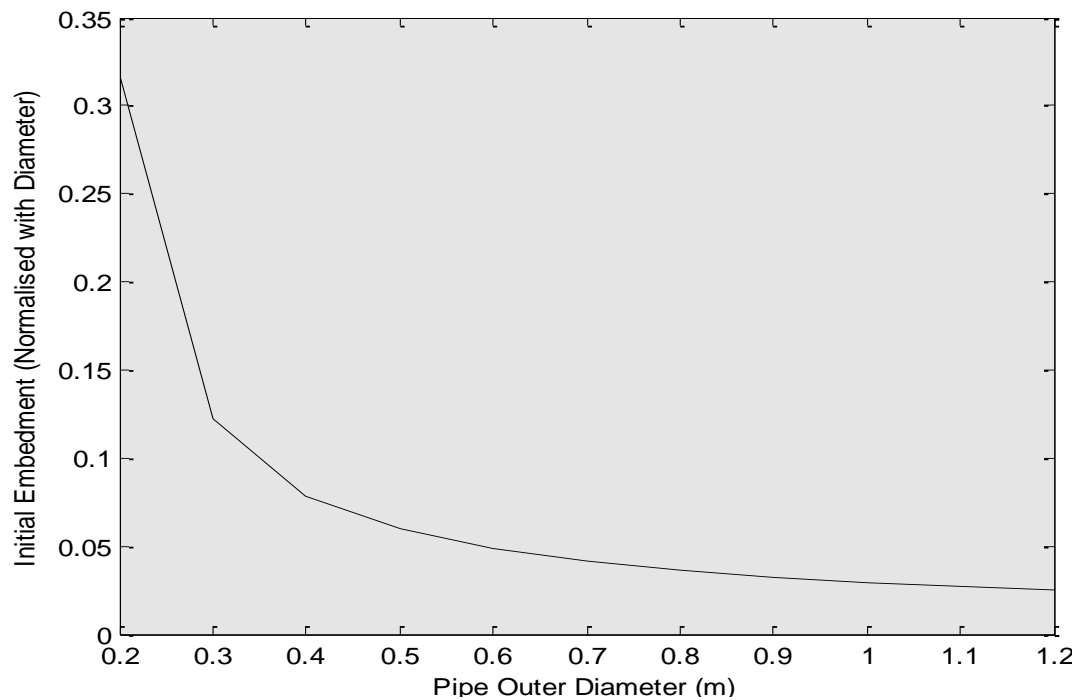
Figure 6.4 Effect of increasing diameter on initial embedment (clay)

Figures 6.5 and 6.6 show the variation of embedment for a 0.5m diameter pipe with increasing weight of pipeline. The plots show that for both sand and clay, as pipe weight increases embedment also increases, with sand having a percentage increase in embedment of approximately 78% and 81% for clay for pipe weight 200N/m to 1200N/m.

To investigate the combined effect of pipe diameter and weight on pipeline embedment, a submerged weight per unit length was assigned to each diameter on the basis of calculated volume per unit length (resulting in a proportional increase in weight as diameter increases). The result for sand (Figure 6.7) show that there is an increase in pipeline embedment with increasing diameter as a result of increasing weight and build-up of a soil ridge. However, when embedment is normalised with diameter (Figure 6.8), there is a decrease in embedment with increasing diameter which is in line with Figures 6.3 and 6.4. This is a result of increased lift force on larger diameter pipelines due to a greater fluid-pipe contact area resulting in a reduced soil ridge and

hence reduced embedment. This implies that pipe diameter has a greater influence on pipeline embedment than pipe weight.
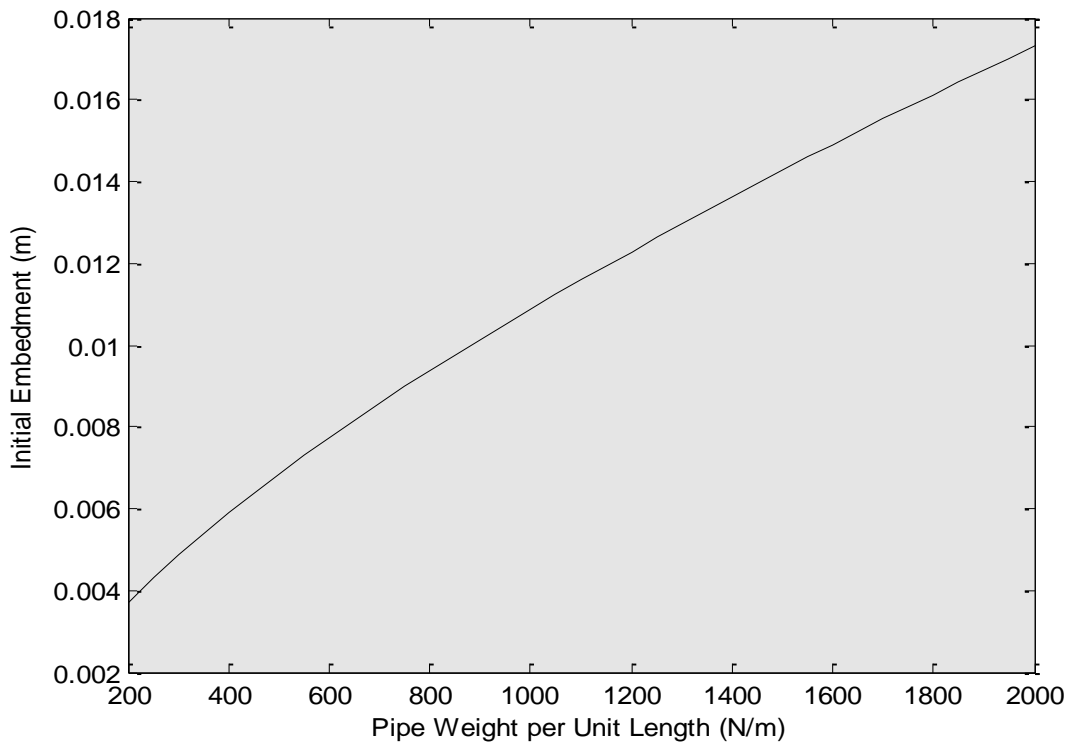
Figure 6.5 Effect of submerged pipe weight on embedment (sand)
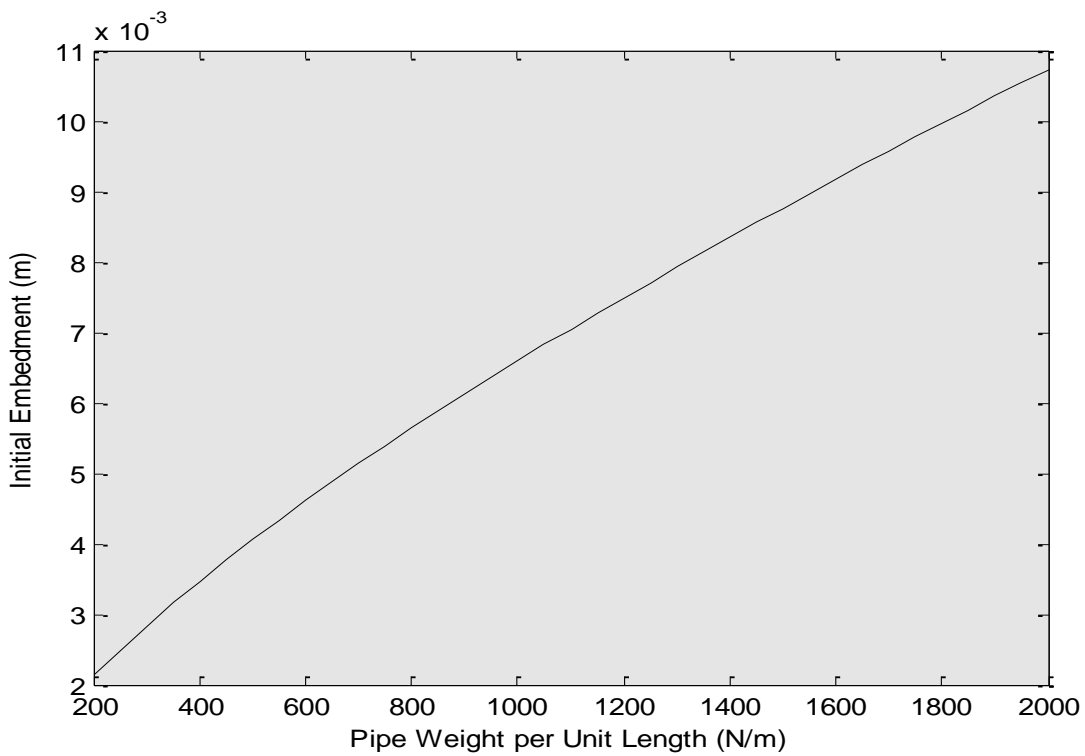
Figure 6.6 Effect of submerged pipe weight on embedment (clay)
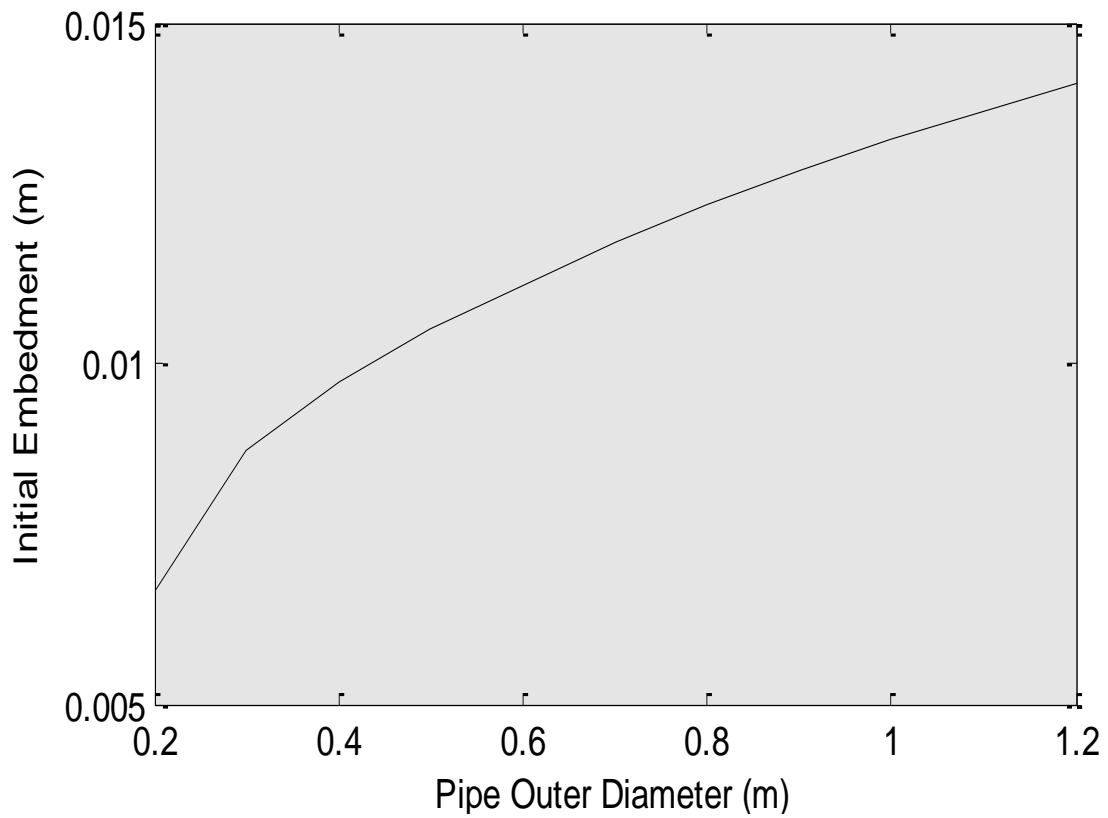
Figure 6.7 Combined effect of pipe diameter and weight on embedment (sand)
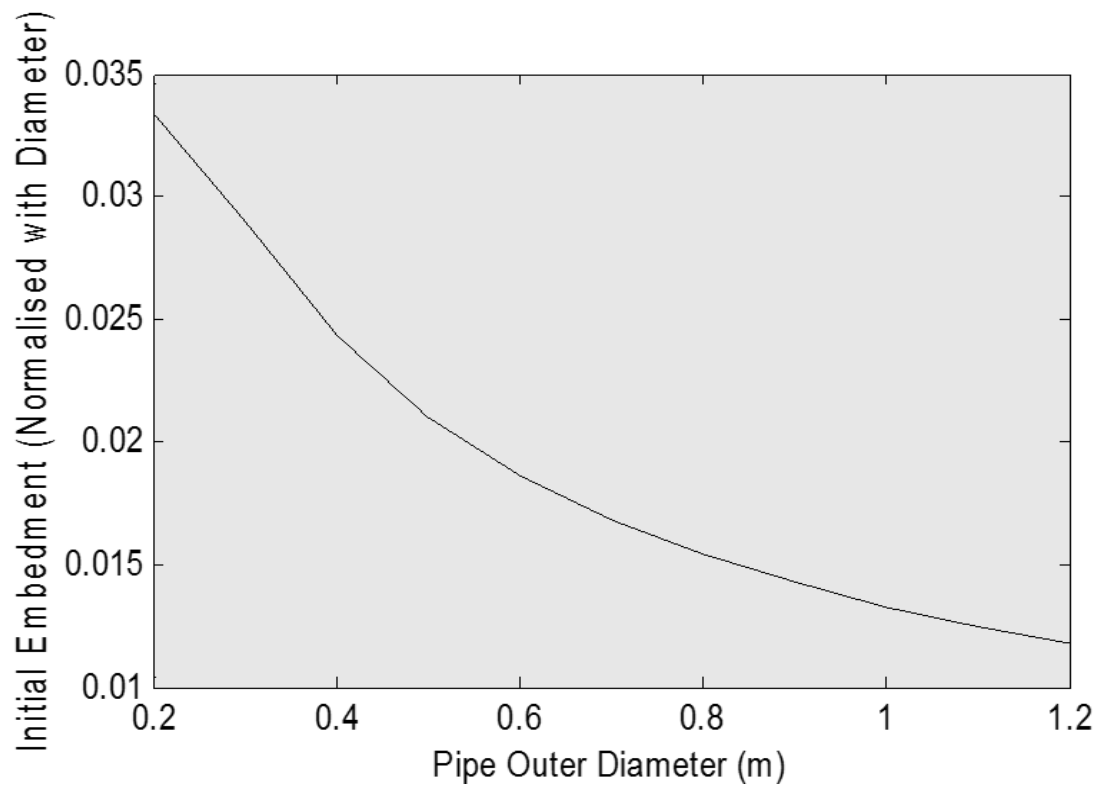
Figure 6.8 Effect of normalised pipe diameter on embedment (sand)

The result for clay show that both actual (Figure 6.9) and normalised embedment (Figure 6.10) increase with increasing diameter, this implies for clay soil, pipe weight has a greater influence on embedment than in sand.
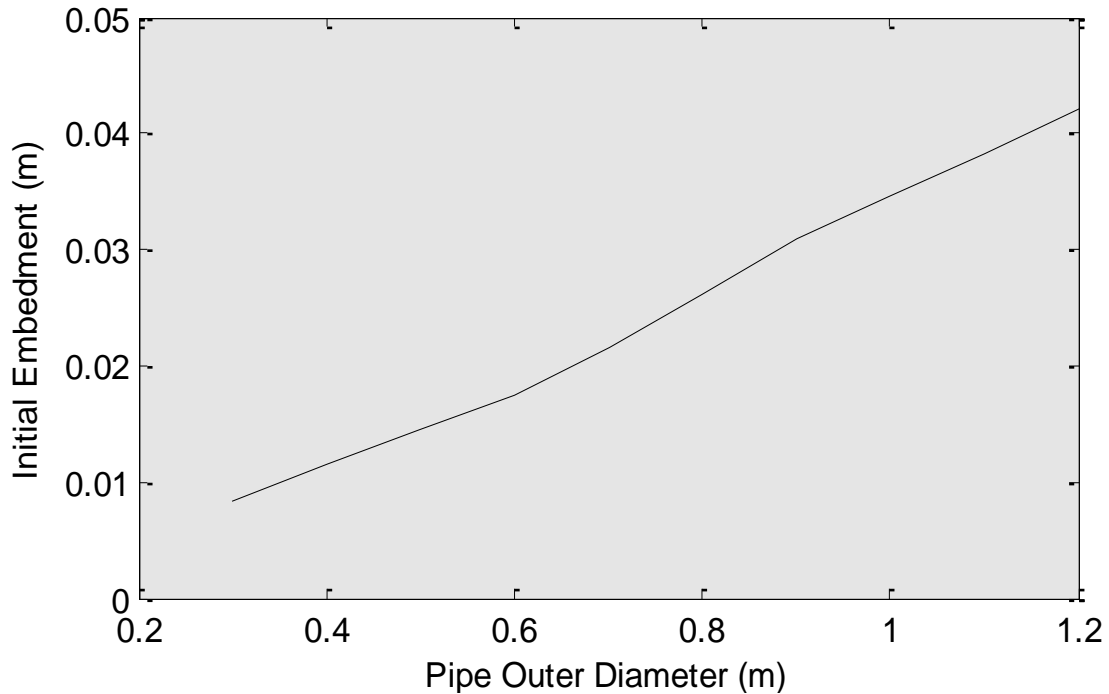
Figure 6.9 Combined effect of pipe diameter and weight on embedment (clay)
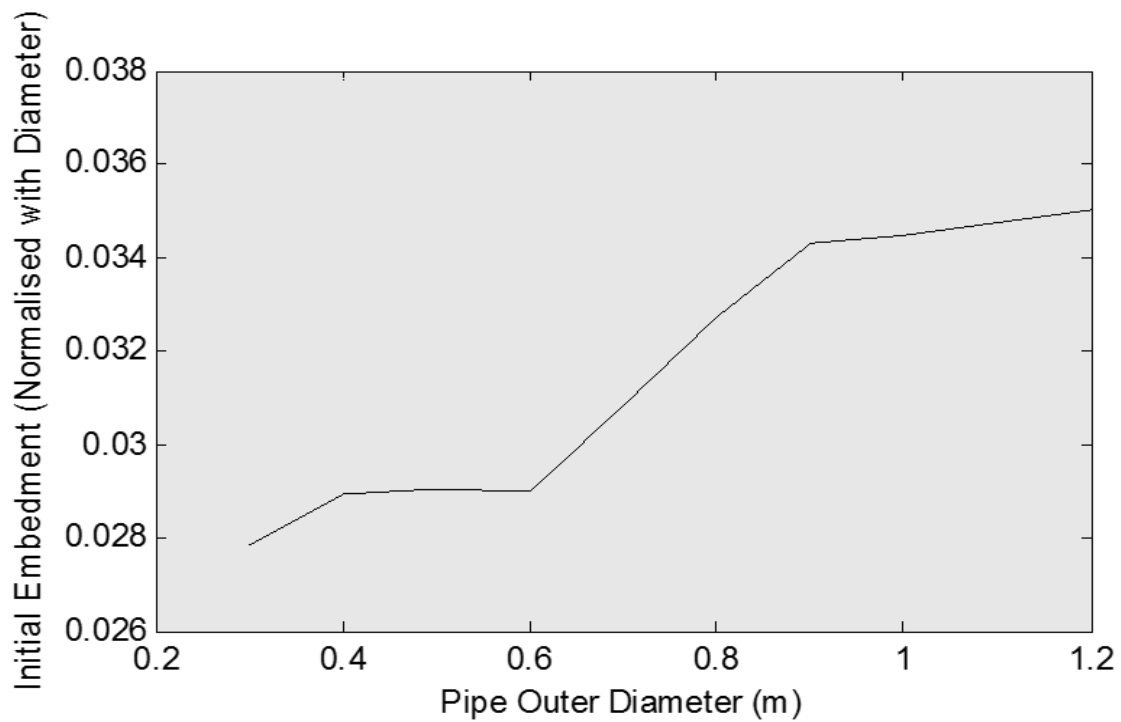
Figure 6.10 Effect of normalised pipe diameter with embedment (clay)

6.2 Results of the effect of unit weight of soil on pipeline embedment

Figure 6.11 and Figure 6.12 show the effect of increasing unit weight of soil on pipeline embedment for sand and clay respectively. Both plots show a decrease in embedment with increasing unit weight of soil. This is a result of decrease in porosity as density (weight and particle size) increases. As discussed in chapter 5 section 5.1.2 a reduction in soil porosity will reduce embedment as the less porous soil reduces the ease with which fluid flows through the soil, thus increasing the upward force on the pipeline. The rate of decrease in embedment with increasing unit weight is greater in sand ($\approx$33%) than in clay ($\approx$7%) as sand has a lower porosity than clay and thus lower degree of embedment.
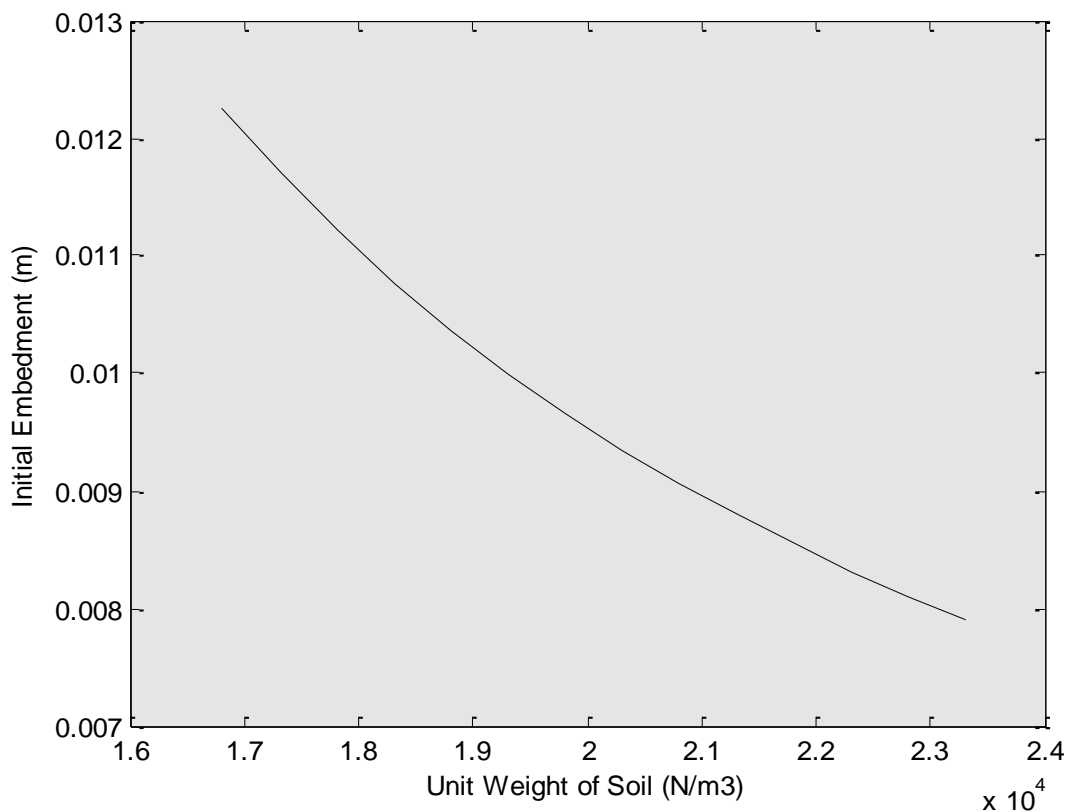
Figure 6.11 Effect of unit weight of soil on embedment (sand)
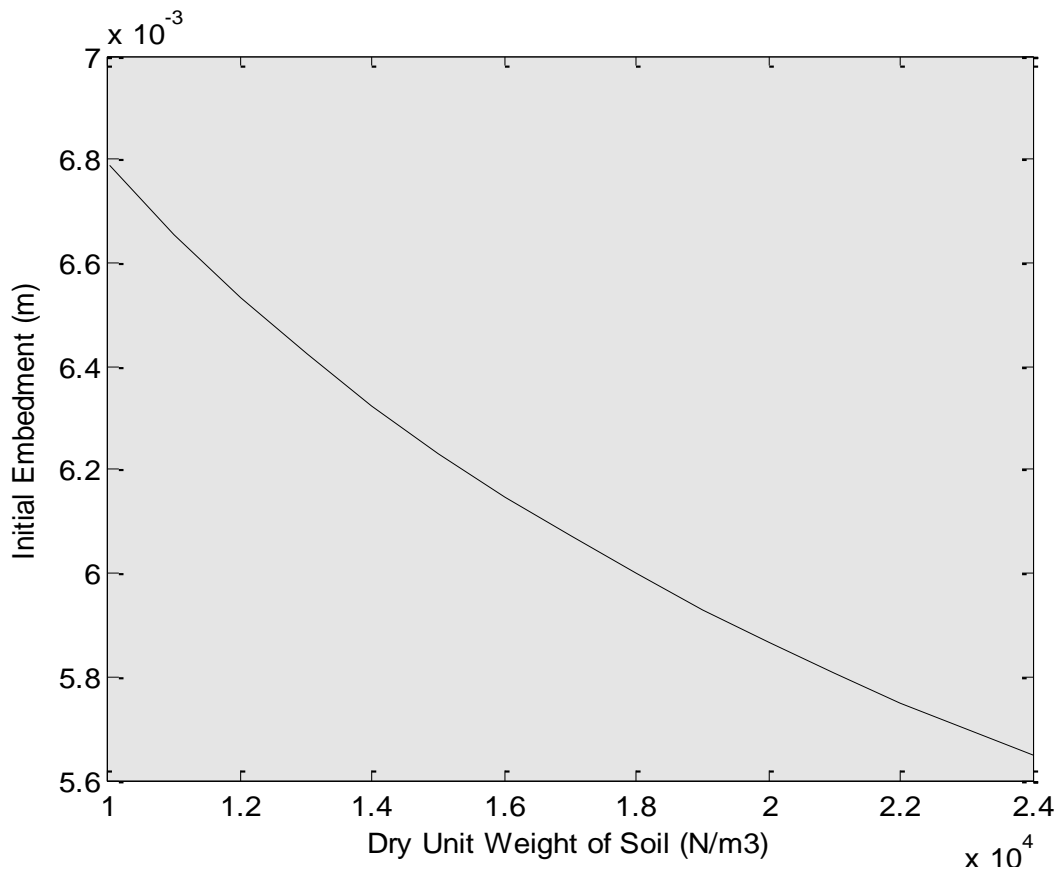
Figure 6.12 Effect of unit weight of soil on embedment (clay)

6.3 Results of the effect of hydrodynamic forces on pipeline embedment

The method used to compute the scour depth was first to determine if scour would occur based on results from initial embedment conditions, then the equilibrium depth was calculated in one step. This reduced the need for a lengthy iterative process. Figures 6.13 and 6.14 show the effect of increasing current velocity on embedment (in loose sand) for a 0.5m and 0.1m diameter pipe respectively.
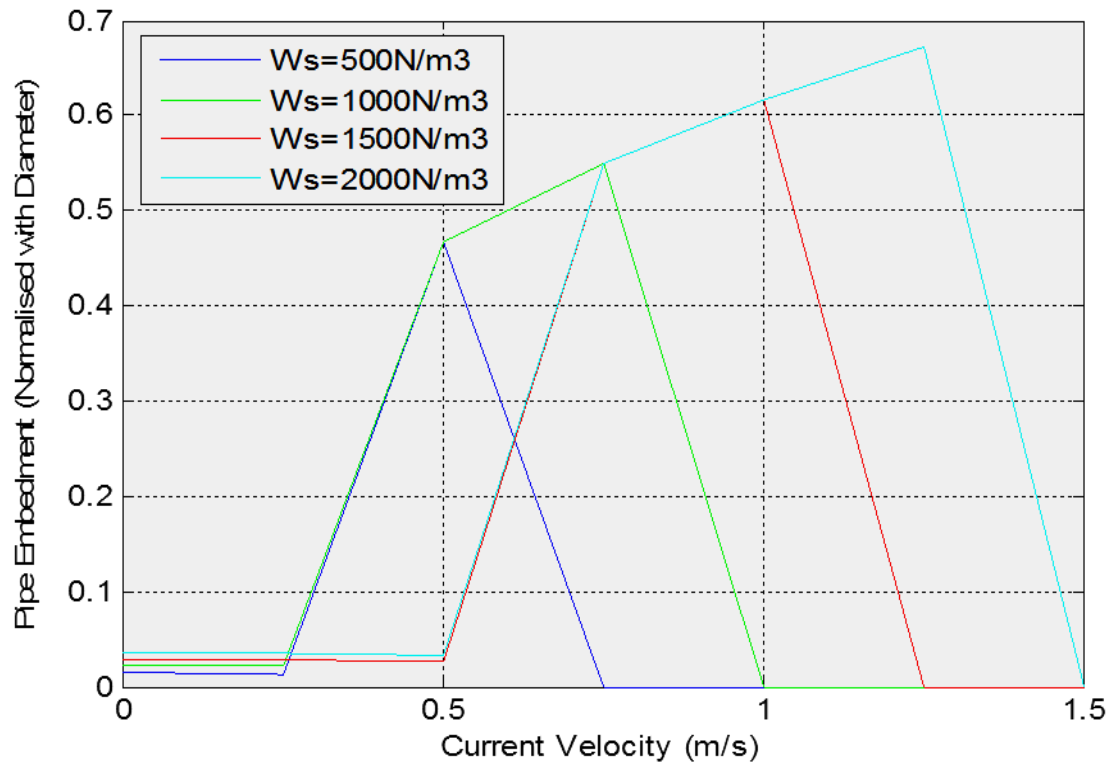
Figure 6.13 Effect of current velocity on embedment (0.5m pipe on loose sand)
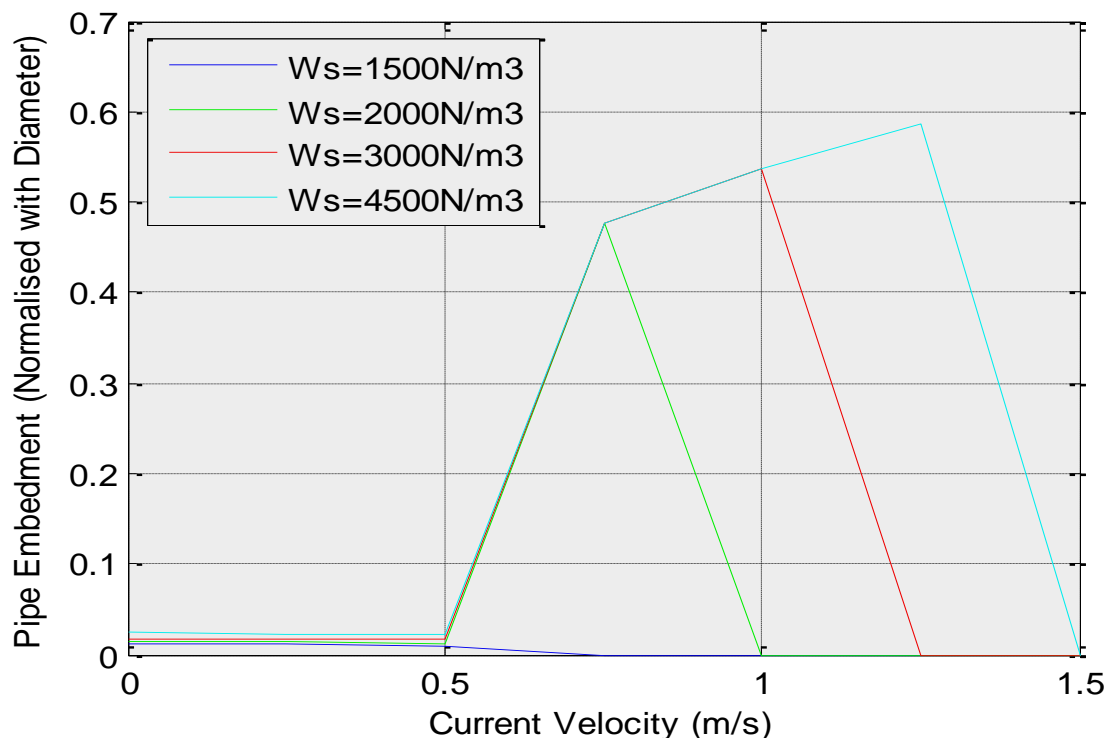
Figure 6.14 Effect of current velocity on embedment (1m pipe on loose sand)

The plots show that other than the initial embedment as a result of pipe weight, there is no change in embedment with initial increase in velocity until the onset of scouring. As scouring progresses with increasing velocity, embedment increases until pipeline breakouts of embedment signifying a decrease in embedment to zero. The results also show that the velocity at which pipe breakout occurs increases with increasing submerged weight of pipe that is the heavier the pipe the higher the velocity required to cause breakout.

Comparing Figures 6.13 (0.5m pipe) and 6.14 (1m pipe) it can be seen that a larger pipe weight is required to prevent pipe breakout at a lower degree of embedment for a 1m diameter pipe than for a 0.5m diameter pipe. This is because hydrodynamic force is proportional to diameter thus the higher diameter pipe has a greater hydrodynamic force acting on it and will require a heavier weight to prevent movement.

Gao et al. (2007), in the experiment on ocean currents-induced pipeline lateral stability on sandy seabed concluded that there is a linear relationship between submerged weight of pipeline and the ratio of inertia force to gravitational force (Froude number) for the lateral stability of pipelines. However, the experiment did not completely verify the combined effect of diameter and submerged weight on pipeline stability. This model has shown the combined effect of pipeline diameter and submerged weight on pipeline embedment which reflects pipeline stability.

6.4 Model Validation

The model was validated by comparing the results of varying pipeline diameter and weight, and soil type on the initial of embedment with the results from experimental work on energy based pipe-soil interaction carried out by Brennodden et al. (1989) as discussed in section 2.12.1.4 and Griffitts et al. (2012) pipe-soil-fluid model (not based on CFD) discussed in section 2.12.2.3 as shown in Table 6.3, Table 6.4 and Table 6.5.

Table 6.3 Initial embedment in loose sand (18400 N/m^3 bulk unit weight)

Diameter (m)	Submerged weight (N/m)	Initial Embedment (m)		
		CFD Model	Brennodden et al	Griffiths et al
0.5	250	0.004	0.004	0.004
0.5	500	0.007	0.006	0.006
1.0	1000	0.009	0.016	0.012
1.0	2000	0.014	0.018	0.018

Table 6.4 Initial embedment in dense sand (19400 N/m^3 bulk unit weight)

Diameter (m)	Submerged weight (N/m)	Initial Embedment (m)		
		CFD Model	Brennodden et al	Griffiths et al
1.0	1000	0.008	0.003	0.010
1.0	2000	0.013	0.004	0.012

Table 6.5 Initial embedment in clay (17300 N/m^3 bulk unit weight)

Diameter (m)	Submerged weight (N/m)	Initial Embedment (m)	
		CFD Model	Brennodden et al
0.5	250	0.011	0.009
1.0	1000	0.032	0.021
1.0	2000	0.043	0.030

The results show that the CFD model is in more in agreement with Griffiths et al. (2012) than Brennodden et al. (1989). CFD model shows a higher degree of initial embedment compared to Brennodden et al. (1989) as the later only considered pipe-soil interaction without the effect of fluid. In the case of Griffiths et al. (2012) which is a pipe-soil-fluid model, the results are almost same as that of the CFD model.

6.5 Results Summary

The results show that pipeline embedment decreases with increasing diameter (a 27% embedment decrease for diameter increase from 0.5m to 1m). This is inverse to the effect of pipeline weight on embedment (embedment increases with increasing weight). The results from the combined effect of pipeline diameter and weight show a variation in embedment based on soil type. Embedment decreased with increasing diameter for sand and remained the same for clay. These results establish that pipeline diameter has a greater influence on embedment in sand while pipeline weight has more influence on embedment in clay. Experimental work by Gao et al. (Gao et al. 2007; Gao, Gu and Jeng 2003; Gao et al. 2002) gave an indication of the influence of diameter in pipeline stability but this was not really established. This work has demonstrated the effect of pipeline diameter and its combined effect with pipeline weight on embedment.

CHAPTER 7: MODELLING SCOURING EFFECT

Model was created as a 2D model representing 0.4m pipeline on a seabed, with seabed scouring effect and eventual breakout of pipe in an unbounded flow. A 383612 node mesh (Figure 7.1) was generated with inflation applied to accurately capture the effect of no-slip condition on the boundary layer region for turbulent flow. Considering turbulent conditions, the k-ε turbulence model was used.
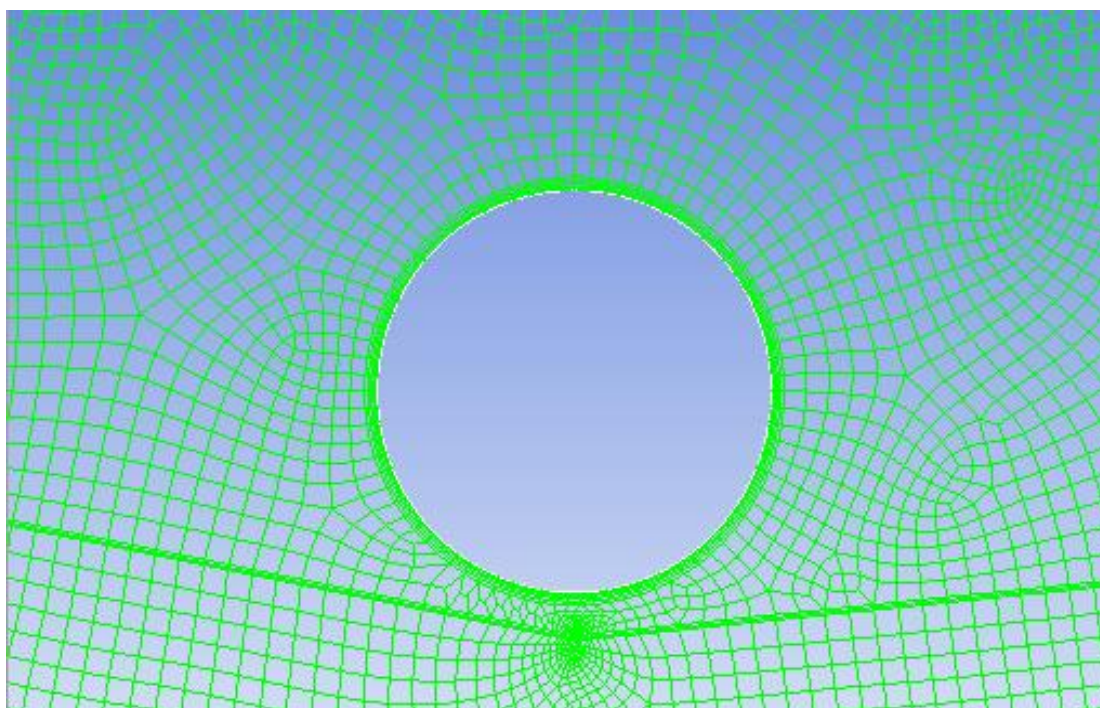
Figure 7.1 Mesh with applied inflation on pipeline wall

Boundary conditions were specified as shown in Figure 7.2. The boundary name and type were set as shown in Table 7.1. Table 7.2 shows the selected parameters.
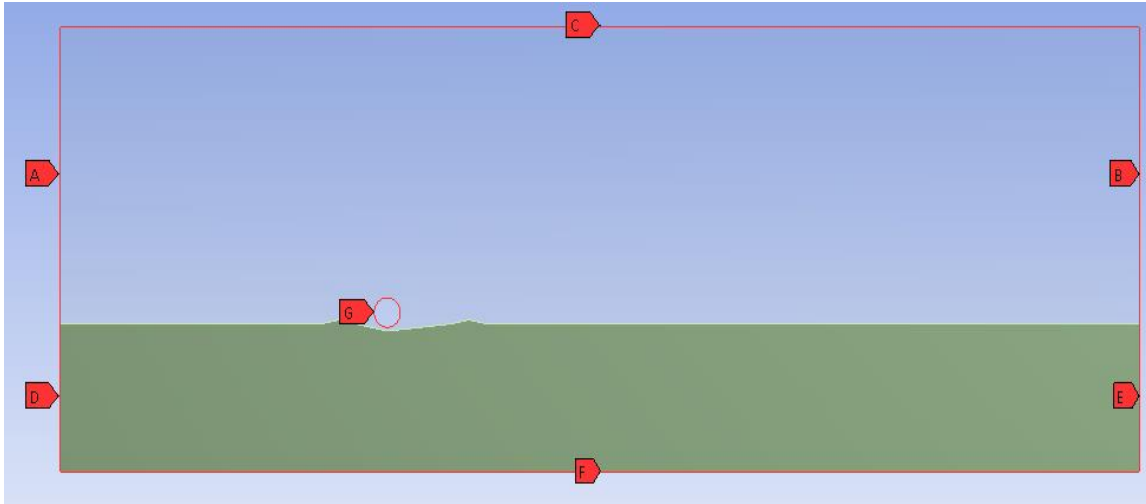
Figure 7.2 Boundary regions (A- inlet; B- outlet; C- symmetry top; D- wall left;

E- wall right; F- wall bottom; G- wall Cylinder)

Table 7.1 Boundary conditions

Boundary Name	Boundary Type
Inlet	Velocity Inlet
Outlet	Pressure Outlet
Symmetry Top	Symmetry
Wall Cylinder	No-Slip Wall
Wall Part Body Surface	Wall
Wall Part Body Surface 1	Wall
Wall Part Body Surface Shadow	Wall

Table 7.2 Selected parameters

Parameter	Value
Density of H_2O	998.2 kg/m^3
Density of Pipe	2719
Viscosity of H_2O	0.001003 Pa-s
Specific Heat of H_2O	4182 J/kg-K
Specific Heat of Pipe	871 J/kg-K
Inlet Velocity	1.5 m/s
Temperature	288.16 K
Time Step	0.001s
Maximum Inner Iteration	20

Simulation was carried out for various pipeline positions (-0.7, -0.3, 0.0, 0.5, 1.0, 1.2) representing pipe movement on the scoured seabed (Figure 7.3). Position -0.7 represents the initial pipeline position before any movement, at position -0.3 embedment is beginning to occur with pipeline gradually be displaced downwards. Position 0.0 represents pipeline at maximum embedment, any further displacement from this position moves pipeline out berm resulting in eventual pipeline breakout. Positions 0.5 and 1.0 represent pipeline movement out of embedment, and position 1.2 represents pipeline at breakout position (i.e. total displacement from embedment).

-0.7   -0.3   0.0   0.5   1.0   1.2
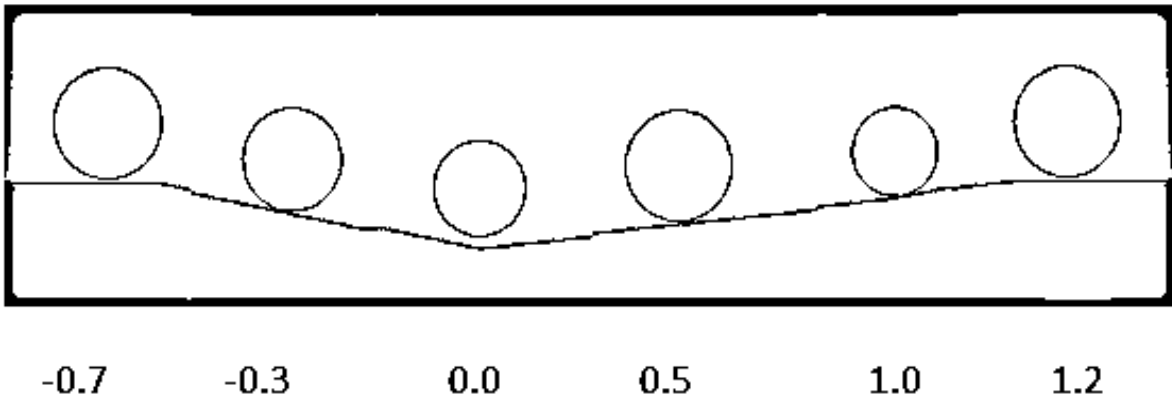
Figure 7.3 Pipeline positions from onset of scour to breakout

Position is with reference to point 0.0 the centre of hydrodynamic scour (see Figure 7.4; arrow shows direction of pipe movement). Simulations were done at 0.001s time step for 10000 time steps at a maximum iteration of 20 per time step with a reporting interval of 1. The seabed scour was modelled as fixed and pipeline position was moved along the scour path as illustrated in figure 7.3.
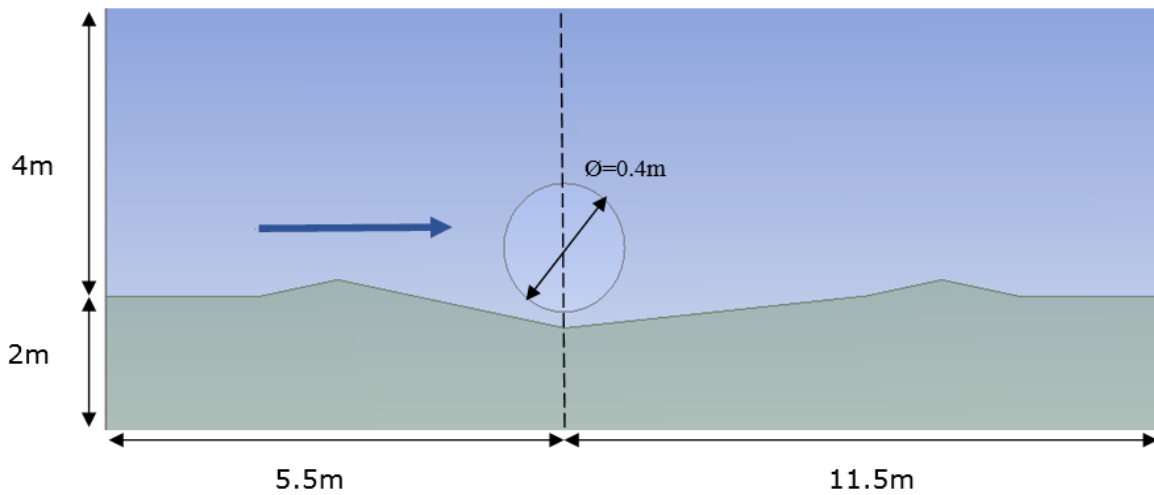
Figure 7.4 Pipeline position at reference point 0.0

7.1 Results on Scouring Effect on Velocity

Figures 7.5a 7.6a, 7.7a, 7.8a, 7.9a and 7.10a show the velocity vector and corresponding contour diagrams (Figures 7.5b, 7.6b, 7.7b, 7.8b, 7.9b and 7.10b) of pipeline from position at -0.7 to position 1.2. At position -0.7 (Figures 7.5a and 7.5b) scouring is yet to occur but a region of high velocity can be seen between the bottom of pipe and seabed. The high velocity combined with the action of vortices (see vorticity plot Figures 7.11a-f) at the downstream side of the pipeline induces seabed erosion (scour). As scouring progresses the region of high velocity is seen at the top of the pipe (Figure 7.6a) indicating negative lift (as shown in the pressure coefficient plot in Figure 7.13b) which signifies pipe embedment. This position (-0.3) also shows an increase in vortex strength. The highest velocity vector is reached at the point (0.0) where maximum scouring (that is maximum embedment) is achieved. Further pipe movement after this position (0.0) causes the pipe to breakout of embedment (Figures 7.8a and 7.8b; 7.9a and 7.9b; 7.10a and 7.10b). These results are in agreement with the wave-pipe-soil interaction experiment by Gao, Gu and Jeng (2006) which showed that there is an increase in the oscillatory flow amplitude (from the onset of scour to pipe rocking and eventual breakout of pipe) during process of pipe losing on-bottom stability. These results are contrary to the conclusion of the PIPESTAB and AGA pipe-soil interaction tests that scouring is not involved in the process of lateral pipeline instability, which is one of the limitations of the study (PIPESTAB and AGA). These results prove that scouring (seabed erosion) is a result of seabed particle movement induced by high velocity region (between pipe and seabed) and vortex formation due to wake effect.

111
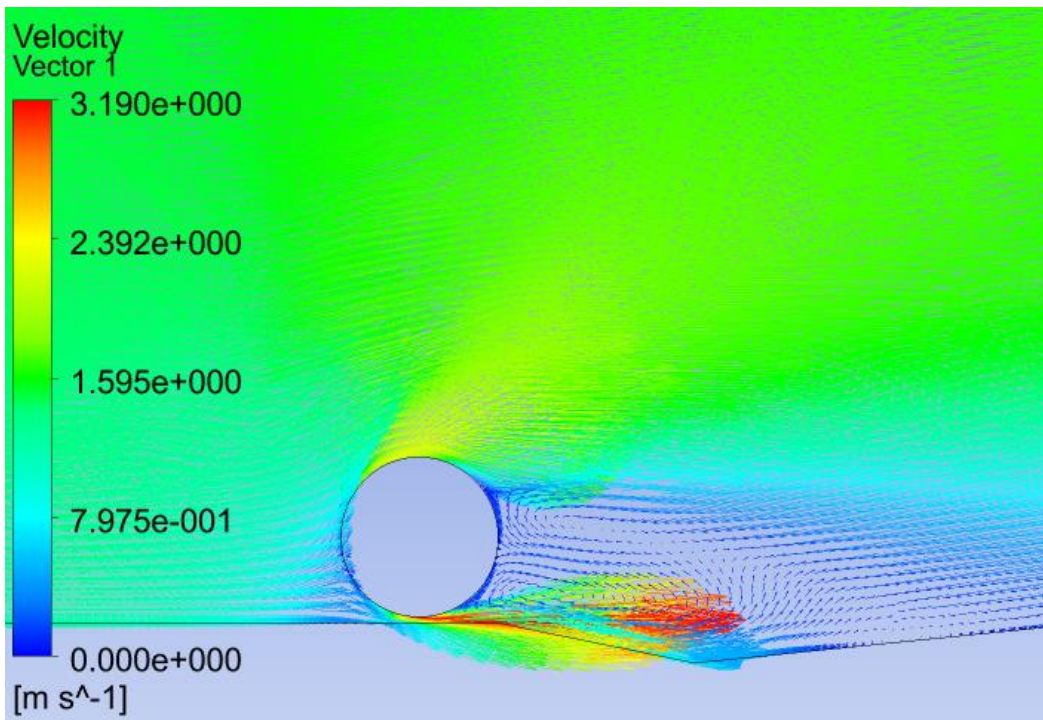
Figure 7.5a Vector of pipeline at position -0.7
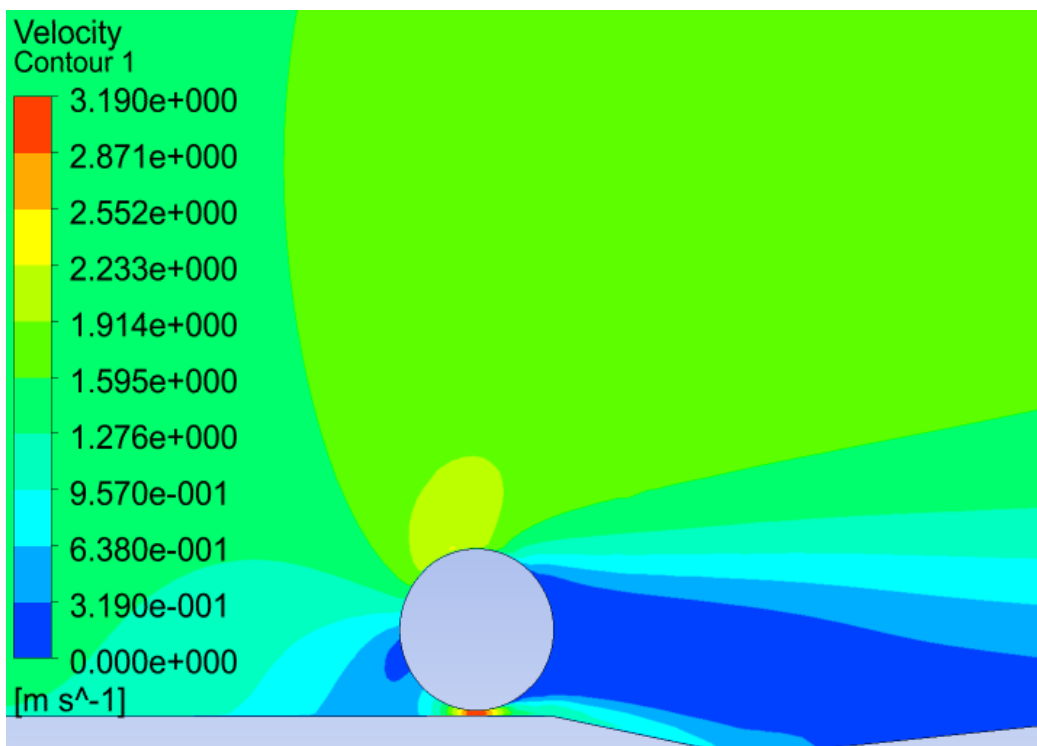
Figure 7.5b Contour of pipeline at position -0.7
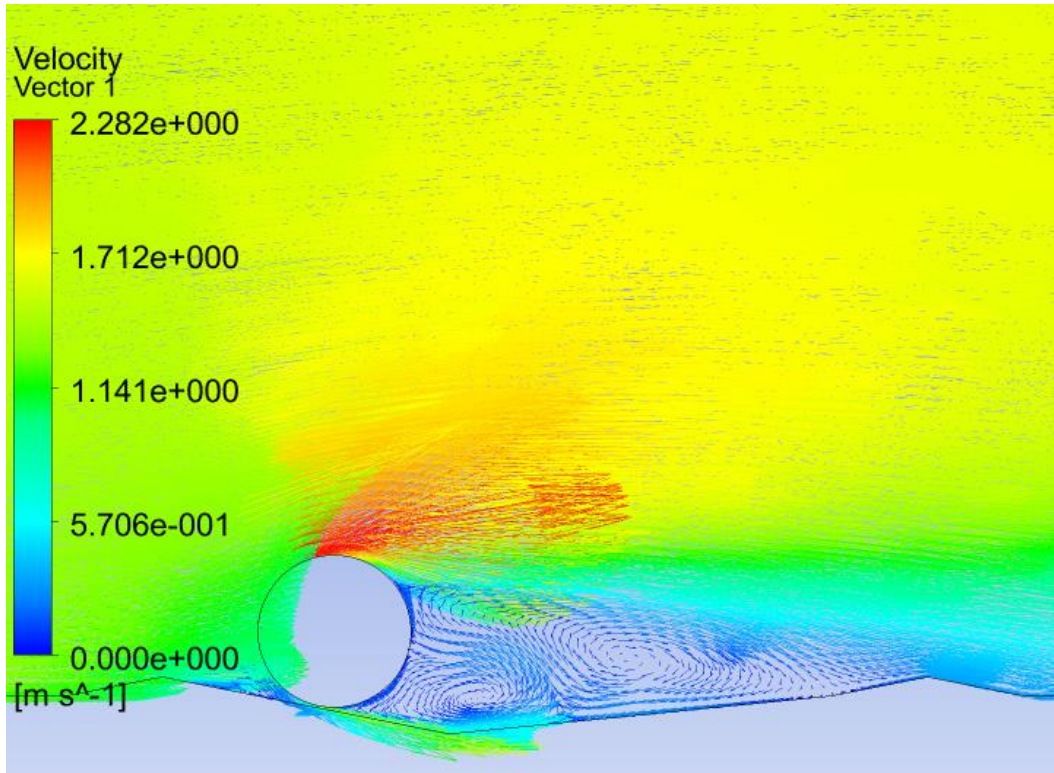
Figure 7.6a Vector of pipeline at position -0.3
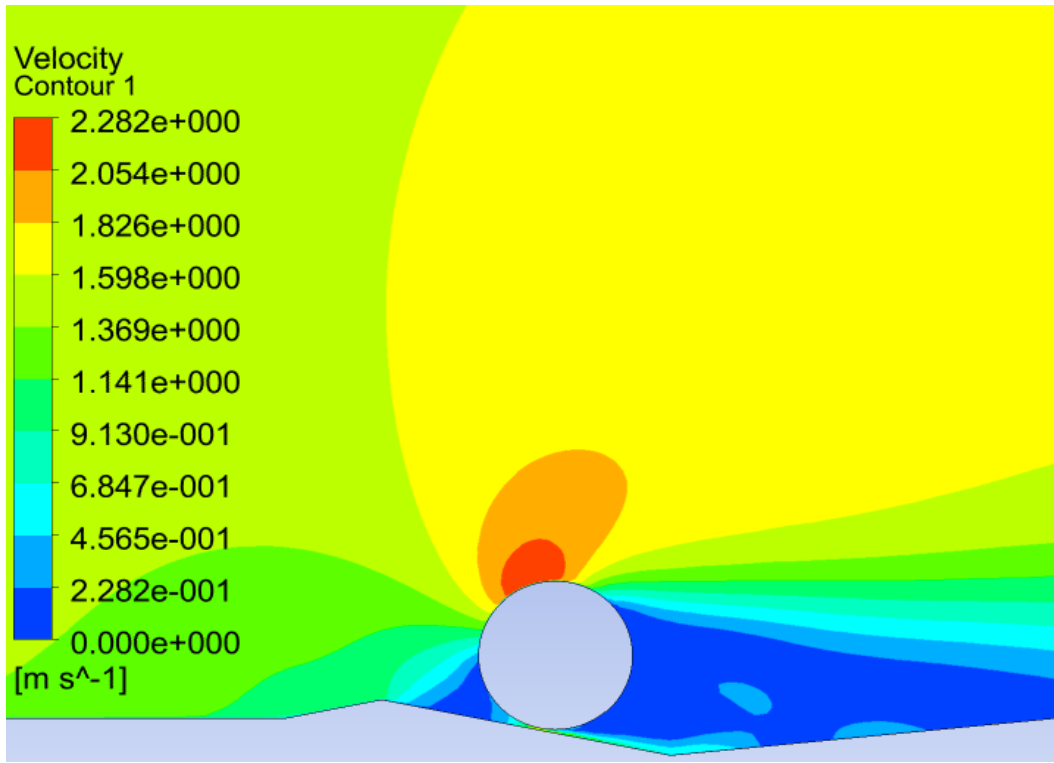
Figure 7.6b Contour of pipeline at position -0.3
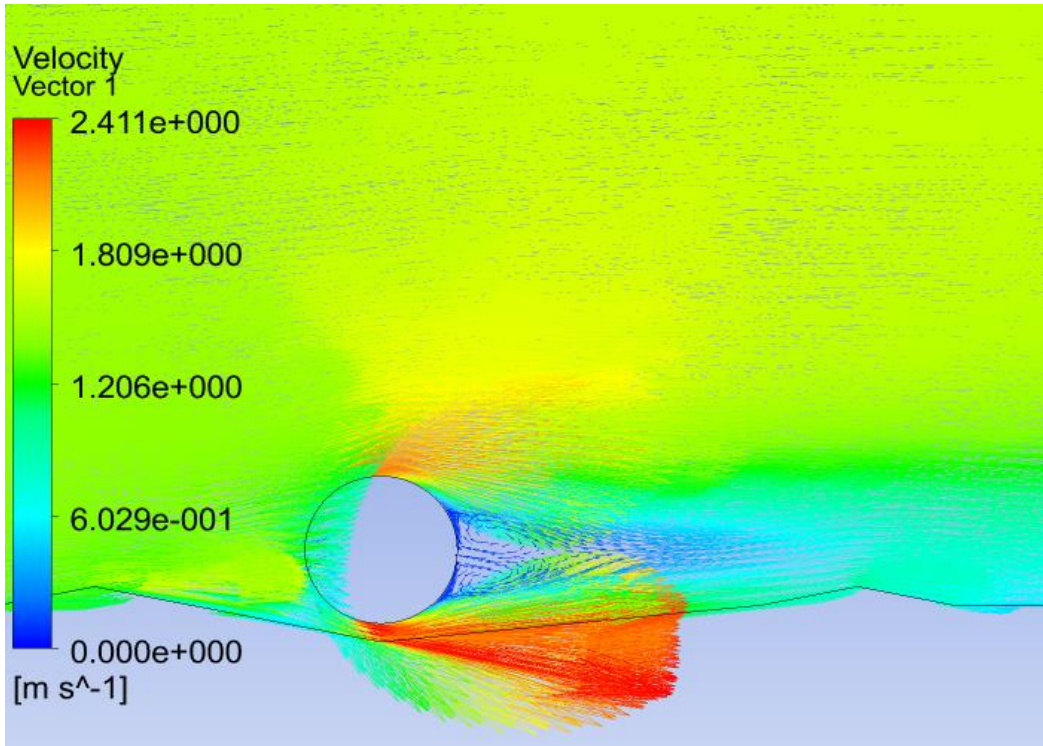
Figure 7.7a Vector of pipeline at position 0.0
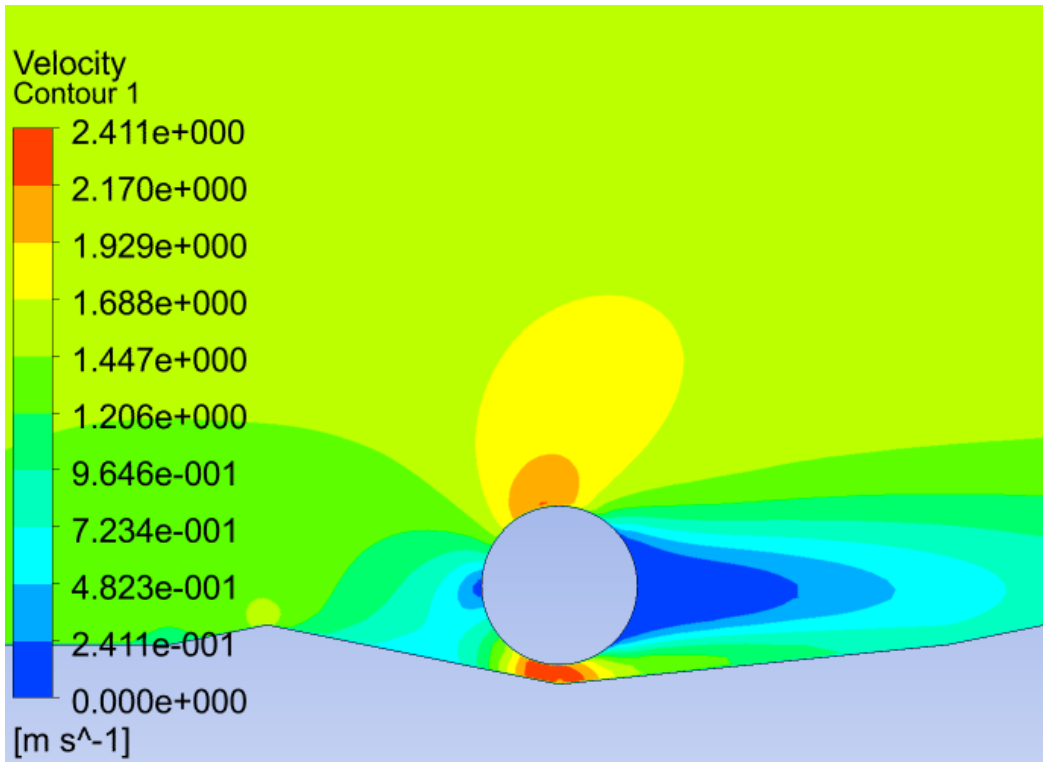
Figure 7.7b Contour of pipeline at position 0.0
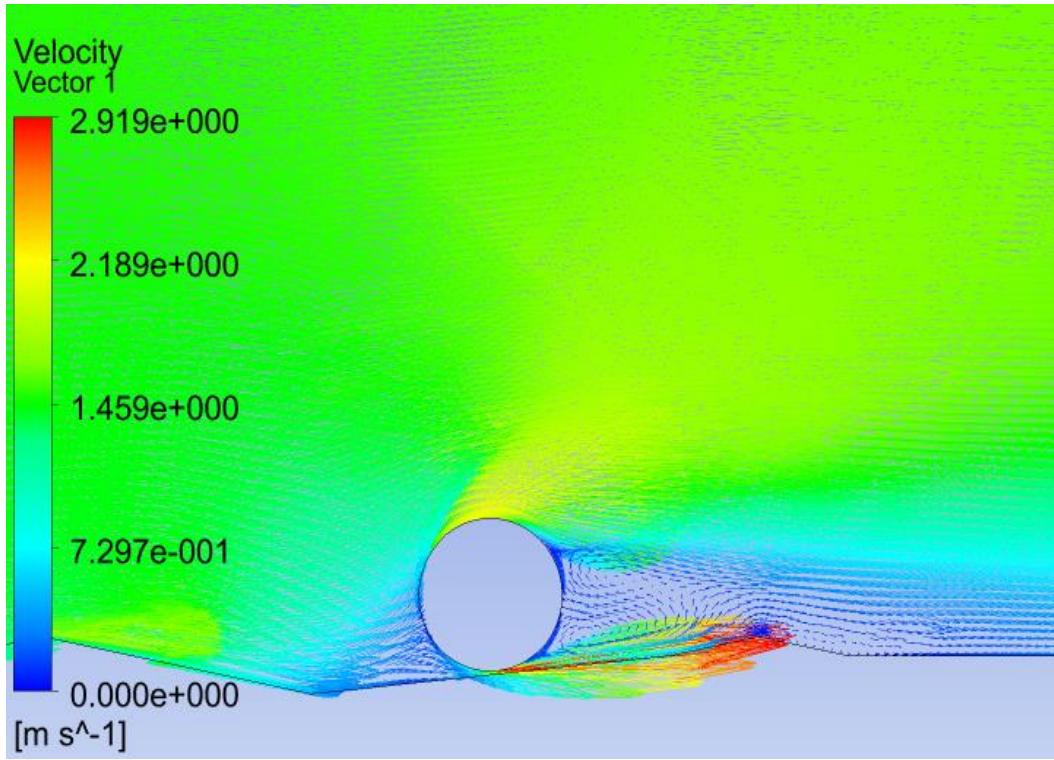
Figure 7.8a Vector of pipeline at position 0.5
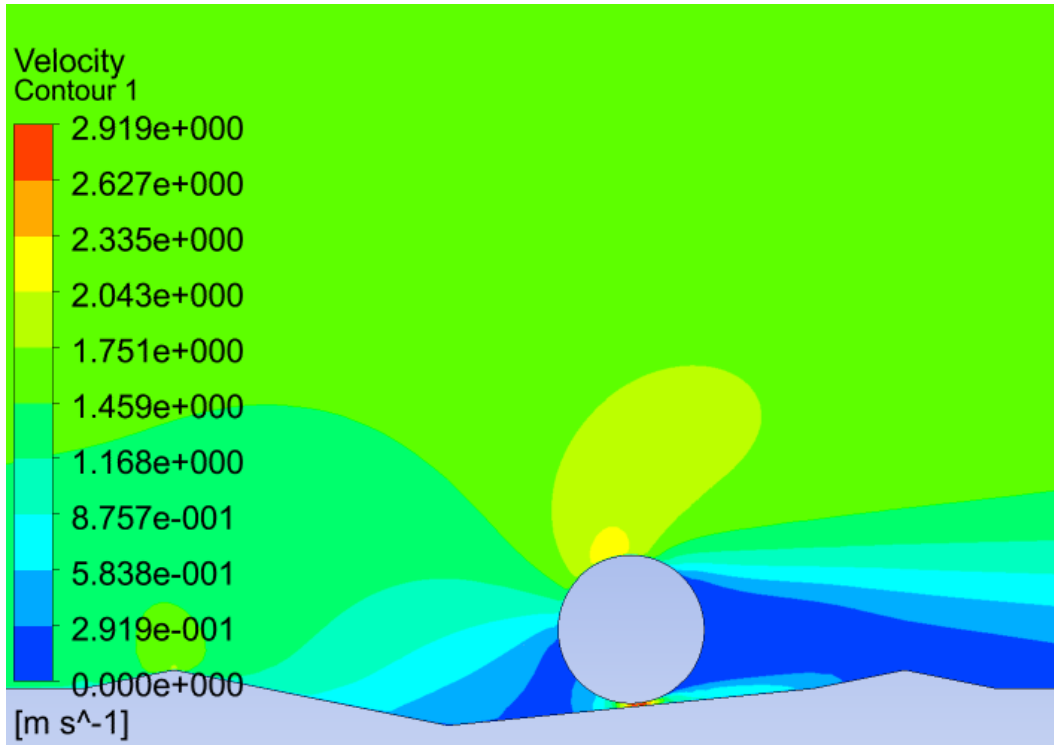
Figure 7.8b Contour of pipeline at position 0.5
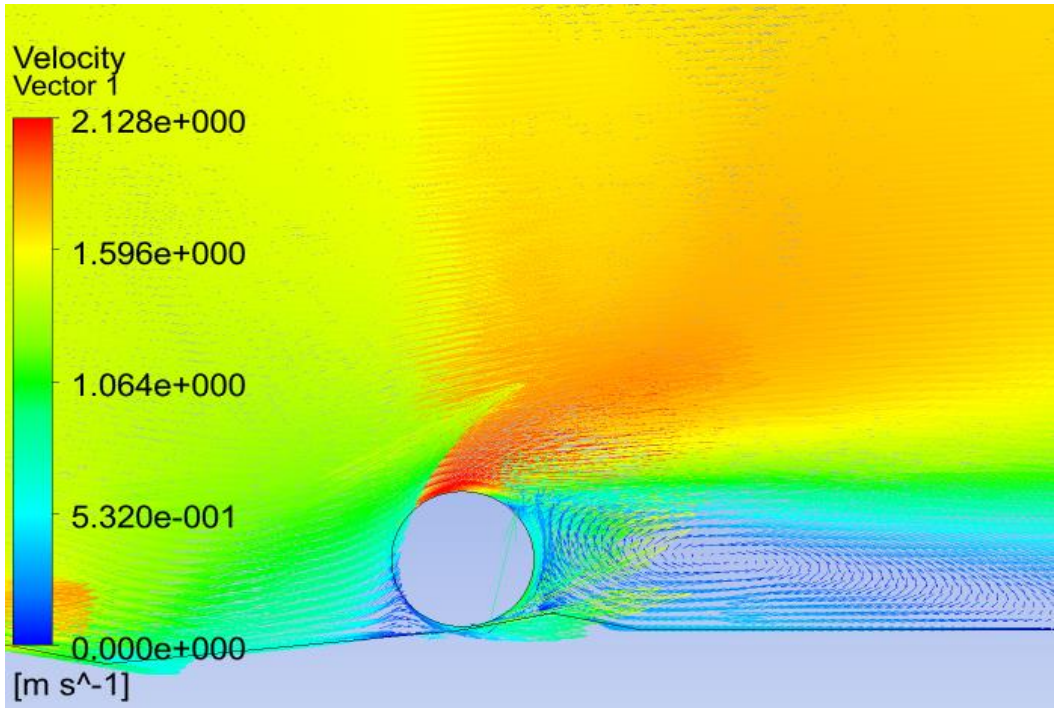
Figure 7.9a Vector of pipeline at position 1.0
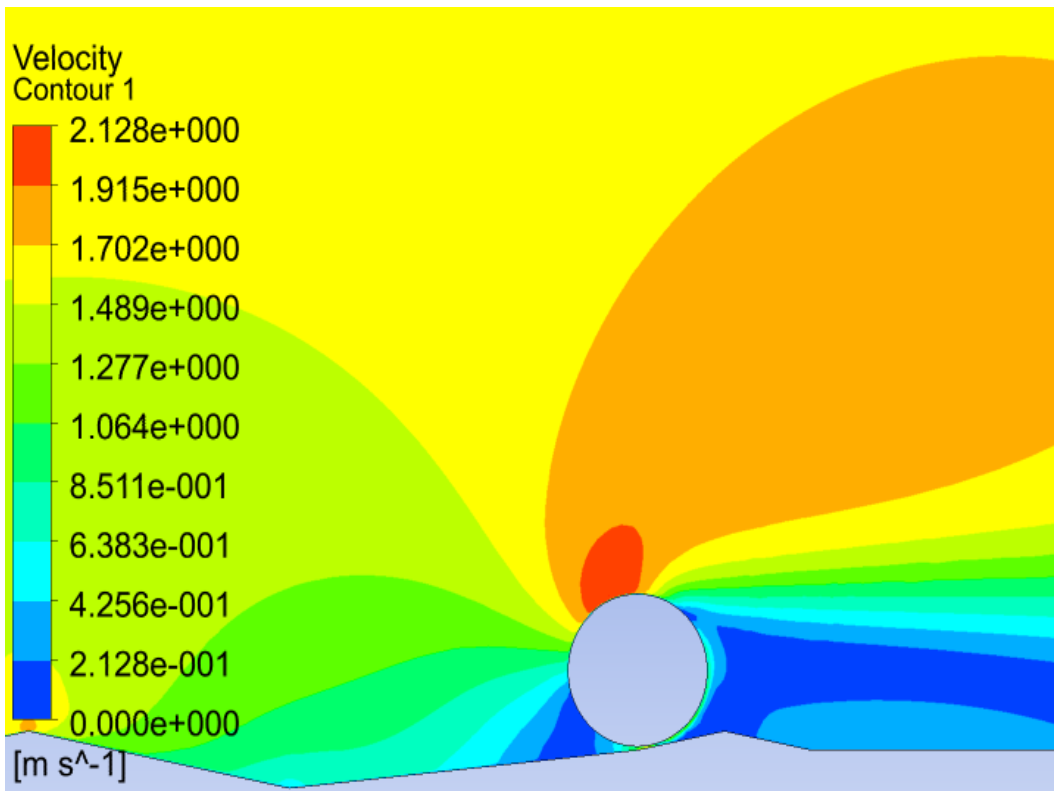
Figure 7.9b Contour of pipeline at position 1.0
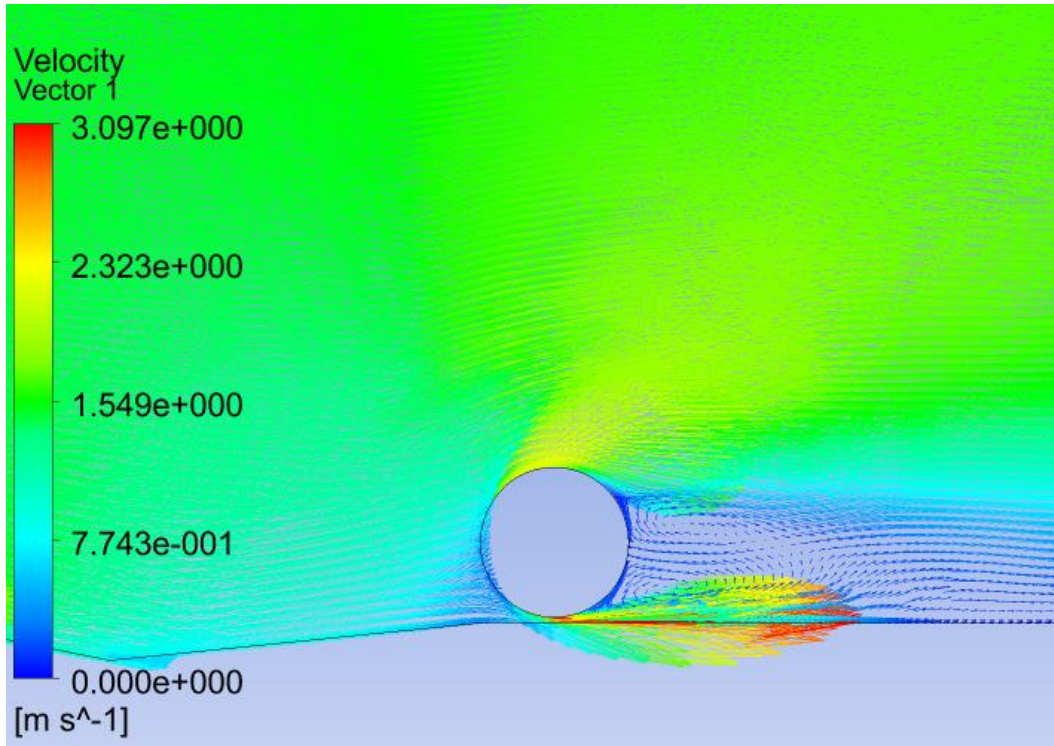
Figure 7.10a Vector of pipeline at position 1.2
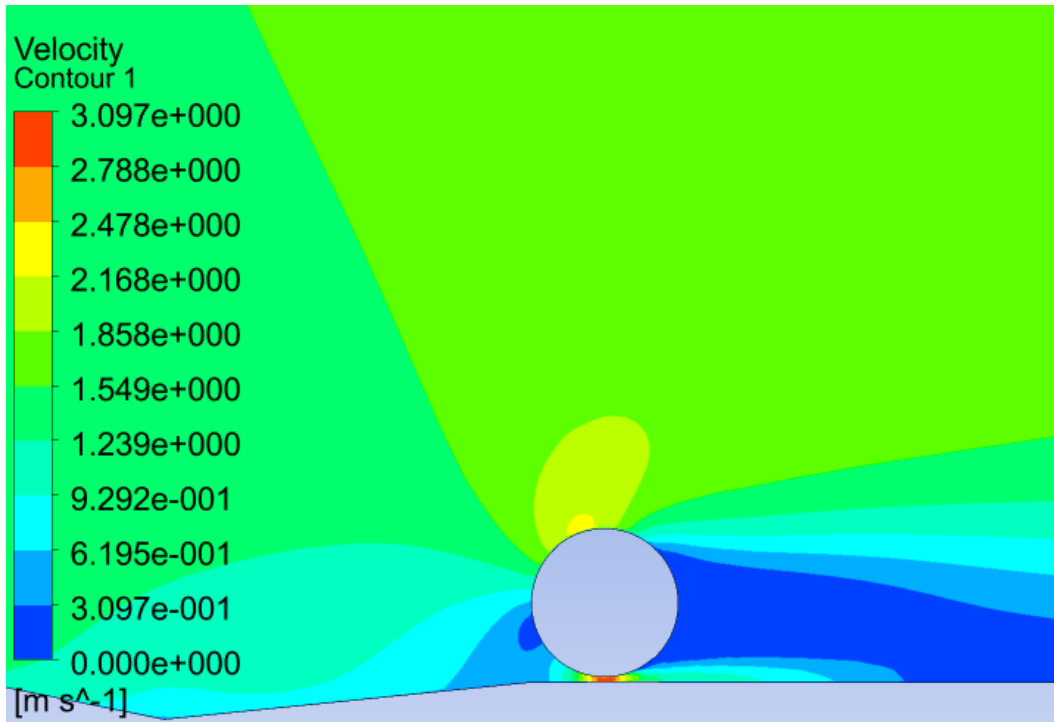
Figure 7.10b Contour of pipeline at position 1.2
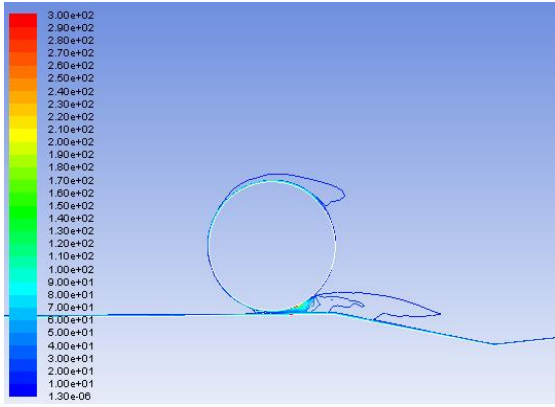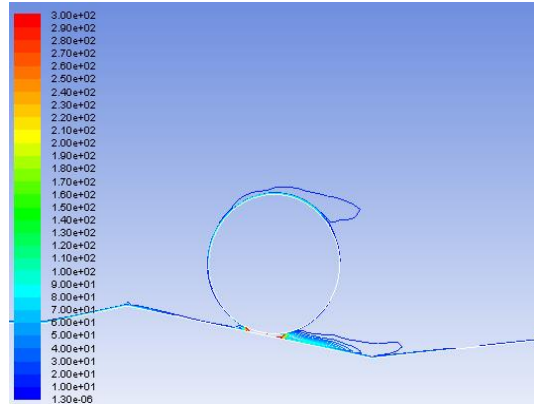
Figure 7.11a -0.7   Figure 7.11b -0.3
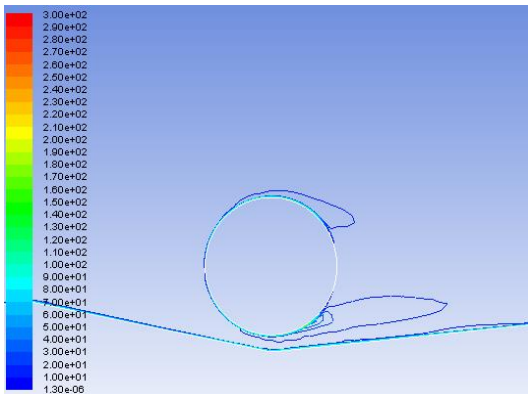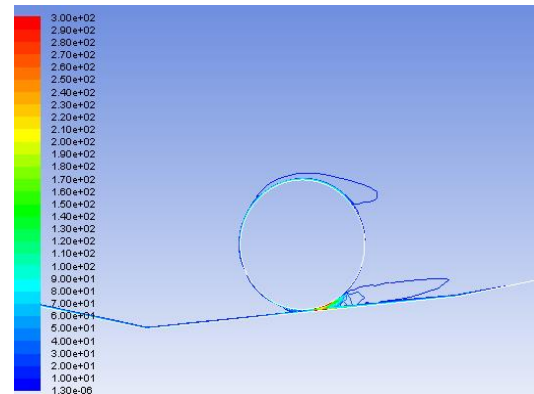
Figure 7.11c 0.0   Figure 7.11d 0.5
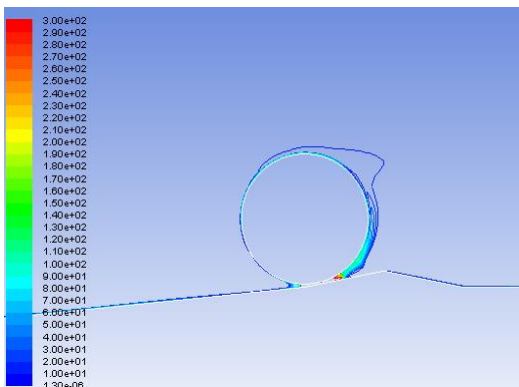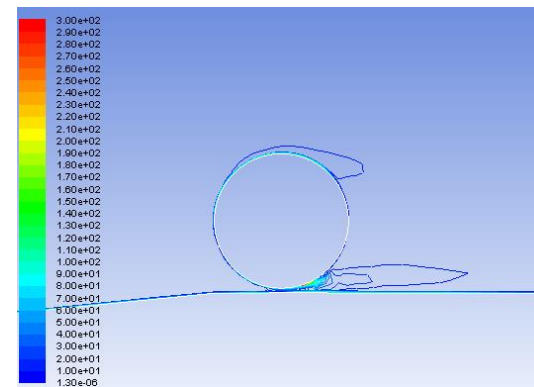
Figure 7.11e 1.0   Figure 7.11f 1.2

Figure 7.11 Vorticity plot for the mechanism of scour under pipeline

7.2 Results for Scouring Effect on Wall Shear Stress and Pressure Coefficient

Figures 7.12a, 7.13a, 7.14a, 7.15a, 7.16a and 7.17a show the wall shear stress plots (that is, shear stress in the layer of the fluid in contact with the pipe wall) and corresponding pressure coefficient plots Figure 7.12b, 7.13b, 7.14b, 7.15b, 7.16b and 7.17b (that is the relative pressure at each point across the pipe wall) for pipeline position -0.7, -0.3, 0.0, 0.5, 1.0 and 1.2. Pressure coefficient plot round circumferential position theta is as shown in Appendix F. Maximum wall shear stress decreases from position -0.7 ($\approx$34 Pa) to position -0.3 ($\approx$15 Pa) as pipeline embedment increases and then increases slightly at position 0.0 ($\approx$20 Pa) maximum embedment. As pipeline breaks out from position 0.5, 1.0 and 1.2 there is an increase in maximum shear stress to $\approx$30 Pa. The point of maximum shear stress which is around the midsection of the pipeline corresponds to the point of highest velocity as shown in the velocity vector plots in Figures 7.5a 7.6a, 7.7a, 7.8a, 7.9a and 7.10a. The plots also generally show that maximum wall shear stress corresponds to a minimum pressure coefficient. This is because the point of maximum shear stress represents the point in the fluid-pipe-soil interface where scouring effect is at its greatest. As shown on the velocity vector plots, the highest velocity is also at the midsection of the pipeline corresponding to the area of scouring. The lift force at the point of maximum shear stress represented by the pressure coefficient is at its minimum as pipeline is at maximum embedment. This is so for all positions except position -0.3 and 1.0 where the maximum wall shear stress is at the top of the pipe as it gets embedded at position -0.3 and breaks out at position 1.0. At both these positions pipeline instability is a result of displacement rather scouring which explains the effect that was observed in the PIPESTAB and AGA

pipe-soil interaction projects. The points of maximum wall shear stress and minimum pressure coefficient also correspond with the point of maximum velocity vector and velocity contour as shown in Figures 7.5a and 7.5b; 7.6a and 7.6b; 7.7a and 7.7b; 7.8a and 7.8b; 7.9a and 7.9b; 7.10a and 7.10b. The highest maximum wall shear stress and lowest minimum pressure coefficient is observed to be at position -0.7. As explained in section 7.1 this is the position where scouring effect is induced.
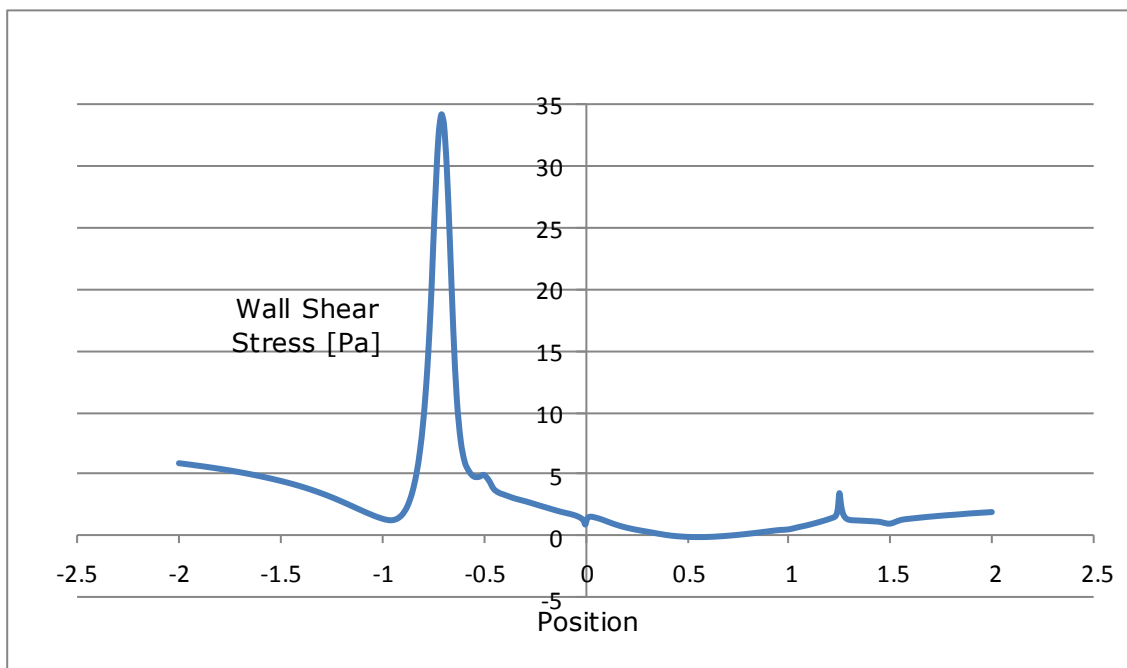
Figure 7.12a Wall shear stress of pipeline at position -0.7
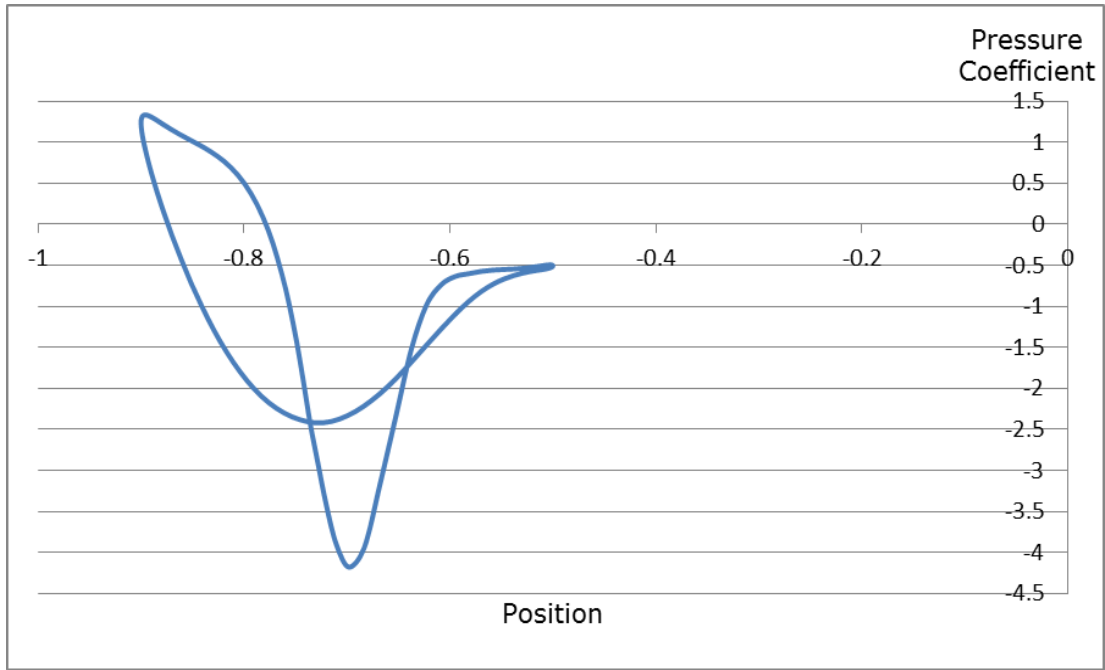
Figure 7.12b Pressure coefficient of pipeline at position -0.7
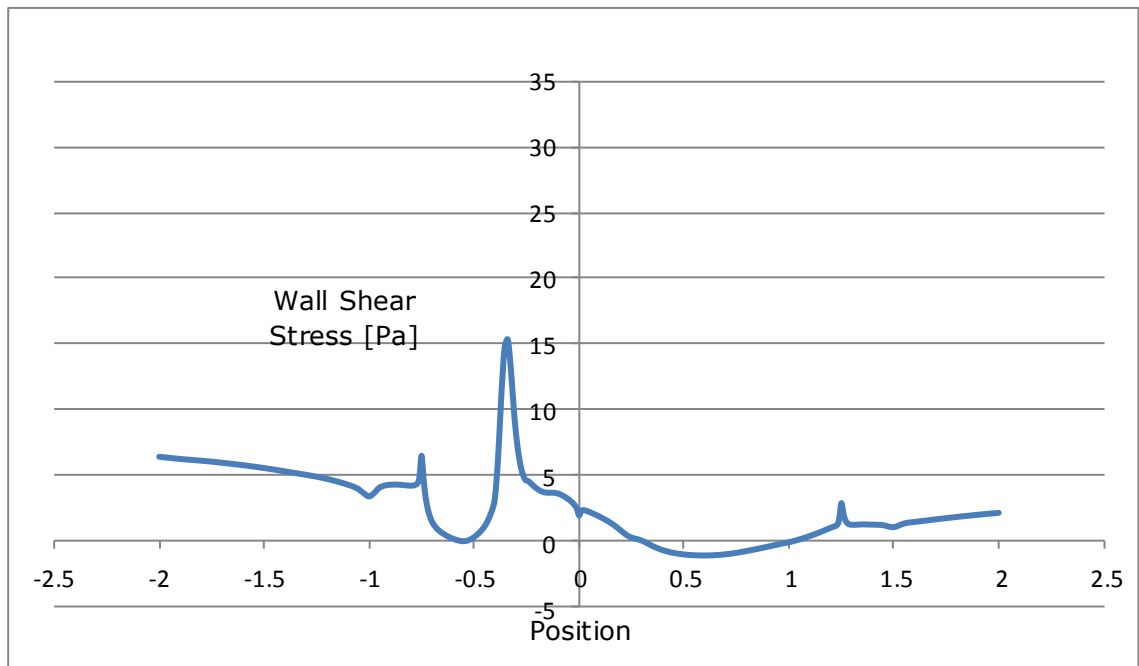
Figure 7.13a Wall shear stress of pipeline at position -0.3
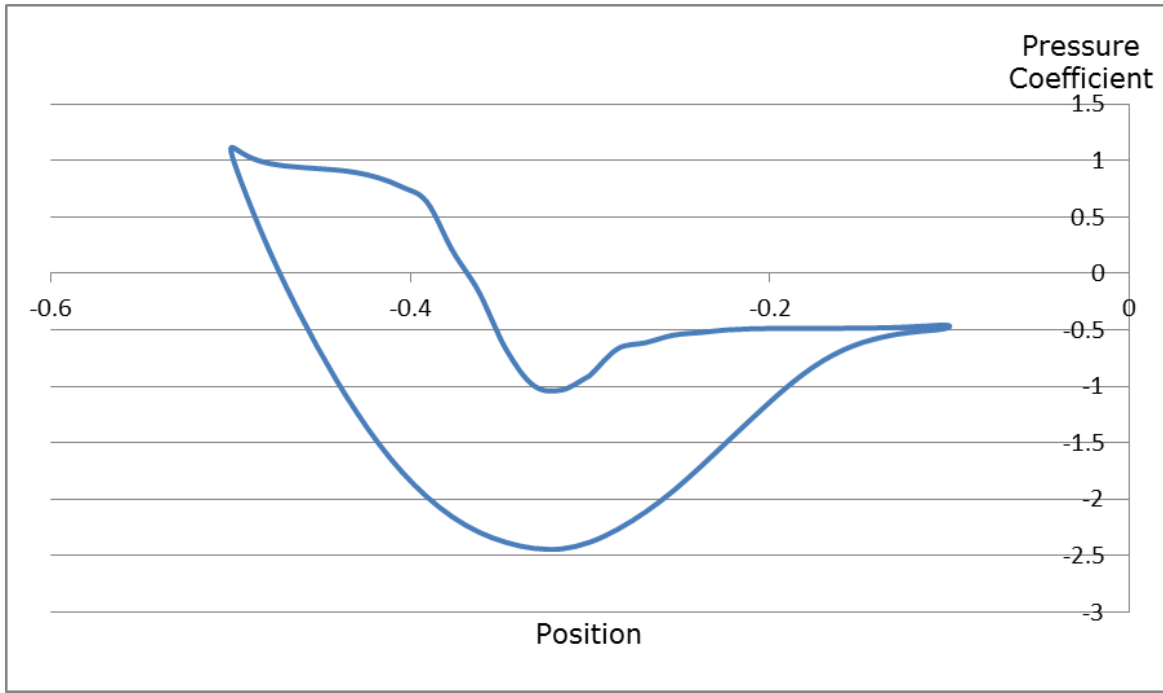
Figure 7.13b Pressure coefficient of pipeline at position -0.3
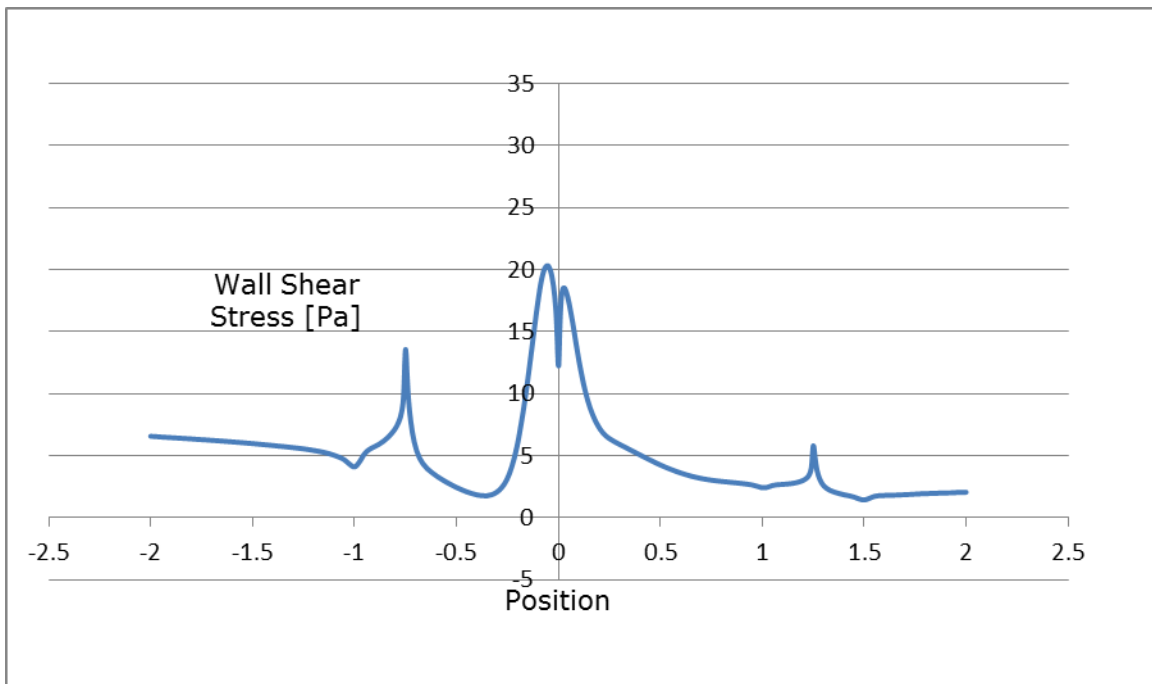
Figure 7.14a Wall shear stress of pipeline at position 0.0
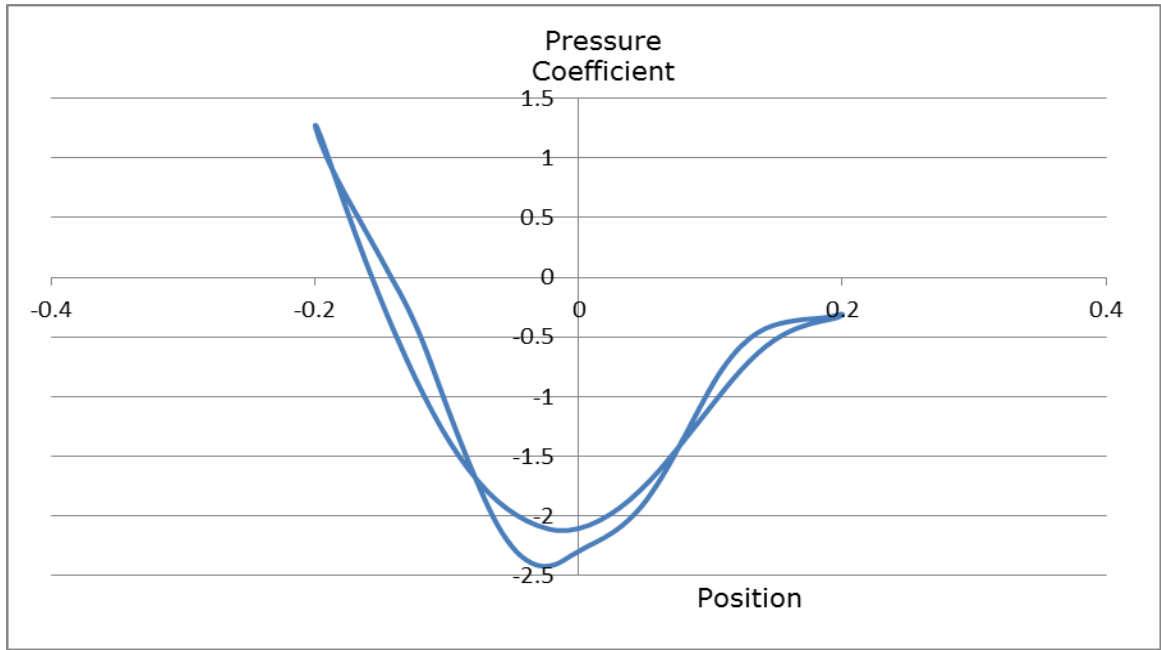
Figure 7.14b Pressure coefficient of pipeline at position 0.0
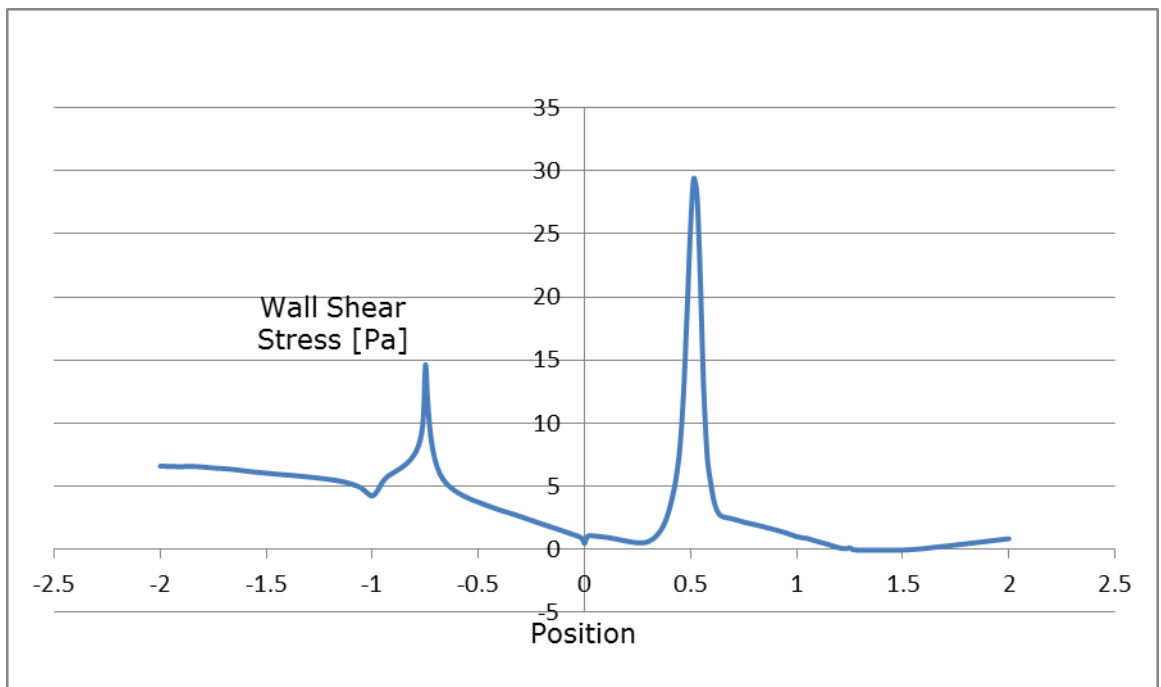
Figure 7.15a Wall shear stress of pipeline at position 0.5
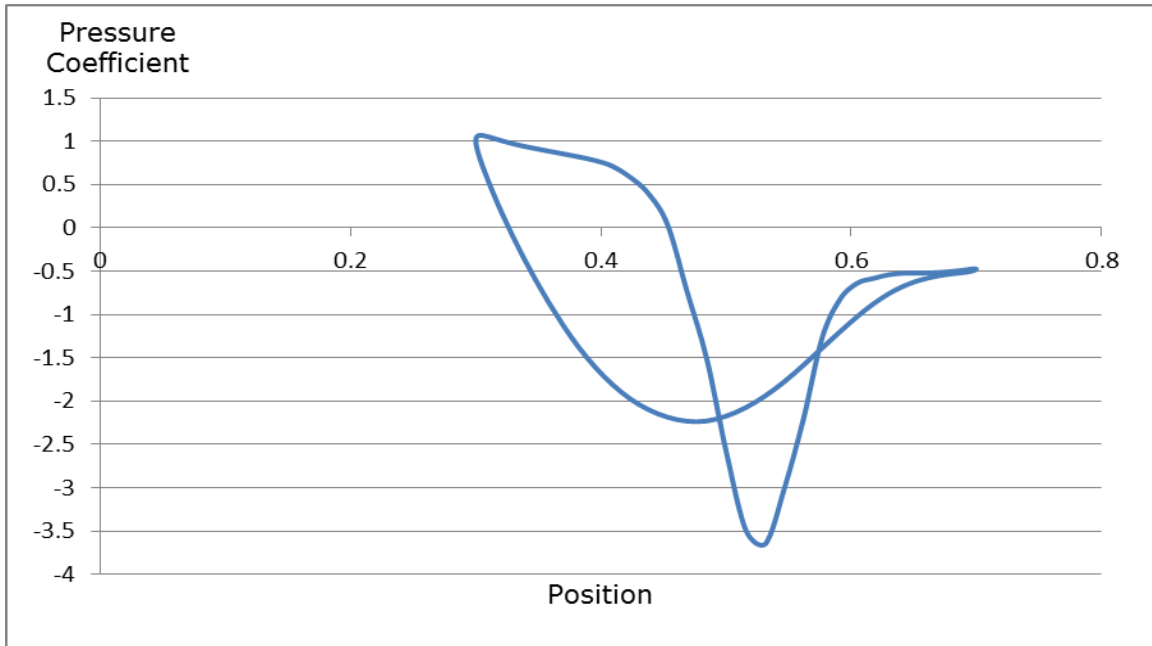
Figure 7.15b Pressure coefficient of pipeline at position 0.5
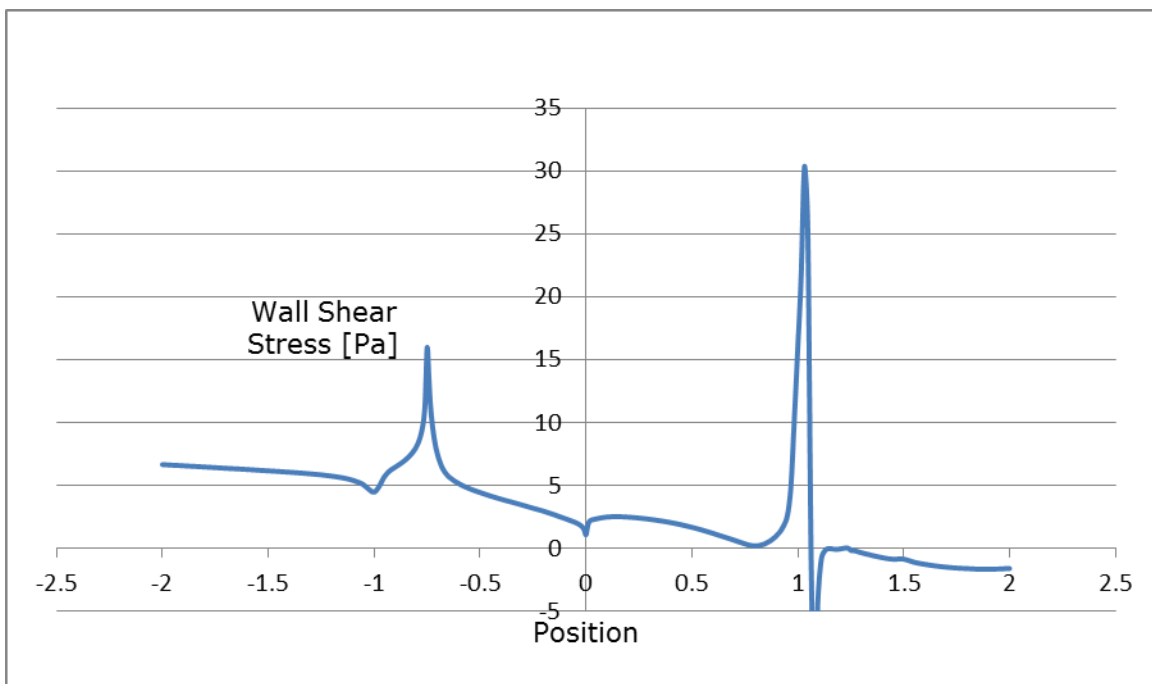
Figure 7.16a Wall shear stress of pipeline at position 1.0
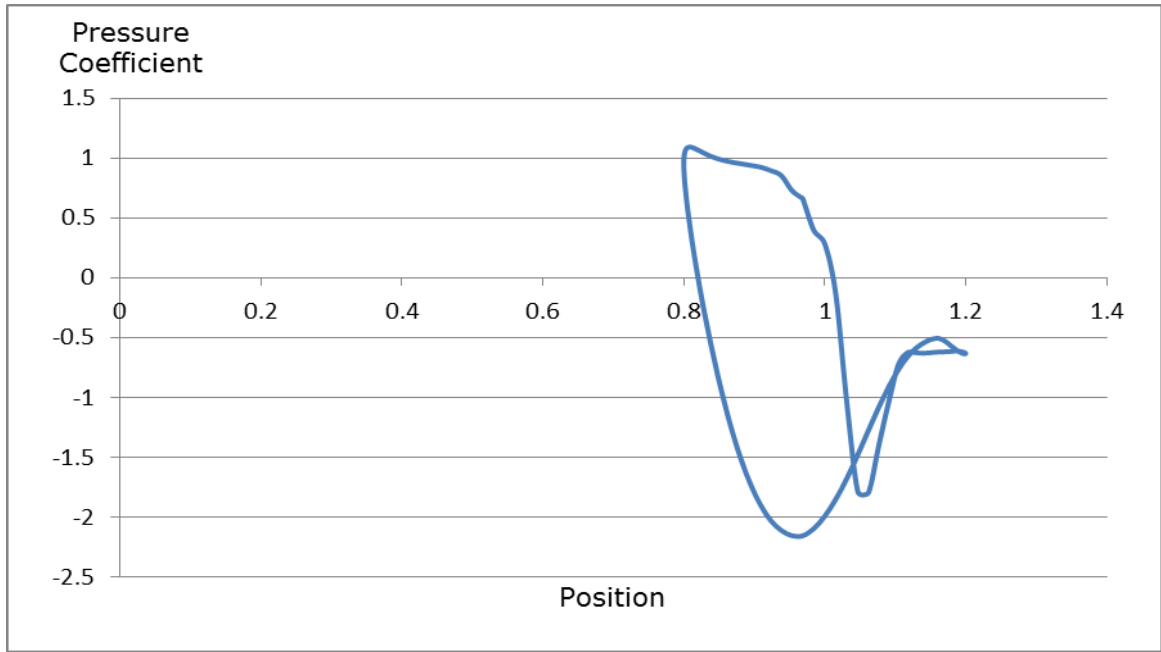
Figure 7.16b Pressure coefficient of pipeline at position 1.0
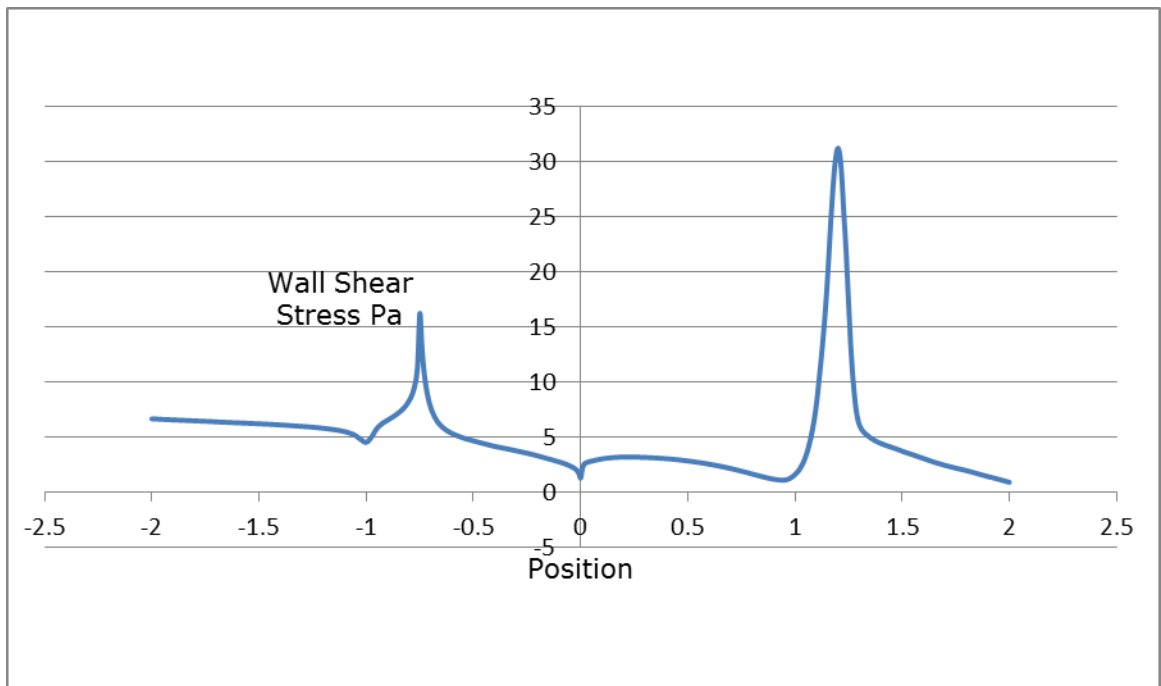
Figure 7.17a Wall shear stress of pipeline at position 1.2

125
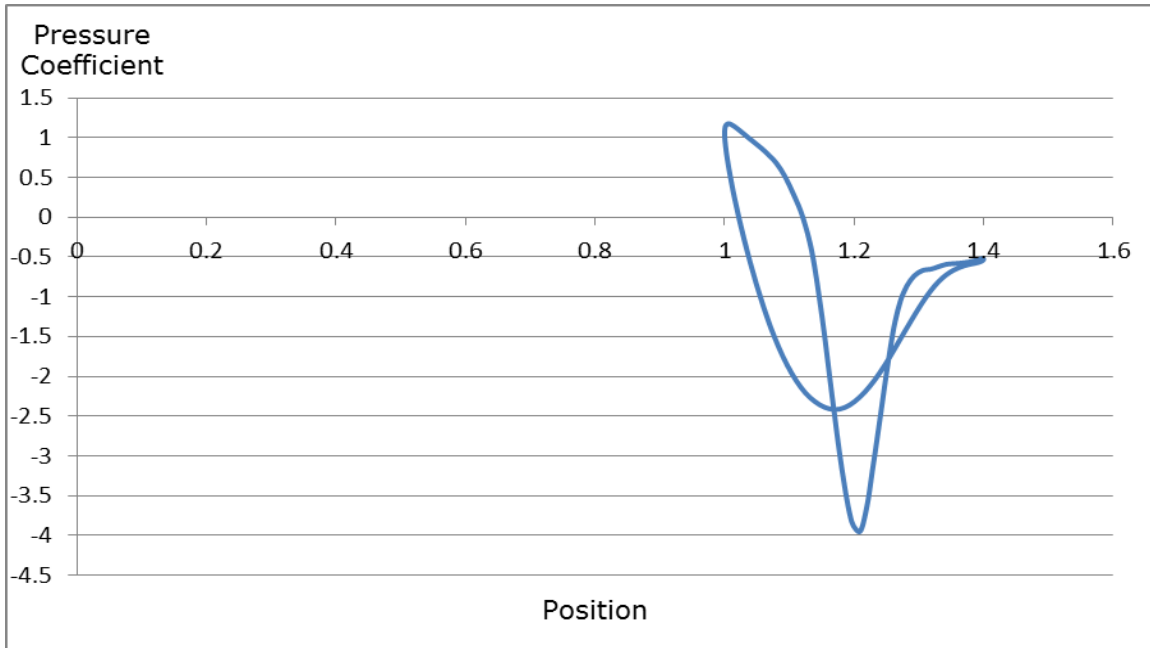
Figure 7.17b Pressure coefficient of pipeline at position 1.2

Table 7.3 and corresponding plot Figure 7.18 below shows the C_D and C_L values at the various pipeline positions 1(-0.7), 2(-0.5), 3(0.0), 4(0.5), 5(1.0) and 6(1.2). The plot shows that C_L increases with decreasing C_D from pipeline initial embedment progressing to the onset of scouring and peaks at position 0.0 (position of maximum embedment) where C_D is at its minimum. This confirms the results of the Pipe-Soil Interaction Model presented by Wagner et al (1987) which showed that there is substantial soil resistance even under high lift forces as there is an increase in pipeline embedment.

126

Table 7.3 C_D and C_L values

Pipeline Position	C_D	C_L
-0.7	2.58	0.57
-0.5	2.03	0.63
0.0	1.83	1.32
0.5	2.10	1.11
1.0	2.52	1.02
1.2	2.47	1.47
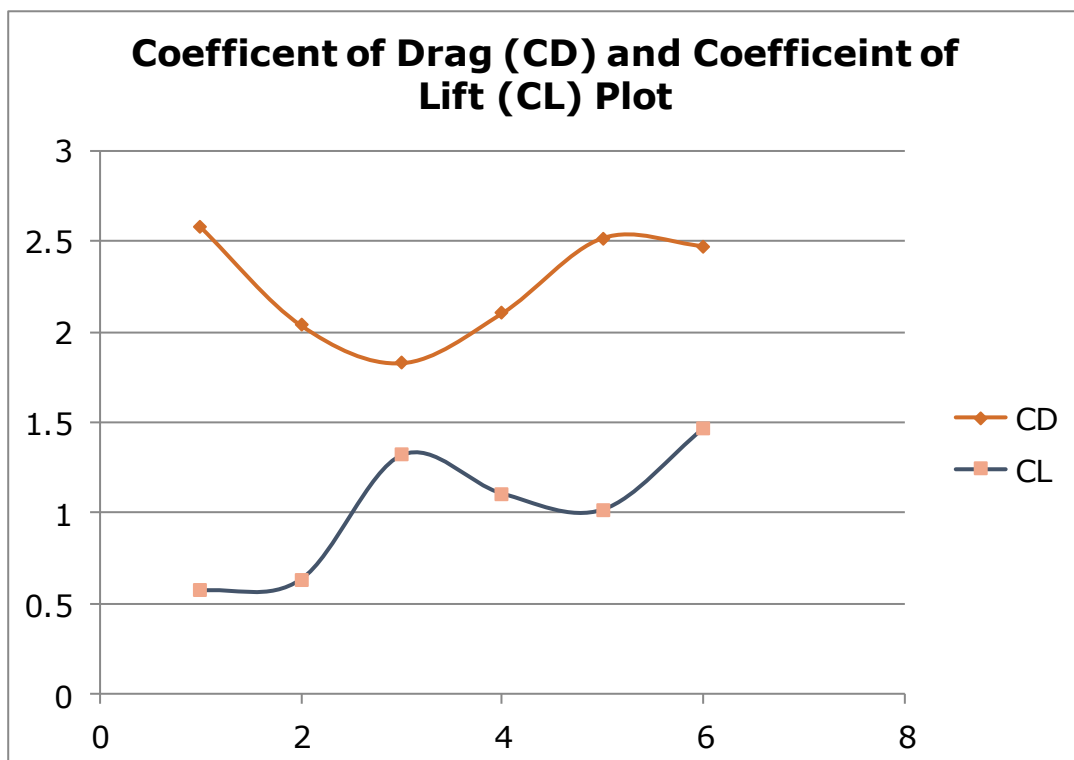
Figure 7.18 C_D and C_L plot at pipeline positions

7.3 Model Validation

This model was validated by comparing the wall interaction effects plot ($\frac{C_d}{C_{d\infty}}$ versus $\frac{H}{D}$) as stated in DNV Recommended Practice C205 (Figure 7.19) (DNV-RP-C205 2010) with that generated by the model considering unbounded flow as shown in Figure 7.20.
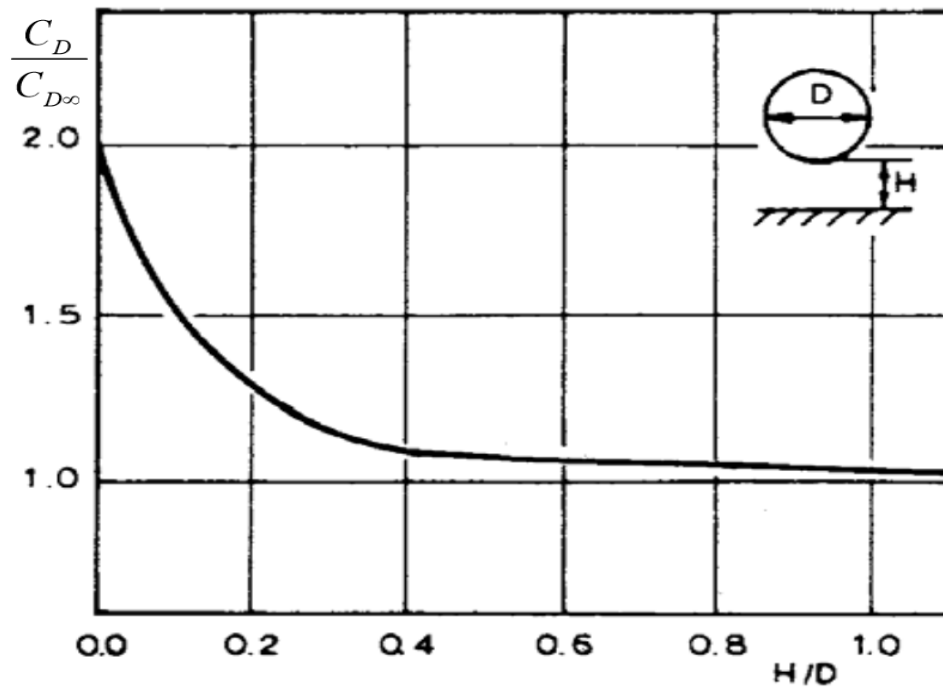
Figure 7.19 Influence of a fixed boundary on drag coefficient of a circular cylinder (DNV-RP-C205, 2010)
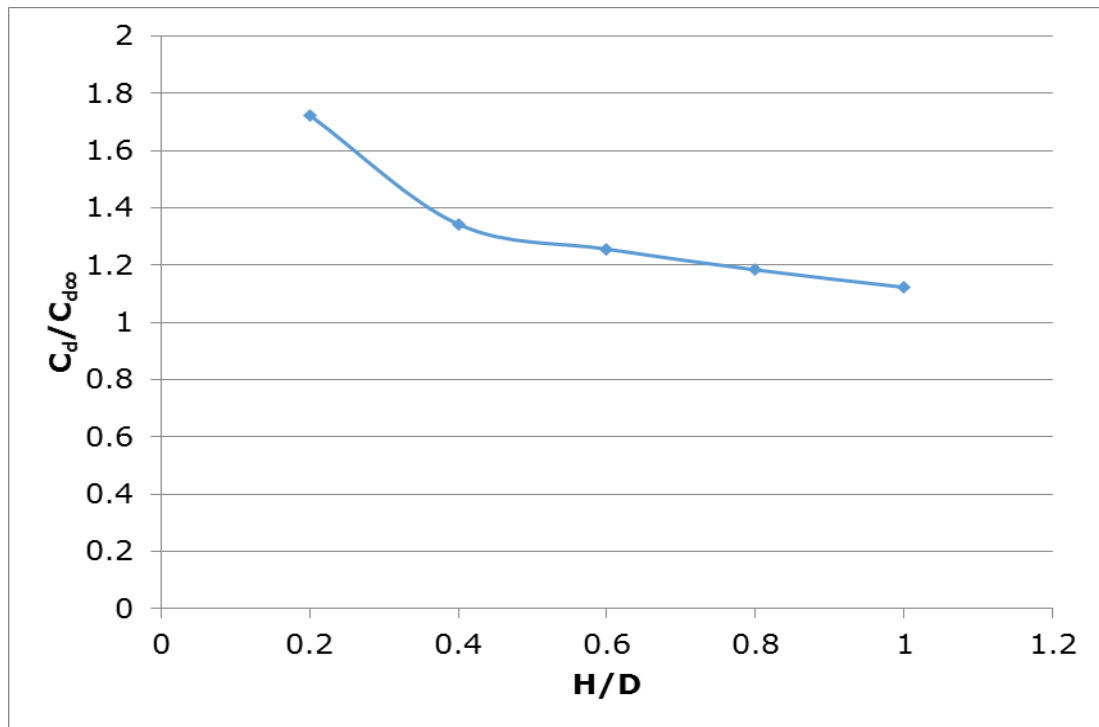
Figure 7.20 Influence of a fixed boundary on drag coefficient of a circular cylinder as generated by CFD model

7.4 Results Summary

The results from modelling scour effect shows maximum embedment (scour) is reached at the point of highest velocity vector, maximum wall shear stress (point of greatest scour effect) corresponds to minimum pressure coefficient (lift force). The model shows that embedment is a result of displacement (initial pipe position before scouring) and scouring. The displacement effect as shown in the results is in agreement with that observed in the PIPESTAB and AGA pipe-soil interaction tests, however the effect of scouring as demonstrated in the results disproves conclusion of the PIPESTAB and AGA pipe-soil interaction tests that scouring is not involved in the process of lateral pipeline instability.

The results also show C_L increases (with maximum at point of maximum embedment) as C_D decreases which confirms previous results that show that soil resistance increases with high lift forces due to increased pipe embedment.

CHAPTER 8: CONCLUSION AND RECOMMENDATION

This thesis presents a numerical study of hydrodynamics loading of a submerged pipe under embedment, passive resistance, porous sea-bed and scoured sea-bed. The computational fluid dynamics (CFD) technique applied in this research took into account the boundary layer effects, wake flow effects, vortex fields, the fluid interaction with both pipeline and seabed, and the interaction between pipeline and seabed. The boundary layer specifications used in this research included pressure outlet in place of pressure outflow to improve convergence, turbulence length scale specified using the intensity and hydraulic method, and inflation applied to ensure accurate prediction of hydrodynamic coefficients.

Wake effect which induces vortex shedding at boundary layer causes an initial reduction in lift force and increase in drag force. Vortex shedding as a result of wake effect induces further interaction between fluid and the seabed (tunnel erosion) leading to sediment mobility which results in scouring of the seabed. As hydrodynamic forces increase, scouring increases resulting in increased pipeline embedment until the break-out point is reached. Hydrodynamic forces also induce pore pressure build-up and vertical pressure on the seabed which results in liquefaction. The CFD model showed an accurate combined effect of fluid flow around a pipeline and on the seabed (considering scouring and liquefaction) when compared with previous work by Gao et al (2007) on wave-pipe-soil interaction model, Brennodden et al (1989) on energy-based

pipe-soil interaction method and Griffiths' (2012) 2D pipe-soil-fluid interaction model.

The simulation results obtained in this research are validated with past experimental and analytical results as stated above. The findings of this research work are summarised as follows;

- Passive soil resistance increases as pipe is displaced and becomes embedded, and decreases as further pipe displacement causes pipe to mount up from embedment. The results show a similar trend for both sand and clay but is approximately twice as much in sand compared to clay for the same lateral displacement.

- Lateral soil resistance increases initially as pipe is displaced then remains fairly constant as pipe displacement increases during period of embedment. Lateral soil resistance then decreases as pipe moves out of embedment and becomes constant after pipe breakout. Passive soil resistance on the other hand increases through the period of embedment until maximum embedment is reached and pipe begins to move out of embedment. As with passive resistance, lateral resistance in both sand and clay show similar trend with sand having the greater (approximately twice) value for the same lateral displacement.

- Overall, passive resistance is of greater significance for on-bottom stability analysis of subsea pipelines as it is by far greater than lateral resistance (passive resistance is about 8-10 times lateral resistance for sand and 10-16 times for clay).

- There is a critical velocity (when horizontal force equals total lateral soil resistance) above which pipe becomes unstable (that is, when horizontal force becomes greater than total lateral soil resistance). Results show

that increasing pipe weight (which induces pipe embedment) increases the critical velocity and thus ensures pipeline stability. The results also show that increasing seabed porosity increases lateral soil resistance (which increases pipe stability). Thus validating the fact that porous seabed provides more stability compared to solid seabed.

- Pipeline embedment decreases with increasing diameter (with sand having a lower degree of embedment than clay), which is the converse for pipe weight. The results from the combined effect of pipe diameter and weight shows that pipe diameter has a greater influence on embedment in sand; decrease in embedment with increasing diameter when normalised diameter. Without normalising increasing diameter will show a corresponding increase in embedment (in sand) due to increase in weight. Embedment in clay remained the same for a normalised and non-normalised case, showing increased embedment with increase in diameter. Thus pipe weight appears to have a greater influence on embedment in clay. The results also show that initial pipe embedment is due to pipe weight, increasing velocity initiates soil scouring which progresses and results in further pipe embedment until pipe moves out of embedment. Thus, a greater degree of embedment is required to maintain on-bottom stability of subsea pipeline in clay than sand.

- Maximum embedment is reached at the point of maximum wall shear stress in the fluid-pipe-soil interface which corresponds to minimum lift force (negative lift coefficient) and represents the point of maximum scour effect. The findings also show that embedment is a result of the combination of displacement (initial pipe position before scouring) and scouring.

- C_L increases as C_D decreases, and reaches maximum at the point of maximum embedment. This further validates the reason for high soil resistance and lift forces as pipeline embedment increases.

- The findings of this research have further shown the weakness of the current approach to pipeline on-bottom stability analysis and its inherent over-conservatism leading to the use of costly stabilisation techniques.

8.1 Future work

Computational fluid dynamics (CFD) model have been developed in this research work to study the complex interaction of fluid, pipeline and soil in the analysis of subsea pipeline on-bottom stability, and the observed results compared with past experimental and analytical results. The findings in this thesis can however be better validated and model refined by carrying out experimental work in line with the practical method for design approach proposed Ryan et al (2011) which is a combination of physical testing and numerical analysis, but with numerical analysis based on CFD rather than FEA as proposed. The future work thus recommended is as follows;

- Experimental study to investigate the combined effect of fluid, soil behaviour and pipeline (weight and diameter effect) on pipeline stability. As discussed in the literature review chapter of this thesis, previous experimental studies were based on modelling wave loads using mechanical actuators (with no water) rather than hydrodynamic methods. Thus an experimental study that will model wave-induced seabed scour and liquefaction and the overall effect on pipeline stability will help validate the findings of this thesis and help optimise the current approach to subsea pipeline stability.

- Conventionally hydrodynamic coefficients of $C_D=0.7$, $C_L=0.9$ $C_I=3.29$ are used in stability analysis calculations. However a large uncertainty is encountered in the application of these coefficients due to varying ambient water conditions, current velocity, Reynolds number effects, fluctuations of pressure fields near pipeline and variations in the geometric layout. These factors are mostly time dependent. Thus an experimental study to investigate the time dependence of hydrodynamic coefficients will also improve widely accepted DNV code for subsea pipeline stability design.

REFERENCES

ALLEN, D.W. et al., 1989. Submarine pipeline on-bottom stability: recent AGA research. *Offshore Technology Conference*. 1-4 May 1989. Texas: Offshore Technology Conference. pp. 121-132.

ANSYS FLUENT [computer program] 2015. Release 16.2. Pennsylvania, PA: ANSYS Inc.

BAI, Y. and BAI, Q., 2005. Pipelines and risers. Oxford: Elsevier. pp. 129-136.

BRANSBY, F. et al., 2014. Sediment mobility effects on seabed resistance for unburied pipelines. *Offshore Technology Conference*. 5-8 May 2014. Texas: Offshore Technology Conference. pp. 2205-2221.

BRENNODDEN, H. et al., 1989. An energy based pipe-soil interaction Model. *Offshore Technology Conference*. May 1-4, 1989. Texas: Offshore Technology Conference. pp. 147-158.

CHAO, J.C., LAMBRAKOS, K.F. and VERLEY, R.L.P., 1989. Hydrodynamic force characteristics for submarine pipelines. *Offshore Technology Conference*. 1-4 May 1989. Texas: Offshore Technology Conference. pp. 181-188.

CONSTANTINIDES, Y., OAKLEY, O. and HOLMES, S., 2005. Modelling GBS hydrodynamics with CFD. *Offshore Technology Conference*. 2-5 May 2005. Texas: Offshore Technology Conference. pp. 1-6.

DAMGAARD, J.S. and PALMER, A.C., 2001. Pipeline stability on a mobile and liquefied seabed: a discussion of magnitudes and engineering implications. *20TH International Conference of Offshore Mechanics and Artic Engineering*. 3-8 June 2001. Rio de Janeiro: Polar and Arctic Pipeline Technology. pp. 195-204

DET NORSKE VERITAS, 2000. Offshore standard DNV-OS-F101: Submarine pipeline systems. Det Norske Veritas.

DET NORSKE VERITAS, 2010. Recommended practice DNV-RP-C205: Environmental conditions and environmental loads. Det Norske Veritas.

DET NORSKE VERITAS, 2011. Recommended practice DNV-RP-H103: Modelling and analysis of marine operations. Det Norske Veritas. pp. 25

DET NORSKE VERITAS, 2010. Recommended practice DNV-RP-F109: On-bottom stability design of submarine pipelines. Det Norske Veritas. pp. 17-19.

DET NORSKE VERITAS, 2013. Offshore standard DNV-OS-F101: Submarine pipeline systems. Det Norske Veritas.

EVANS, D.J., 1970. Analysis of wave force data. *Journal of Petroleum Technology*, pp. 347-358.

FALTINSEN, O.M., 1993. Sea loads on ships and offshore structures. Cambridge: Cambridge University Press. pp. 223-252.

GAO, F. and JENG, D., 2005. A new design method for wave-induced pipeline stability on a sandy seabed. [online]. The University of Sydney. Available from: http://www.civil.usyd.edu.au/publications/r860.pdf [Accessed 30 June 2009].

GAO, F. et al., 2002. An experimental study for wave-induced instability of pipelines: the breakout of pipelines. *Journal of Applied Ocean Research*, 24(2), pp. 83-90.

GAO, F. et al., 2005. Wave-Induced pipeline on-bottom stability: comparison between pipe-soil and wave-pipe-soil interaction models. In: *Proceedings of the fifteenth International Offshore and Polar Engineering Conference*. 19-24 June 2005. Seoul: The International Society of Offshore and Polar Engineers. pp. 109-114.

GAO, F. et al., 2006. Experimental study of pipeline stability on sandy seabed under the influence of ocean currents. In: *Proceedings of the Seventh International Society of Offshore and Polar Engineers Pacific/Asia Offshore Mechanics Symposium*. 17-21 September 2006. Dalian: International Society of Offshore and Polar Engineers. pp. 152-156.

GAO, F. et al., 2007. Ocean currents-induced pipeline lateral stability on sandy seabed. *Journal of Engineering Mechanics*, 133(10), pp. 1086-1092.

GAO, F.P., GU, X.Y. and JENG, D.S., 2003. Physical modelling of untrenched submarine pipeline instability. *Journal of Ocean Engineering*, 30(10), pp. 1283-1304.

GAO, F., JENG, D.S. and WU, Y., 2006. Improved analysis method for wave-induced pipeline stability on sandy seabed. *Journal of Transportation Engineering*, 132(7), pp. 590-595

GRIFFITHS, T., 2012. Development of a novel 2D pipe-soil-fluid interaction model for subsea pipeline stability design. *Proceedings of the 22nd International Offshore and Polar Engineering Conference*. 17-22 June 2012. Rhodes: International Society of Offshore and Polar Engineers. pp. 327-336.

GROH, R., 2016. *Boundary layer separation and pressure drag* [online]. 15 October 2016. Available from:

http://aerospaceengineeringblog.com/boundary-layer-separation-and-pressure-drag/ [Accessed 24 February 2017].

HALE, J.R., LAMMERT, W.F. and ALLEN, D.W., 1991. Pipeline on-bottom stability calculations: comparison of two state-of-the-art methods and pipe-soil model verification. *Offshore Technology Conference*. 6-9 May 1991. Texas: Offshore Technology Conference. pp. 567-582.

KAMARUDIN, M.H., 2005. Numerical Modelling of Hydrodynamics Coefficients for Piggyback Pipelines. Thesis, UWA.

KIRCA, O., SUMER, B.M. and FREDSOE, J., 2012. Wave liquefaction in soils with clay content. *Proceedings of the 8th International Conference on Coastal and Port Engineering in Developing Countries.* 20 -24 Feb. Chennai, India: pp. 395-402

KNUT, T. et al., 2009. A stability design rationale – a review of present design approaches. *Proceedings of the ASME 28th International Conference on Ocean, Offshore and Artic Engineering*. 31 May-5 June 2009. Hawaii: ASME. pp. 717-729.

LAMBRAKOS, K.F., 1982. Seabed wave boundary layer measurements and analysis. *Journal of Geophysics*, 87(C6), pp. 4171-4189.

LAMBRAKOS, K.F., et al., 1987. Wake Model of hydrodynamic forces on pipelines. *Journal of Ocean Engineering*, 14(2). pp. 117-136

LUO, C. and GAO, F., 2008. Numerical investigation on the onset of tunnel erosion underneath a submarine pipeline in currents. *Proceedings of the Fourth International Conference on Scour and Erosion.* 5-7 November 2008. Tokyo. pp. 214-219.

LYONS, C.G., 1973. Soil Resistance to lateral sliding of marine pipelines. *Offshore Technology Conference*. 29 April-2 May1973. Texas: Offshore Technology Conference. pp. 479-484.

MARBUS, G.D., 2007. Verification of the water forces on stinger of Allseas' Solitaire. Delft: Allseas Engineering BV. pp. 7-12.

MOUSSELLI, A.H., 1981. Offshore pipeline design, analysis, and methods. Tulsa: Pennwell. pp. 33-69.

PALMER, A.C., 1996. A flaw in the conventional approach to stability design of pipelines. *Proceedings of the 19th Annual Offshore Pipeline Technology Conference*. 15-16 February 1996. Amsterdam: Offshore Pipeline Technology. pp. 1-10.

PALMER, A.C. and KING, R.A., 2011. Subsea Pipeline Engineering. 2nd ed. Tulsa: Pennwell. pp. 361-389.

REN, Y. and LIU, Y., 2013. The analysis of pipeline's penetration laid on the elastic-plastic seabed based on the ABAQUS software. *Journal of Advanced Materials Research*, 748, pp. 416-420.

RYAN, J. et al., 2011. A fluid-pipe-soil approach to stability design of submarine pipelines. *Offshore Technology Conference*. 2-5 May 2011. Texas: Offshore Technology Conference. pp. 1-13

SABAG, R., 1999. Wake II Model for hydrodynamic forces on marine pipelines for the wave plus current case. Texas: Texas A & M University.

SABAG, S.R., EDGE, B.L. and SOEDIGDO, I., 2000. Wake II Model for hydrodynamic forces on marine pipelines including waves and currents. *Journal of Ocean Engineering*, 27(12), pp. 1295-1319.

SCHLICHTING, H., 1979. *Boundary-layer theory*. 7th ed. New York: McGraw-Hill. pp. 1-17.

SOEDIGDO, I.R., LAMBRAKOS, K.F. and EDGE, B.L., 1998. Prediction of hydrodynamic forces on submarine pipelines using an improved Wake II Model. *Journal of Ocean Engineering*, 26(5), pp. 431-462.

SUMER, B.M. and FREDSOE, J., 1999. Wave scour around structure. In: LUI, P.L.F., ed. *Advances in Coastal and Ocean Engineering*. Vol. 4. New Jersey: World Scientific Publishing Company. pp. 191-249.

SUMER, B.M. and FREDSOE, J., 2002. *The mechanics of scour in the marine environment*. Vol 17. London: World Scientific Publishing Co. Pte. Ltd. pp. 15-66

SUMER, B.M. and FREDSOE, J., 2006. Hydrodynamics around cylindrical structures. Revised Ed. Singapore; London: World Scientific Publishing. pp. 1-120.

SUMER, B.M., 2014. *Liquefaction around marine structures*. Singapore; London: World Scientific Publishing. pp. 6-150

THUSYANTHAN, N.I., 2012. Seabed soil classification, soil behaviour and pipeline design. Proceedings of the Offshore Technology Conference. 30 April–3 May. Houston, Texas: Offshore Technology Conference. pp. 1793-1803.

TU, J., YEOH, G. and LIU, C., 2013. Computational fluid dynamics a practical approach. 2nd ed. Amsterdam; Boston: Elsevier/Butterworth-Heinemann.

UNIVERSITY OF CAMPINAS. FACULTY OF MECHANICAL ENGINEERING. Flow around a cylinder in steady current. [online]. Campinas, Sao Paulo Brasil: University of Campinas. Available from: http://www.fem.unicamp.br/~phoenics/SITE_PHOENICS/AULAS/GRADE%20&%20MALHA/wake%20of%20bodies%206248_chap01.pdf [Accessed 18 September 2015]

VERLEY, R.L.P., LAMBRAKOS, K.F. and REED, K., 1987. Prediction of hydrodynamic forces on seabed pipelines. *Offshore Technology Conference*. 27-30 April 1987. Texas: Offshore Technology Conference. pp. 171-180.

VERSTEEG, H.K. and MALALSEKERA, W., 2007. An introduction to computational fluid dynamics: the finite element method. Essex: Longman Scientific & technical. pp. 1-20

WADE, B.G. and DWYER, M., 1978. Application of Morison's equation to fixed offshore platforms. *Journal of Petroleum Technology*, pp. 447-454.

WAGNER, D.A. et al., 1987. Pipe-Soil interaction model. *Offshore Technology Conference*. 27-30 April 1987. Texas: Offshore Technology Conference. pp. 181-190.

WANG, J. et al., 2010. Uplift resistance of buried pipelines at low cover-diameter ratios. *Offshore Technology Conference*. 3-6 May 2010. Texas: Offshore Technology Conference. pp. 1-11.

WILSON, J.F., 2002*. Dynamics of offshore structures*. New Jersey: John Wiley & Sons Inc.

WOLFRAM, W.R., GETZ, J.R. and VERLEY, R.L.P., 1987. PIPESTAB project: improved design basis for submarine pipeline stability. *Offshore Technology Conference*. 27-30 April 1987. Texas: Offshore Technology Conference. pp. 153-158.

ZHAO, M. et al., 2007. Hydrodynamics Forces on Dual Cylinders of Different Diameters in Steady Currents. *Journal of Fluid and Structures*, 23, pp. 59-83.

ZIETOUN, H.O. et al., 2008. Pipeline stability-state of the art. *Proceedings of the ASME 27th International Conference on Offshore Mechanics and Artic Engineering*. 15-20 June 2008. Estoril: ASME. pp. 213-228.

BIBLIOGRAPHY

ABEELE, V.F. and VOORDE, V.J., 2011. Stability of offshore pipelines in close proximity to the seabed. *6TH Pipeline Technology Conference*. 4-5 April 2011. Hannover: Pipeline Technology Conference.

BEATTIE, J.F., BROWN, L.P. and WEBB, B., 1971. Lift and drag forces on a submerged circular cylinder. *Offshore Technology Conference*. 19-21 April 1971. Texas: Offshore Technology Conference. pp. 319-328.

BRAESTRUP, M.W. et al., 2005. Design and Installation of Marine Pipelines. First Edition Oxford: Blackwell Publishing Co. pp. 107-108.

BRYNDUM, M.R. and JACOBSEN, V.B., 1983. Hydrodynamic forces from wave and current loads on marine pipelines. *Offshore Technology Conference*. 2-5 May 1983. Texas: Offshore Technology Conference. pp. 95-102.

CARDOSO, C.O. and SILVEIRA, R.M.S., 2010. Pipe-soil interaction behavior for pipelines under large displacements on clay soils - a model for lateral residual friction factor. *Offshore Technology Conference*. 3-6 May 2010. Texas: Offshore Technology Conference. pp. 1-15.

CHEUK, C.Y. and BOLTON, M.D., 2006. A technique for modelling the lateral stability of on-bottom pipelines in a small drum centrifuge. In: NG,

C.W.W., ZHANG, L.M. and WANG, Y.H., ed. *Physical modelling in geotechnics*. *Proceedings of the sixth International Conference of Physical Modelling in Geotechnics.* 4-6 August 2006. Hong Kong: ICPMG. pp. 715-721.

FODA, M.A., CHANG, J. and LAW, A., 1990. Wave-induced breakout of half-buried marine pipes. *Journal of Waterways, Port, Coastal Ocean Engineering*, 116(2), pp. 267-286.

GAO, F.P., JENG, D.S. and SEKIGUCHI, K., 2003. Numerical study on the interaction between non-linear wave, buried pipeline and non-homogenous porous seabed. *Journal of Computers and Geotechnics Engineering*, 30(6), pp. 535-547.

GRIFFITHS, T.J., WHITE, D.J. and CHENG, L., 2010. Progress in investigating pipe-soil-fluid interaction: the STABLEpipe JIP. *Proceedings of the 20th International Offshore and Polar Engineering Conference*. 20-25 June 2010. Beijing: International Society of Offshore and Polar Engineers. Pp. 115-122.

GUO, B. et al., 2005. Offshore pipelines. Oxford: Elsevier Inc.

HELFINSTINE, R.A. and SHUPE, J.W., 1972. Lift and drag on a model offshore pipeline. *Offshore Technology Conference*. 1-3 May 1972. Texas: Offshore Technology Conference. pp. 563-572.

HUSE, E. and MUREN, P., 1987. Drag in oscillatory flow interpreted from wake considerations. *Offshore Technology Conference*. 27-30 April 1987. Texas: Offshore Technology Conference. pp. 135-142.

JAS, E. et al., 2012. Pipeline stability revisited. *The Journal of Pipeline Engineering*, 4th Quarter, pp. 259-269.

JENG, D.S. and CHENG, L., 2000. Wave-induced seabed instability around a buried pipeline in a poro-elastic seabed. *Journal of Ocean Engineering*, 27(2), pp. 127-146.

JO, C.H., KIM, K. and HONG, S.G., 2000. Subsea pipeline stability in various trench sections. *Proceedings of the 10th International Offshore and Polar Engineering Conference*. 28 May-2 June 2000. Seattle: International Society of Offshore and Polar Engineers. pp. 218-225.

LAM, K.Y., WANG, Q.X. and ZONG, Z., 2002. A nonlinear fluid–structure interaction analysis of a near-bed submarine pipeline in a current. *Journal of Fluids and Structures*, 16(8), pp. 1177-1191.

LAMBRAKO, K.F., 1985. Marine pipeline soil friction coefficients from in-situ testing. *Journal of Ocean Engineering*, 12(2), pp. 131-150.

LAMMERT, W.F. and HALE, J.R., 1989. Dynamic response of submarine pipelines exposed to combined wave and current action. *Offshore Technology*

Conference. 1-4 May 1989. Texas: Offshore Technology Conference. pp. 159-170.

LIANG, D. and CHENG, L., 2005. Numerical modeling of flow and scour below a pipeline in currents: Part I. flow simulation. *Journal of Coastal Engineering*, 52(1), pp. 25-42.

LIANG, D., CHENG, L. and LI, F., 2005. Numerical modeling of flow and scour below a pipeline in currents: Part I. scour simulation. *Journal of Coastal Engineering*, 52(1), pp. 43-62.

ONG, C.M. et al., 2011. Near-Bed flow mechanisms around a circular marine pipeline close to a flat seabed in the subcritical flow regime using a k-ε model. *Journal of Offshore Mechanics and Arctic Engineering,* 134(2), pp. 021803-021803-11

RANDOLPH, M.F. and WHITE, D.J., 2008. Pipeline embedment in deep water: processes and quantitative assessment. *Offshore Technology Conference*. 5-8 May 2008. Texas: Offshore Technology Conference. pp. 1-16.

SHEN, W.O et al., 2013. 2D and 3D CFD investigation of seabed and shear stresses around subsea pipelines. *Proceedings of the ASME 32nd International Conference on Ocean, Offshore and Artic Engineering*. 9-14 June 2013. Nantes: ASME. pp. 1-15.

TEH, T.C. et al., 2006. Stability of submarine pipelines on liquefied seabeds. *Journal of Waterway, Port, Coastal and Ocean Engineering*, 132(4), pp. 244-251.

TEH, T.C., PALMER, A.C. and DAMGAARD, J.S., 2003. Experimental study of marine pipelines on unstable and liquefied seabed. *Journal of Coastal Engineering*, 50(1-2), pp. 1-17.

TIAN, Y. and CASSIDY, M.J., 2008. A practical approach to numerical modeling of pipe-soil interaction. *Proceedings of the 18th International Offshore and Polar Engineering Conference*. 6-11 July 2008. Vancouver: International Society of Offshore and Polar Engineers. pp. 533-538.

YANG, B. et al., 2008. Forces acting on the seabed around a pipeline in unidirectional ocean currents. *The Open Civil Engineering Journal*, (2), pp. 148-155.

YANG, L., et al., 2010. A study in motion on seabed with submarine pipeline. In: *Proceedings of the 20th (2010) International Offshore and Polar Engineering Conference.* 20-25 June 2010. Beijing: International Society of Offshore and Polar Engineers. pp. 98-103.

TRYGGESTAD, S., KOLLSTAD, T. and SELANGER, K.A., 1987. Measuring technique and field data for pipeline stability studies. *Offshore Technology Conference*. 27-30 April 1987. Texas: Offshore Technology Conference. pp. 199-210.

ZANG, Z. et al., 2009. A numerical model for onset of scour below offshore pipelines. *Journal of Coastal Engineering*, 56(4), pp. 458-466.

ZHAO, M. and CHENG, L., 2009. Numerical investigation of local scour below a vibrating pipeline under steady currents. *Journal of Coastal Engineering*, 57(4), pp. 397-406.

ZIETOUN, H.O. et al., 2009. Advanced dynamic stability analysis. *Proceedings of the ASME 28th International Conference on Ocean, Offshore and Artic Engineering*. 31 May-5 June 2009. Hawaii: ASME. pp. 661-673.

APPENDIX A

Flowchart of Matlab Program for Embedment Calculation for varying Pipeline Diameter
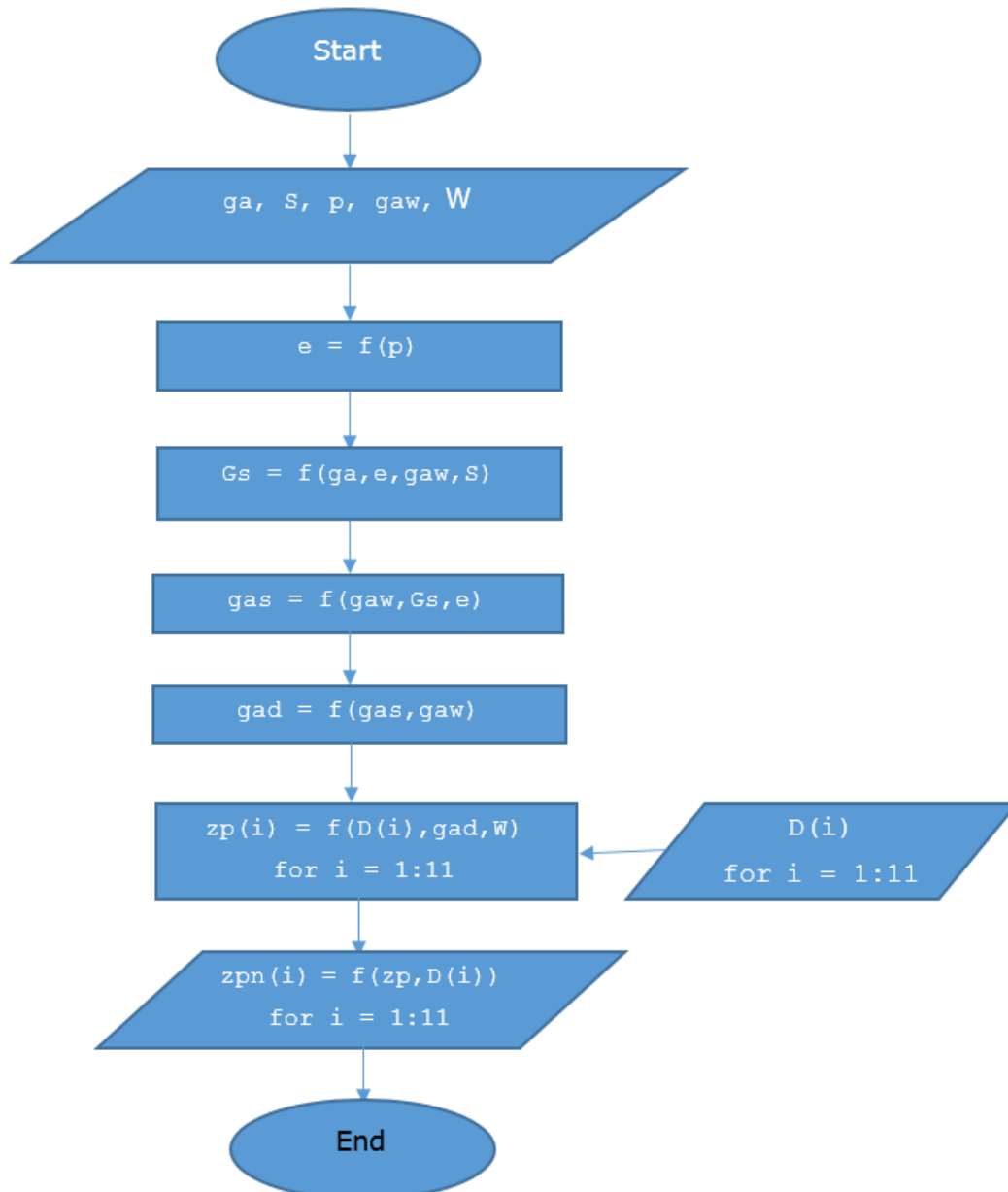
APPENDIX A(ɪ)

Embedment Calculation for each Pipeline Diameter on Sand Matlab

Code

```
clear all
clf

ga = input('Bulk Unit Weight of Sand (N/m³) = ');
S = input('Saturation of Sand (%) = ');
p = input('Porosity of Sand (%) = ');
gaw = 9810;                          % Unit Weight of Water

e = p/(1-p);                         % Voids Ratio
Gs = ((ga*(1+e))/gaw)-(e*S);         % Specific Gravity of Soil
gas = (gaw*(Gs+e))/(1+e);            % Saturated Unit Weight of Soil
gad = gas - gaw;                     % Submerged Unit Weight of Soil

D = 0.2:0.1:1.2;            % Pipe Diameter Range
W = 1000;                   % Submerged Weight per Unit Length of Pipe
zp = zeros(1,11);
zpn = zeros(1,11);          % Storage Matrices


for i = 1:11

    zp(i) = 0.037*D(i)*((gad*(D(i))^2)/W)^-0.67;
    zpn(i) = zp(i)/D(i);
                         % Embedment Calculation for Each Diameter
end


figure(1)
plot(D,zpn)
xlabel('Pipe Outer Diameter (m)')
ylabel('Initial Embedment (Normalised with Diameter)')
```

APPENDIX A(II)

Embedment Calculation for each Pipeline Diameter on Clay Matlab

Code

```
clear all
clf

Ga = 11500;              % Dry unit soil weight
Su = 30000;              % Undrained shear strength
D = 0.2:0.1:1.2;         % Pipe Diameter Range
W = 1000;                % Submerged Weight per Unit Length of Pipe
zp = zeros(1,11);
zpn = zeros(1,11);       % Storage Matrices


for i = 1:11

    Gc = Su/(D(i)*Ga);
    Kc = (Su*D(i))/W;

    zp(i) = D(i)*(0.0071*(((Gc^0.3)/Kc)^3.2) +
0.062*(((Gc^0.3)/Kc)^0.7));

    zpn(i) = zp(i)/D(i);
                            % Embedment Calculation for Each Diameter
end


figure(1)
plot(D,zpn)
xlabel('Pipe Outer Diameter (m)')
ylabel('Initial Embedment (Normalised with Diameter)')
```

APPENDIX B

Flowchart of Matlab Program for Embedment Calculation for varying Pipeline Weight
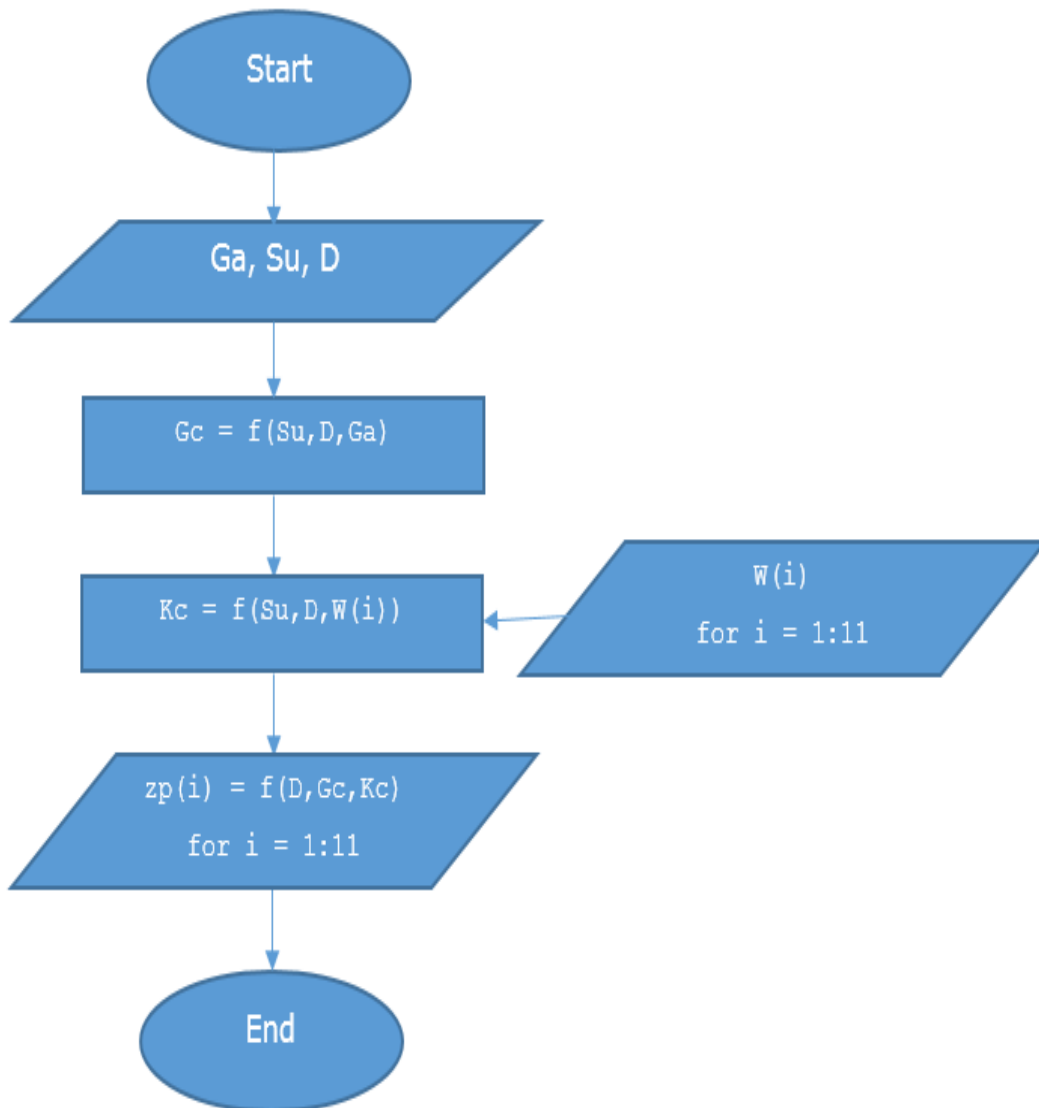
APPENDIX B(ɪ)

Embedment Calculation for each Pipeline Weight on Sand Matlab Code

```
clear all
clf

D = input('Diametr (m) = ');
ga = input('Bulk Unit Weight of Sand (N/m3) = ');
S = input('Saturation of Sand (%) = ');
p = input('Porosity of Sand (%) = ');
gaw = 9810;                      % Unit Weight of Water

e = p/(1-p);                     % Voids Ratio
Gs = ((ga*(1+e))/gaw)-(e*S);     % Specific Gravity of Soil
gas = (gaw*(Gs+e))/(1+e);        % Saturated Unit Weight of Soil
gad = gas - gaw;                 % Submerged Unit Weight of Soil

Ws = 200:50:2000;                % Pipe Submerged Unit Weight Range
zp = zeros(1,37);                % Storage Matrix


for i = 1:37

    zp(i) = 0.037*D*((Ga*D^2)/Ws(i))^-0.67;
                       % Embedment Calculation for Each Weight
end
```

APPENDIX B(ɪɪ)

Embedment Calculation for each Pipeline Weight on Clay Matlab Code

```
clear all
clf

Ga = 11500;                        % Dry unit soil weight
Su = 30000;                        % Undrained shear strength
D =input('Diameter (m) = ');

W = 200:50:2000;                   % Pipe Submerged Unit Weight Range
zp = zeros(1,37);                  % Storage Matrix


for i = 1:37

    Gc = Su/(D*Ga);
    Kc = (Su*D)/W(i);

    zp(i) = D*(0.0071*(((Gc^0.3)/Kc)^3.2) + 0.062*(((Gc^0.3)/Kc)^0.7));
                          % Embedment Calculation for Each Weight
end
```

APPENDIX C

Flowchart of Matlab Program for Embedment Calculation for combined Pipeline Diameter and Weight
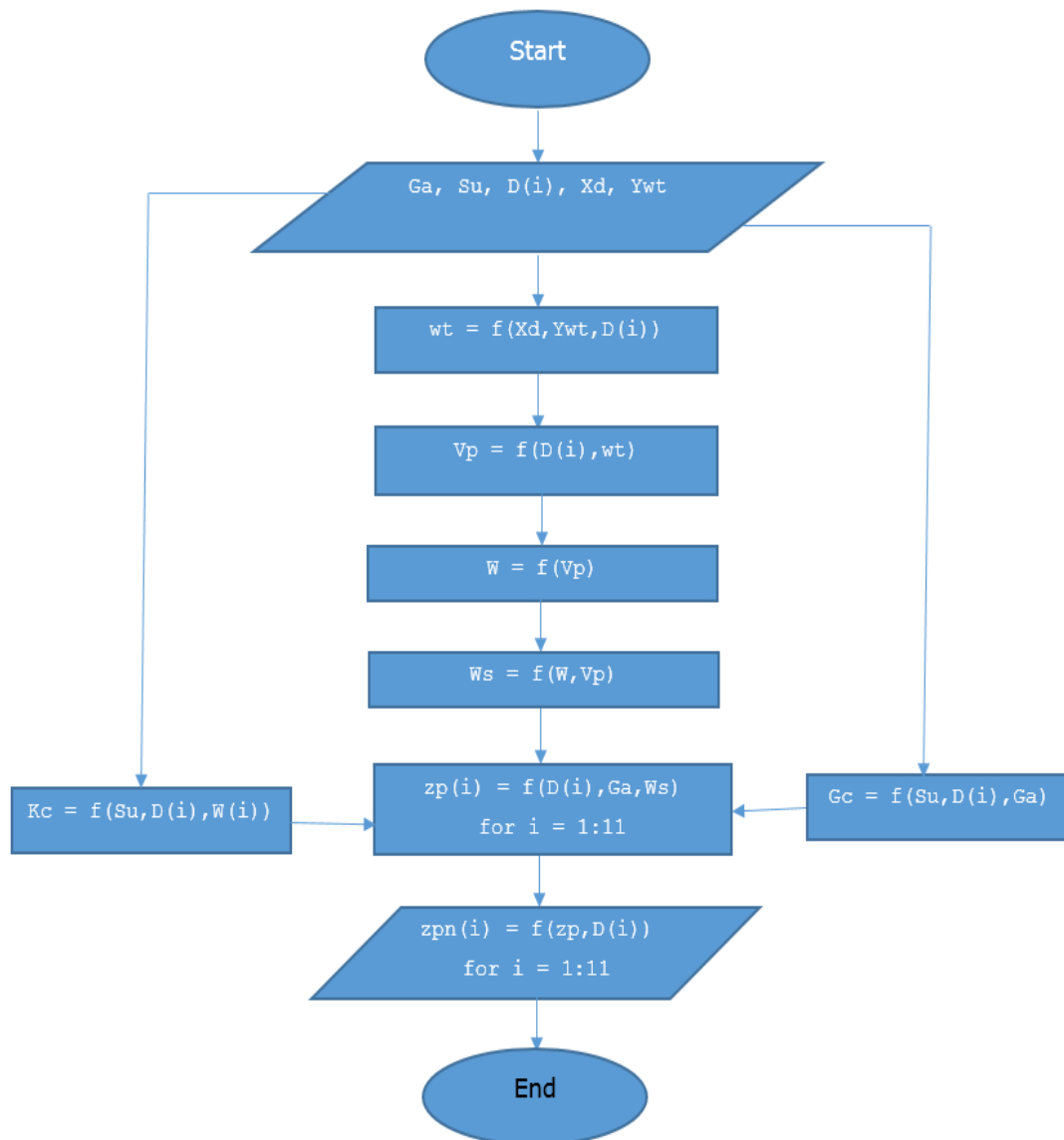
APPENDIX C(1)

Embedment Calculation for combined Pipeline Diameter and Weight

on Sand Matlab Code

```matlab
clear all
clf

Ga = 8836;                          % Submerged Unit Weight of Soil
D = 0.2:0.1:1.2;                    % Pipe Diameter Range
zp = zeros(1,11);
zpn = zeros(1,11);                  % Storage Matrices

for i = 1:11

    Xd = [0.1016, 0.1143, 0.1413, 0.1683, 0.2191, 0.273, 0.3238, 0.66, 0.965,
1.219];
    Ywt = [0.00574, 0.00602, 0.00655, 0.00711, 0.00818, 0.00927, 0.00953,
0.00953, 0.00953, 0.00953];
            % Range of Standard Pipe Diameters and Wall Thicknesses

    wt = interp1(Xd, Ywt, D(i));        % Wall thickness for Diameter

    Vp = (pi*(D(i)^2 - (D(i)-(wt*2))^2))/4;      % Volume of Pipe
    W = Vp*7600*9.81;                            % Weight of Pipe
    Ws = W - Vp*1025*9.81;                       % Submerged Weight of Pipe

    zp(i) = 0.037*D(i)*((Ga*(D(i))^2)/Ws)^-0.67;
    zpn(i) = zp(i)/D(i);
                        % Embedment Calculation for Each Diameter
end
```

APPENDIX C(II)

Embedment Calculation for combined Pipeline Diameter and Weight

on Clay Matlab Code

```
clear all
clf

Ga = 18000;                      % Dry Unit Weight of Soil
Su = 30000;                      % Undrained Shear Strength
D = 0.2:0.1:1.2;                 % Pipe Diameter
zp = zeros(1,11);
zpn = zeros(1,11);               % Storage Matrices

for i = 1:11

    Xd = [0.1016, 0.1143, 0.1413, 0.1683, 0.2191, 0.273, 0.3238, 0.66, 0.965,
1.219];
    Ywt = [0.00574, 0.00602, 0.00655, 0.00711, 0.00818, 0.00927, 0.00953,
0.00953, 0.00953, 0.00953];
        % Range of Standard Pipe Diameters and Wall Thicknesses

    wt = interp1(Xd, Ywt, D(i));   % Wall thickness for Diameter

    Vp = (pi*(D(i)^2 - (D(i)-(wt*2))^2))/4;      % Volume of Pipe
    W = Vp*7600*9.81;                            % Weight of Pipe
    Ws = W - Vp*1025*9.81;              % Submerged Weight of Pipe

    Gc = Su/(D(i)*Ga);
    Kc = (Su*D(i))/Ws;

    zp(i) = D(i)*(0.0071*(((Gc^0.3)/Kc)^3.2) + 0.062*(((Gc^0.3)/Kc)^0.7));
    zpn(i) = zp(i)/D(i);
                        % Embedment Calculation for Each Diameter
end
```

APPENDIX D

Flowchart of Matlab Program for Embedment Calculation for varying unit Weight of Soil

```
                    ┌───────────────┐
                    │     Start     │
                    └───────┬───────┘
                            │
                            ▼
              ╱─────────────────────────╲
             ╱  Gad(i), Su, D, Xd,       ╲
            ╱───────────────────────────╱
                            │
                            ▼
            ┌───────────────────────────┐
            │   wt = f(Xd,Ywt,D(i))     │
            └───────────────┬───────────┘
                            │
                            ▼
            ┌───────────────────────────┐
            │     Vp = f(D(i),wt)       │
            └───────────────┬───────────┘
                            │
                            ▼
            ┌───────────────────────────┐
            │       W = f(Vp)           │
            └───────────────┬───────────┘
                            │
                            ▼
            ┌───────────────────────────┐
            │     Ws = f(W,Vp)          │
            └───────────────┬───────────┘
                            │
                            ▼
          ╱─────────────────────────────╲
         ╱  zp(i) = f(D,Gad(i),Ws)       ╲
        ╱       for i = 1:11             ╱
       ╱────────────────────────────────╱
                            │
                            ▼
                    ┌───────────────┐
                    │      End      │
                    └───────────────┘
```

160

APPENDIX D(1)

Embedment Calculation for each unit Weight of Soil (Sand) Matlab Code

```
clear all
clf

Gad = 7000:500:13500;          % Submerged Unit Weight of Soil Range
Ga = Gad+9810;                 % Unit Weight of Soil Range
D = input('Pipe Diameter (m) - ');
zp = zeros(1,14);
zpn = zeros(1,14);             % Storage Matrices

Xd = [0.1016, 0.1143, 0.1413, 0.1683, 0.2191, 0.273, 0.3238, 0.66, 0.965,
1.219];
Ywt = [0.00574, 0.00602, 0.00655, 0.00711, 0.00818, 0.00927, 0.00953,
0.00953, 0.00953, 0.00953];
          % Range of Standard Pipe Diameters and Wall Thicknesses

wt = interp1(Xd, Ywt, D(i));    % Wall thickness for Diameter

Vp = (pi*(D(i)^2 - (D(i)-(wt*2))^2))/4;   % Volume of Pipe
W = Vp*7600*9.81;                         % Weight of Pipe
Ws = W - Vp*1025*9.81;                    % Submerged Weight of Pipe

for i = 1:14

    zp(i) = 0.037*D*((Gad(i)*D^2)/(Ws))^-0.67;
              % Embedment Calculation for Each Unit Weight of Soil
end
```
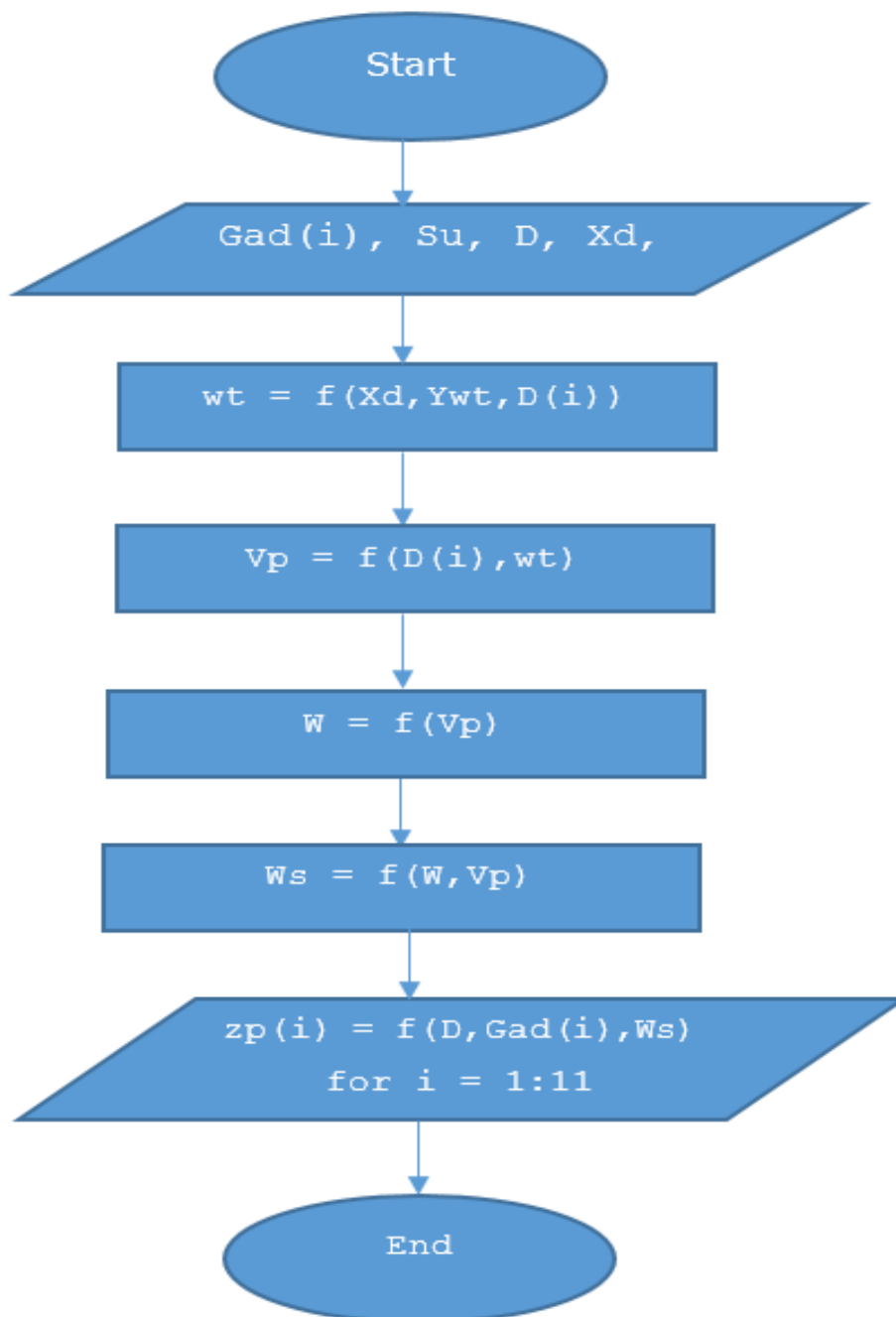
161

APPENDIX D(II)

Embedment Calculation for each unit Weight of Soil (Clay) Matlab Code

```
clear all
clf

Ga = 10000:1000:24000;            % Dry unit soil weight
Su = 30000;                       % Undrained shear strength

D = input('Pipe Diameter (m) - ');
zp = zeros(1,14);
zpn = zeros(1,14);                % Storage Matrices

Xd = [0.1016, 0.1143, 0.1413, 0.1683, 0.2191, 0.273, 0.3238, 0.66, 0.965,
1.219];
Ywt = [0.00574, 0.00602, 0.00655, 0.00711, 0.00818, 0.00927, 0.00953,
0.00953, 0.00953, 0.00953];
        % Range of Standard Pipe Diameters and Wall Thicknesses

wt = interp1(Xd, Ywt, D(i));      % Wall thickness for Diameter

Vp = (pi*(D(i)^2 - (D(i)-(wt*2))^2))/4;     % Volume of Pipe
W = Vp*7600*9.81;                           % Weight of Pipe
Ws = W - Vp*1025*9.81;                      % Submerged Weight of Pipe

for i = 1:15

    Gc = Su/(D*Ga(i));
    Kc = (Su*D)/W;

    zp(i) = D*(0.0071*(((Gc^0.3)/Kc)^3.2) + 0.062*(((Gc^0.3)/Kc)^0.7))
                % Embedment Calculation for Each Unit Weight of Soil
end
```

162

APPENDIX E

Embedment Calculation due to Scouring Matlab Code

```
clear all
clf

D = 0.5;                        % Pipe Diameter
gad = 8836;                     % Submerged Weight of Soil
mu = 0.6;                       % Pipe/Soil Friction Coefficient
ph = 9*(pi/180);                % Soil Response Angle


Fl = zeros(1,7);
Fd = zeros(1,7);
Fc = zeros(1,7);
Ff = zeros(1,7);
Ks = zeros(1,7);
Fr = zeros(1,7);
Fx = zeros(1,7);
P1 = zeros(1,7);
P2 = zeros(1,7);
Fln = zeros(1,7);
Fcn = zeros(1,7);
Zp = zeros(1,7);
ZP = zeros(4,7);                % Storage Matrices


zpR = 0:0.05:0.25;              % Embedment Range
Uc = 0:0.25:1.5;                % Current Velocity Range
Ws = 500:500:2000;              % Pipe Submerged Weight

FlR = [0 0 0 0 0 0; 40.77 37.92 32.11 29.84 25.99 22.96; 171.32 158.34 155.7
124.11 105.5 86.33; 394.41 364.73 346.11 286.25 242.55 197.76; 665.36 655.02
597.6 511.34 436.75 350; 1094.7 1031.7 1027.3 727.74 675.17 543; 1593.6
1512.3 1493.1 1183.7 1105.5 808.4];

FdR = [0 0 0 0 0 0; 26.28 21.98 18.65 17.1 14.82 12.59; 99.25 82.49 80.68
64.16 54.87 46.26; 216.2 178.62 157.86 139.56 119.07 100.68; 353.72 306.28
271.34 240.83 205.24 173.74; 598.55 468.92 460.95 342.5 312.4 265.77; 848.28
671.63 651.92 527.06 468.26 383];

P1R = [0 0 0 0 0 0; 32.14 32.79 33.17 32.1 30.58 27.86; 126.87 130.35 118.61
127.6 126.27 124.32; 283.83 292.17 276.62 284.86 283.58 279.22; 522.04 541.13
526.93 529.53 353.77 509.09; 773.02 823.96 717.31 861.95 778.37 782.37;
1110.6 1162.1 1030.1 1131.7 979.06 1114.7];

P2R = [0 0 0 0 0 0; -23.1 -19.99 -16.21 -14.73 -12.34 -10.44; -88.48 -75.56
-87.86 -54.58 -40.11 -27.11; -192.02 -163.68 -145.93 -118.67 -84.39 -56.59;
-286.72 -254.35 -232.58 -178.12 -151.1 -84.41; -624.57 -413.21 -501.05
-207.01 -219.81 -137.35; -885.56 -613 -705.4 -437.99 -430.33 -198.64];
                                % Ansys Results


for n = 1:4     % Sets Up Loop for 4 Pipe Weights

    zpin = 0.037*D*((gad*D^2)/Ws(n))^-0.67;   % Initial Embedment

    for j=2:7   % Sets Up Loop for 6 Current Velocities
            Fl(j) = interp1(zpR, FlR(j,:), zpin);
            Fd(j) = interp1(zpR, FdR(j,:), zpin);
                    % Lift and Drag Forces at Initial Embedment
```

163

```matlab
            Fc(j) = Ws(n)-Fl(j);          % Contact Force
            Ff(j) = mu*Fc(j);             % Friction Force

            Ks(j) = (gad*D^2)/Fc(j);

                if Ks(j) > 26.7
                    Fr(j) = Fc(j)*Ks(j)*(zpin/D)^1.25;
                else
                    Fr(j) = Fc(j)*(5*Ks(j)-0.15*Ks(j)^2)*(zpin/D)^1.25;
                end              % Passive Reaction Force Calculation

            Fx(j) = Fr(j) + Ff(j);     % Total Reaction Force

            if (Fx(j) > Fd(j))         % Condition for Pipe Break-Out

                Zp(1) = zpin;  % Sets First Element in Embedment
                            Storage Matrix to Initial Embedment

                P1(j) = interp1(zpR, P1R(j,:), zpin);
                P2(j) = interp1(zpR, P2R(j,:), zpin);
                                    % Pressures at Initial Embedment

                Fln(j) = interp1(zpR, FlR(j,:), zpin);
                Fcn(j) = Ws(n)-Fln(j);
                    % New Lift and Contact Force with Current Flowing

                al = acos(1-((2*zpin)/D));
                Pdc = gad*(al*D*tan(ph))/(cos(al)+(sin(al)*tan(ph)));

                if P1(j)-P2(j) >= Pdc;
            % Condition for Onset of Scour

                    Zp(j) = 0.972*((((Uc(j))^2)/(2*9.81))^0.2)*(D^0.8);
                                    % Equilibrium Scour Hole Depth
                else
                        Zp(j) = 0.037*D*((gad*D^2)/Fcn(j))^-0.67;
                            % Embedment with New Contact Force
                end
            else
                display('Pipe will break out of embedment')
            end
        end

    ZP(n,:) = Zp;     % Stores Embedment Values for Each Pipe Weight
end
ZPN = ZP./D;          % Normalised Embedment Results
```
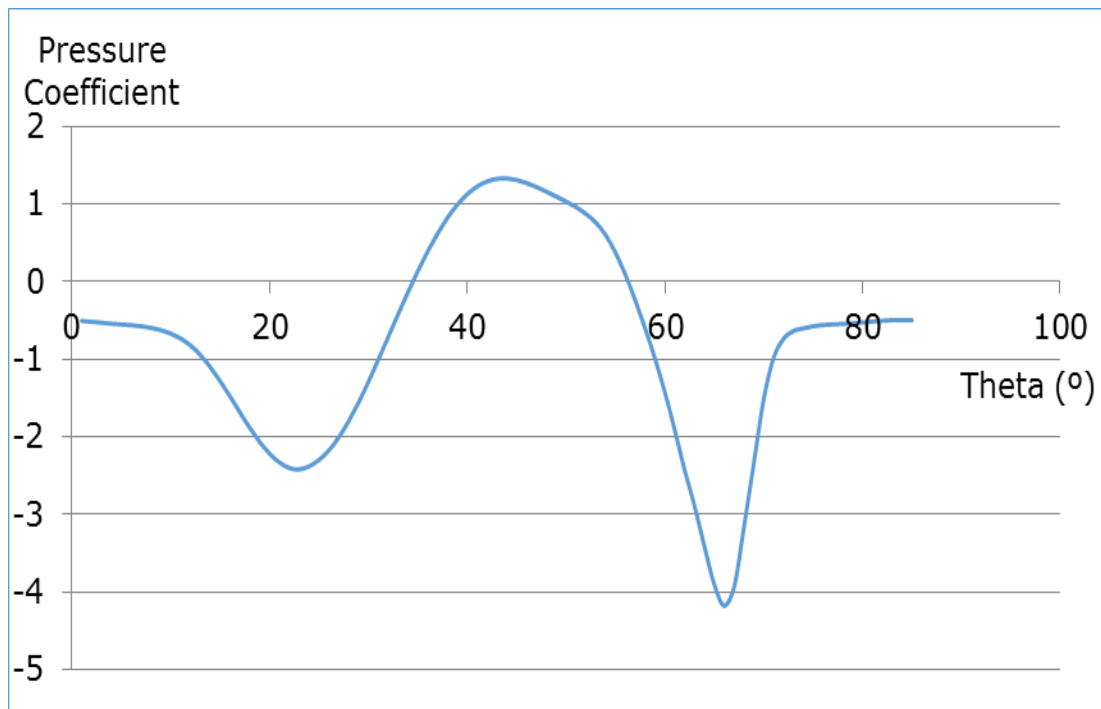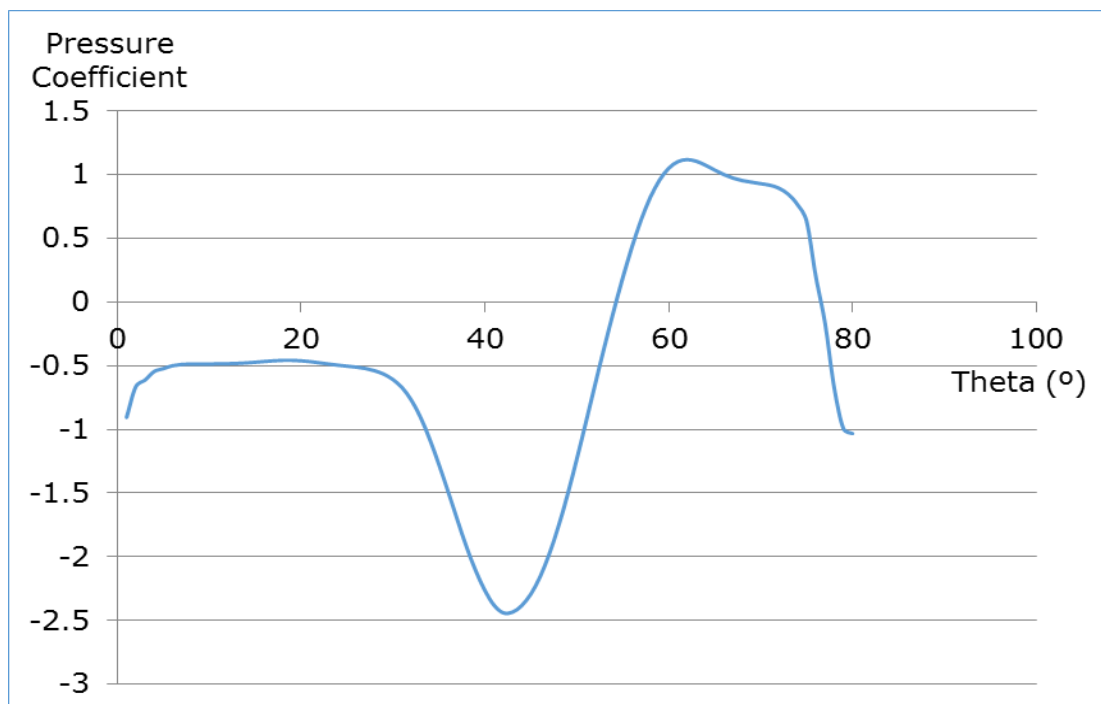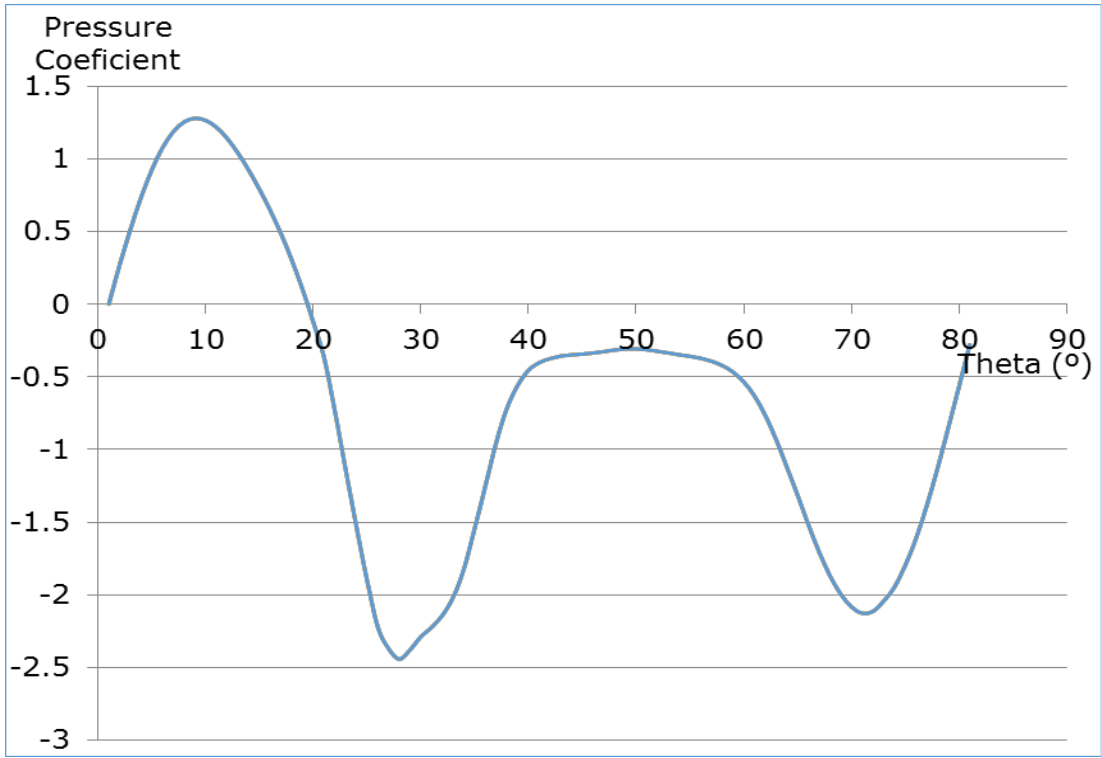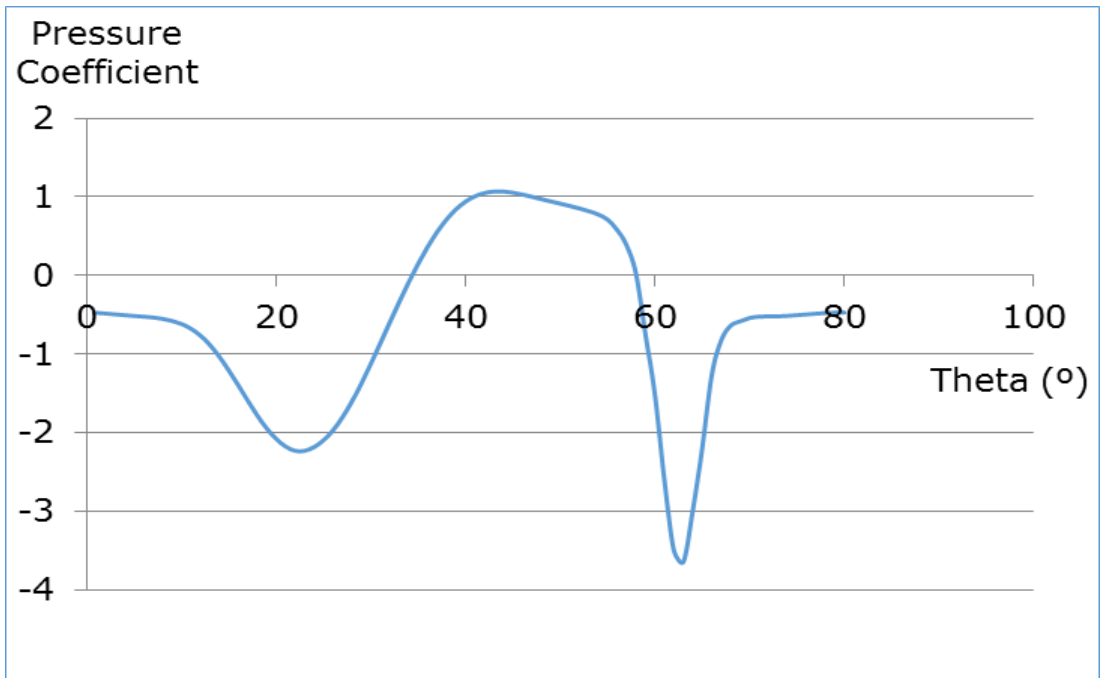
164

APPENDIX F

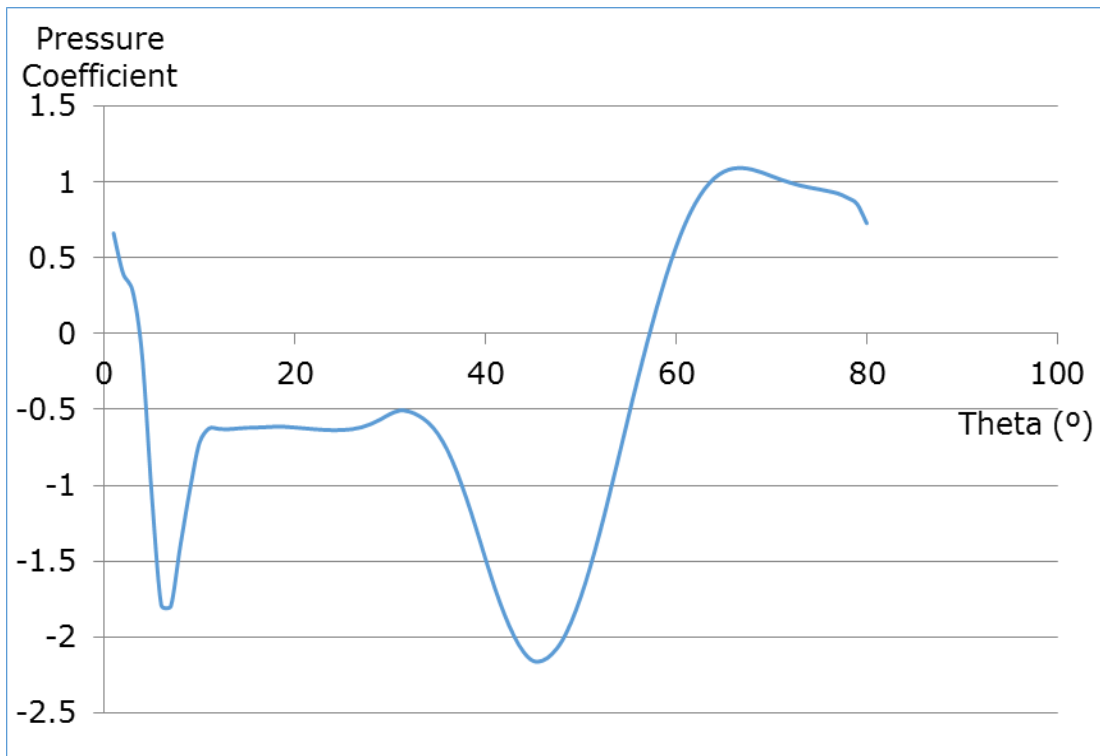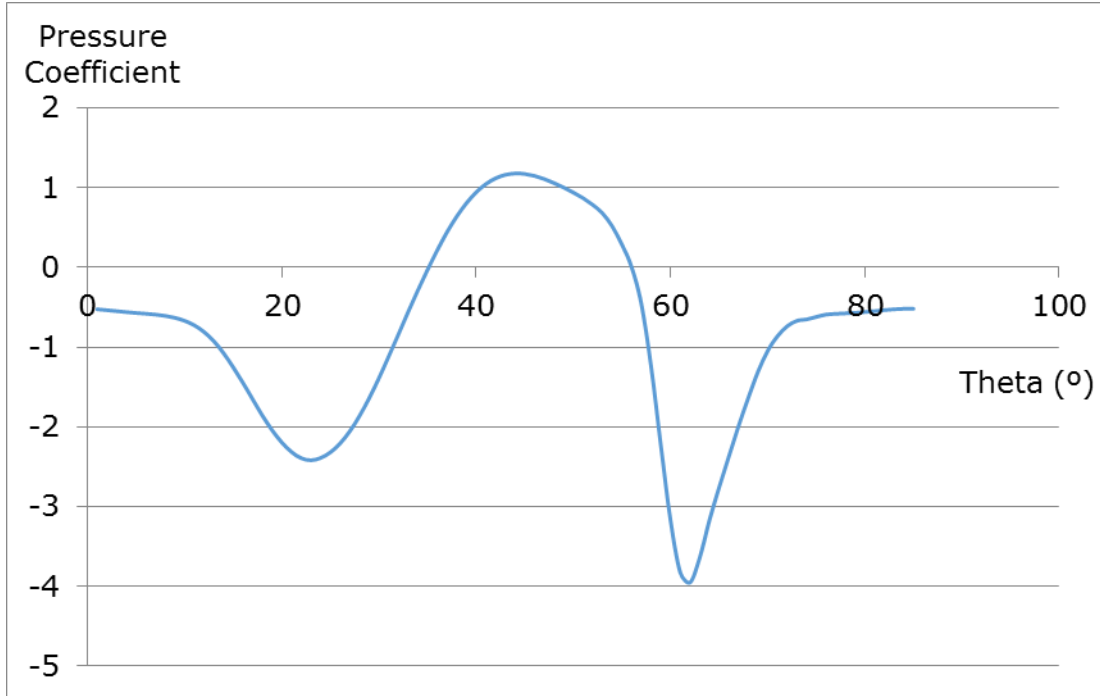Pressure coefficient as a function of Theta for pipeline at position -0.7

Pressure coefficient as a function of Theta for pipeline at position -0.7

Pressure coefficient as a function of Theta for pipeline at position 0.0

Pressure coefficient as a function of Theta for pipeline at position 0.5

166

Pressure coefficient as a function of Theta for pipeline at position 1.0

Pressure coefficient as a function of Theta for pipeline at position 1.2

PUBLICATIONS

1. **I Iyalla**, K Umah and M Hossain. Computational Fluid Dynamics Modelling of Pipe-Soil Interaction in Current. Proceedings of the IAENG World Congress on Engineering. 2010 June 30- August 2. London: IAENG, 2010. Vol II p. 1539-1543.

2. **Ibiye Iyalla**, Mamdud Hossain and Jesse Andrawus. Calculating Hydrodynamic Loads on Pipelines and Risers: Practical Alternative to Morison's Equation. Proceedings of the 3rd International Conference of Engineering Research and Development (ICERD). 2010 September 7-9. Benin. ICERD10101.

3. **Iyalla I**, Hossain M, Andrawus J. Calculating hydrodynamic loads in pipelines and risers: practical alternative to Morison's equation. *Advanced Materials Research*. 2012; 367.